Timing of the Quaternary Elazığ Volcanism, Eastern Turkey, and its Significance for Constraining Landscape Evolution and Surface Uplift

ALİ SEYREK[1], ROB WESTAWAY[2], MALCOLM PRINGLE[3],
SEMA YURTMEN[4], TUNCER DEMİR[5] & GEORGE ROWBOTHAM[6]

[1] Department of Soil Science, Harran University, TR–63300 Şanlıurfa, Turkey
[2] Faculty of Mathematics and Computing, The Open University,
Eldon House, Gosforth, Newcastle-upon-Tyne NE3 3PW, UK
(E-mail: robwestaway@tiscali.co.uk)
[Also at: School of Civil Engineering and Geosciences, Newcastle University,
Newcastle-upon-Tyne NE1 7RU, UK]
[3] Scottish Universities' Environmental Research Centre, Rankine Avenue,
East Kilbride, Glasgow G75 0QF, UK
[Present address: Laboratory for Noble Gas Geochronology, Department of Earth,
Atmospheric, and Planetary Sciences, Massachusetts Institute of Technology,
77 Massachusetts Avenue, Building 54 TR–1013, Cambridge, MA 02139 TR–4307, USA]
[4] Department of Geology, Çukurova University, TR–01330 Adana, Turkey
[Present address: 41 Kingsway East, Westlands, Newcastle-under-Lyme, Staffordshire, ST5 5PY, UK]
[5] Department of Geography, Harran University, TR–63300 Şanlıurfa, Turkey
[6] School of Earth Sciences and Geography, Keele University, Keele, Staffordshire ST5 5BG, UK

Abstract: The eastern part of the Anatolian plateau in eastern Turkey has experienced dramatic landscape evolution in the Late Cenozoic, surface uplift having been associated with the disruption of former lake basins and the development of the modern high-relief landscape, incised by the upper reaches of the River Euphrates and its major tributary, the Murat. Overall, the altitude of the plateau decreases gradually westward, and it has been assumed that uplift on any given timescale has varied regionally in a similar manner. However, using the Ar-Ar method, we have dated an episode of basaltic volcanism around the city of Elazığ to ~1.8–1.9 Ma (two alternative calculation procedures give ages of 1885±16 ka and 1839±16 ka; both ±2σ). The disposition of this basalt indicates no more than ~100 m of incision by the River Murat on this timescale in this area, in marked contrast to neighbouring localities where much more incision on similar timescales is indicated by the geomorphology. We interpret these variations as consequences of flow in the lower continental crust induced by surface processes, the flow being vigorous because the lower crust in this region is highly mobile due to the high Moho temperature. We thus suggest that the ~1.8–1.9 Ma Elazığ volcanism was triggered by outflow of lower crust following the emptying at ~2 Ma of the adjacent Malatya lake basin; the resulting local removal of part of this lower-crustal layer can also account for the limited amount of subsequent net crustal thickening and surface uplift that has occurred locally. Local patterns such as this are superimposed onto the regional westward tilting of the surface of the Anatolian Plateau, which has facilitated the disruption of former lake basins such as this.

Key Words: Turkey, Anatolia, Miocene, Pliocene, Pleistocene, volcanism, Ar-Ar dating

Doğu Anadoluda Elazığ Kuvaterner Volkanizmasının Yaşı ve Bölgenin Jeomorfolojik Evrimi ile Yükselimi Açısından Önemi

Özet: Anadolu Platosunun doğu kesimi Geç Senozoik'te dikkat çekici bir evrim geçirmiştir. Tektonik yükselmeler daha önce var olan göl havzalarının tahrip olmasına ve bu havzalarda Fırat nehri ve onun ana kolu olan Murat nehri tarafından derince yarılmış, yüksek rakımlı topografyanın meydana gelmesine sebep olmuştur. Genel olarak Anadolu Platosunun yükseltisi batıya doğru azalmaktadır. Bu durum tektonik yükselme oranlarının batıya doğru azalma eğiliminde olduğunu ortaya koymaktadır. Bununla birlikte, Ar-Ar metodunun uygulanmasıyla Elazığ yakınında yüzeyleyen bazaltik karakterdeki volkanizmanın yaşının 1.8–1.9 milyon yıl olduğunu ortaya konmuştur (iki farklı hesaplama metodu Elazığ volkanizması yaşının 1885±16 ka ve 1839±16 ka arasında değiştiğini göstermektedir). Bazaltların topografik durumundan anlaşıldığı üzere volkanizmanın meydana geldiği zamandan

günümüze kadar geçen sürede Murat nehri çalışma sahasında yatağını 100 m den fazla derinleştirememiştir. Buna karşılık, çalışma sahasına komşu alanların günümüzdekü jeomorfolojik durumu aynı zaman diliminde nehirlerin yataklarını derine kazma miktarlarının daha fazla olduğunu göstermektedir. Nehirlerin yataklarını derine kazma oranlarındaki bu farklılıkları yüzey proseslerinin sebep olduğu alt kıtasal kabuktaki akıntıların rolüne bağlamaktayız. Bu bölgedeki alt kıtasal kabuk yüksek moho sıcaklığından dolayı daha mobil olup, kabuk içerisinde oluşan akıntılar ise daha güçlüdür. Böylece 1.8–1.9 milyon yaşındaki Elazığ volkanizması yaklaşık olarak 2 milyon yıl önce komşu Malatya göl havzasının dış drenaja (boşalmasını) bağlanmasını takip eden dönemde çalışma sahasındaki alt kıtasal kabuğun civar alanlara doğru akışının tetiklediği varsayılmaktadır. Alt kıtasal kabuktaki bu türden hareketlenmeler bazı sahalarda yerel olarak kabuk kalınlaşmasına ve tektonik yükselmelere sebep olmuştur. Bu türdeki yerel tektonik yükselmeler aynı zamanda batıya doğru topyekün eğimlenmiş olan Anadolu Platosu üzerine eklenmiştir. Bu durum Malatya göl havzasında olduğu gibi daha önce var olan göl havzalarının ortadan kalkmasına sebep olmuştur.

Anahtar Sözcükler: Türkiye, Anadolu, Miyosen, Pliyosen, Pleyistosen, volkanizma, Ar-Ar yaşlandırma

Introduction

Eastern Turkey (Figure 1) forms the modern boundary zone between the African (AF), Arabian (AR), Eurasian (EU) and Turkish (TR) plates. The right-lateral North Anatolian Fault Zone (NAFZ) takes up westward motion of the Turkish plate relative to Eurasia; the left-lateral East Anatolian Fault Zone (EAFZ) accommodates WSW motion of the Turkish plate relative to Arabia. The overall effect of both fault systems is to accommodate north–northwestward motion of Arabia relative to Eurasia. The NAFZ and EAFZ converge at Karlıova (Figure 1), which is thus regarded as the notional TR-AR-EU 'triple junction'. Geodetic studies (e.g., McClusky *et al.* 2000) indicate that internal deformation of these plates is not significant, given the limits of measurement precision. This modern geometry of the NAFZ and EAFZ is thought to have developed at ~4 Ma (e.g., Westaway 2003, 2004a, 2006a; Westaway *et al.* 2006b). It is thought (e.g., by Westaway & Arger 2001; Westaway 2003, 2004a; cf. Kaymakcı *et al.* 2006) that, beforehand, the relative motion between the Turkish and Arabian plates was acommodated by slip on the Malatya-Ovacık Fault Zone (MOFZ; Figure 2). The SW part of this structure, the SSW-trending Malatya Fault, was shown by Kaymakcı *et al.* (2006) to have accommodated transtension, involving left-lateral slip and extension, resulting in subsidence in the interior of the lacustrine Malatya Basin.

For most of their length the NAFZ and EAFZ transect the Anatolian plateau. As many people have noted, the typical altitude of the land surface within this plateau rises eastward from ~500–1000 m a.s.l. in the west to ~3000 m in the east. The large negative Bouguer gravity anomaly (e.g., Ateş *et al.* 1999) indicates that this plateau is underlain by a thick lower-crustal 'keel' or 'root'.

Studies of seismic wave propagation indicate that the crustal thickness is 30 km in the west (Saunders *et al.* 1998) and up to 50 km in the east (Zor *et al.* 2003). Eastern Anatolia is adjoined to the south, across the suture of the former southern Neotethys ocean (Figure 2), by the northern part of the Arabian Platform crustal province, where the land surface is much lower (typically ~500–1000 m a.s.l.). As many people have previously discussed, the Cenozoic continental collision between Arabia and Anatolia has evidently resulted in much more intense deformation of the latter than of the former, indicating that the Arabian Platform crust is much stronger than that of Anatolia (see Demir *et al.* 2007, for a recent analysis of this topic).

Recent studies have begun to constrain the detailed history of Late Cenozoic regional surface uplift within the northern Arabian Platform, using heights of terraces of the rivers Tigris and Euphrates that are capped by dated basalt flows (e.g., Bridgland *et al.* 2007; Demir *et al.* 2007, 2008; Westaway *et al.* 2008). These investigations indicate a general southward tapering in uplift. For instance, the fluvial incision estimated since ~0.9 Ma decreases southward from ~70 m near Diyarbakır in SE Turkey (near the northern margin of the Arabian Platform) to as little as ~15 m near Deir ez-Zor in NE Syria, ~250 km farther south; the incision estimated since ~2 Ma decreases southward between these localities from ~100 m to ~40–50 m. Much greater amounts of fluvial incision, equated to regional surface uplift, are evident in western Anatolia; for instance dating of basalt flows and other evidence indicates that in the vicinity of Kula the River Gediz has incised by ~140 m since ~1 Ma and by as much as ~400 m since ~3 Ma (e.g., Westaway *et al.* 2004, 2006c). If the uplift during each span of time varied across Anatolia in proportion to
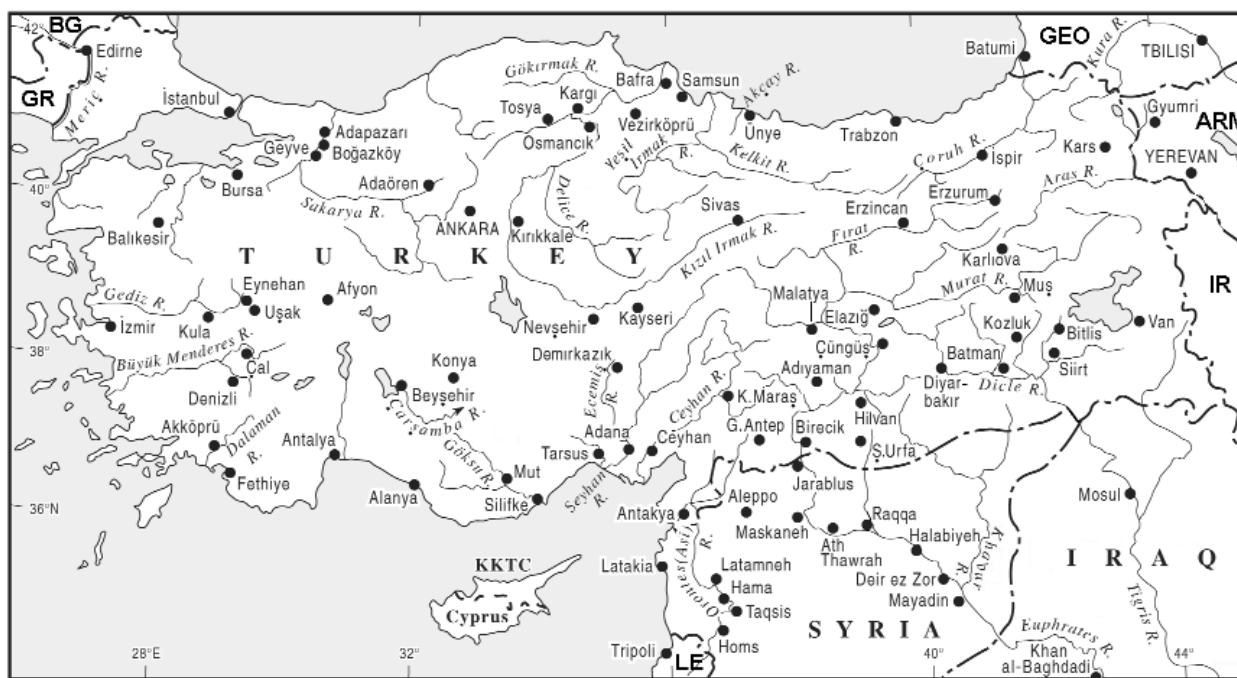
Figure 1. Map of Turkey showing the locations of the cities of Malatya and Elazığ and of the Euphrates river system, together with localities outside our immediate study region that are mentioned in the text. K. Maraş, G. Antep, and Ş. Urfa are abbreviations for Kahramanmaraş, Gaziantep, and Şanlıurfa. The NAFZ runs westward from Karlıova past Erzincan, along the Kelkit valley, then past Vezirköprü, Kargı, Tosya, and Adapazarı to the vicinity of İstanbul. The EAFZ runs generally WSW from Karlıova along the Murat valley, past Lake Hazar between Elazığ and Çüngüş, then between Malatya and Adıyaman to the vicinity of Kahramanmaraş.

the overall topography, one would expect to observe incision several times greater than each of these estimates in eastern Anatolia on corresponding time scales. However, there has as yet been no equivalent investigation of any age-height relationship for basalts that cascade into river valleys in eastern Anatolia.

The present study region, adjoining the city of Elazığ, is located well north of the EAFZ (Figure 2), within eastern Anatolia; the crust being locally 42 km thick (Zor *et al.* 2003). This region is now drained by the upper reaches of the River Euphrates and its major left-bank tributary, the Murat. As previously noted (e.g., Huntington 1902; Westaway & Arger 2001) the gorges of these rivers (now flooded by hydro-electric reservoirs) in some localities attain depths of many hundreds of metres, having been incised into former lake basins across much of the region. Basalt flows have cascaded partway down tributary gorges leading into the Murat valley, terminating at levels that can be presumed to mark the contemporaneous Murat valley floor. Dating of such basalts can indicate amounts of subsequent fluvial incision

(and thus, after appropriate corrections, discussed below, regional uplift), for comparison with surrounding regions.

This study will, first, discuss the disposition of basalts and lake sediments in and around the study region, then present dating evidence for the basalts, which will demonstrate that a brief phase of volcanism occurred in the Elazığ area at ~1.8–1.9 Ma. The possible cause-and-effect relationship between the chronology of this volcanism (and the limited subsequent fluvial incision and local surface uplift indicated by it) and that of the disruption at ~2 Ma of the youngest lake basin in the region, the Malatya Basin, will then be discussed.

Overview of Late Cenozoic Lacustrine Deposits and Basalts

This study region is within the eastern part of the Turkish plate, adjoining the Eurasian and Arabian plates, south of the NAFZ and north of the EAFZ (Figure 2). Both these active fault zones are well-known from both GPS satellite
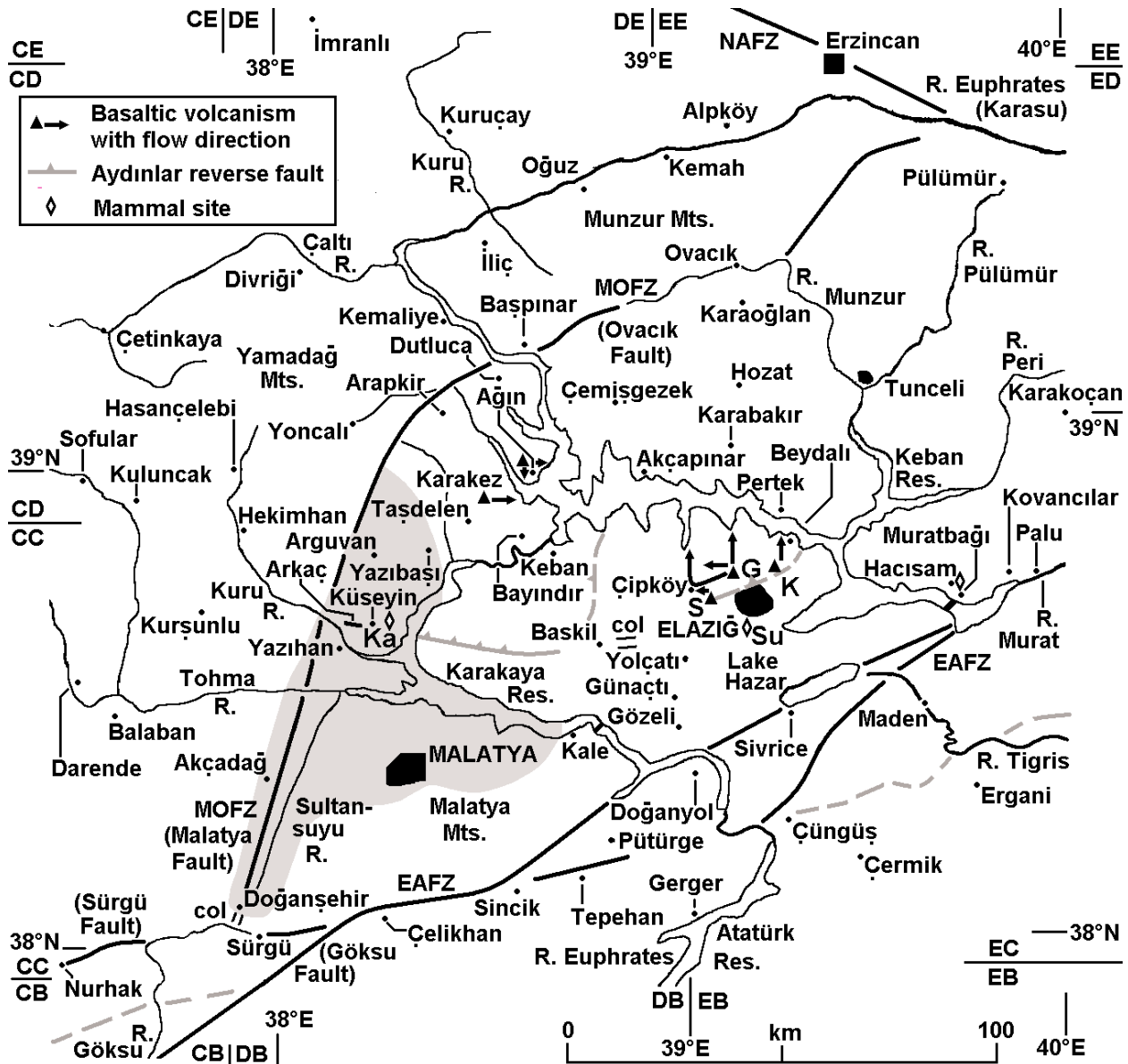
Figure 2. Map of the study region, showing sites of (?) Late Miocene Pliocene basaltic volcanism (triangles; omitted outside the Elazığ region) and mammal sites (diamond symbols) in relation to the Euphrates river system and to major strike-slip fault zones: the NAFZ, MOFZ and EAFZ. Light grey shading illustrates schematically the Malatya Basin. As discussed in the text, its northern limit marks the end of continuous outcrop, and is somewhat arbitary, as the (?) Late Miocene and Pliocene lacustrine deposits in localities farther north and east evidently formed part of the same palaeo-lake. Dashed dark grey line marks the Neotethys suture, as delimited by the northern margin of outcrop of rocks of the Cenozoic carbonate sequence of the Arabian Platform (after Altınlı 1961; Baykal 1961; Tolun 1962). Between points marked, this suture roughly coincides with strands of the EAFZ. Triangles indicate young basaltic necks, with arrows indicating schematic directions of basalt flow from them; G, K and S denote the Gümüşbağlar, Karataş, and Sarıbuçuk necks; Ka and Su denote the Karababa (Mamaar) and Sürsürü mammal sites. For geological maps of this area see Westaway & Arger (2001).

geodesy and geological evidence (e.g., McClusky *et al.* 2000; Westaway 2003, 2004a; Westaway *et al.* 2006b) to involve transform faulting for most of their lengths, which requires no vertical component of crustal motion. This modern geometry of strike-slip faulting is thought to

have superseded a different geometry that existed between ~7–6 and 4 Ma (e.g., Westaway & Arger 2001; Westaway 2006a), which involved left-lateral slip on the MOFZ rather than the EAFZ (Figure 2).

Prior to this latest Miocene development of strike-slip faulting, the region accommodated northward (or northwestward) convergence of the African and Arabian plates relative to Eurasia by active folding and reverse faulting. It is thought that this earlier phase of crustal deformation became active in the Late Eocene, at the start of the continental collision between Africa/Arabia and Eurasia; beforehand, the convergence between Africa and Eurasia was instead accommodated by northward subduction of the southern Neotethys Ocean beneath Anatolia (e.g., Aktaş & Robertson 1984). Rocks associated with this subduction, which began in the Late Cretaceous (~90 Ma), known locally as the 'Elazığ Complex', indeed form much of the bedrock outcrop in the study region. These rocks are unconformably overlain by latest Cretaceous to earliest Cenozoic limestone, thought to mark the Maastrichtian–Paleocene hiatus in relative motion between the African and Eurasian plates. The subsequent resumption of subduction is marked by deposition of the claystone-dominated Kırkgeçit Formation, biostratigraphically dated to the Middle to Late Eocene (e.g., Bingöl 1984), apparently in a back-arc extensional basin overlying the subduction zone. Recent detailed accounts of the magmatism, sedimentation, and structural development associated with these Late Cretaceous and Early Cenozoic events include work by Cronin *et al.* (2000), Rızaoğlu *et al.* (2006), and Robertson *et al.* (2007). This summary was provided to facilitate later discussion, given the stratigraphic and structural relationships of the region's young basalts and lake sediments, and the associated landscape, to older rocks and structures.

Previous studies of the incised Late Cenozoic lacustrine sequences around Elazığ (Figure 3) include Tonbul (1987), Kerey & Türkmen (1991), and Westaway & Arger (2001). Westaway & Arger (2001) also summarised the limited information then accessible regarding the lacustrine Malatya Basin. Kaymakçı *et al.* (2006) have subsequently resolved the structure of this basin in greater detail using seismic reflection profiling. West of this basin, comparable lacustrine deposits of inferred Middle–Late Miocene age are known as the Kuzgun Formation (e.g., Perinçek & Kozlu 1984); they crop out in the flanks of the present Tohma River gorge, upstream and downstream of Darende (Figure 2).

Excluding evidence derived from dating of basalts, age control for these lacustrine successions is available from mammalian biostratigraphy at three significant sites: at Sürsürü (~2.5 km S of Elazığ; Figures 2 & 4), Hacısam (~50 km east of Elazığ; ~20 km west of Palu; Figure 2), and, within the Malatya Basin, Karababa (~80 km west of Elazığ; ~35 km north of Malatya; Figure 2). As is noted below, ages have also been assigned to the lacustrine sediments of the Malatya Basin using pollen, but the ages thus obtained conflict with the mammalian evidence.

Lacustrine Deposits in the Elazığ Region

The stacked lacustrine sequence in the western and central Elazığ region is known as the Karabakır Formation (e.g., Tonbul 1987; Asutay 1988; Figure 3), after a type locality ~17 km NW of Pertek at c. [ED 185 165] (Figure 2); farther east, similar deposits have been called the Palu Formation (Kerey & Türkmen 1991). This sediment was originally thought to be Late Miocene, based on microfossils (Sirel *et al.* 1975; Bingöl 1984). However, at Hacısam and Sürsürü (Figures 2 & 4) evidence from mammalian biostratigraphy now places these lacustrine deposits in the Early and Middle Pliocene, respectively (Ünay & de Bruijn 1998; see below).

As already noted, amounts of Late Cenozoic uplift have increased eastward across the Anatolian Plateau, reflecting the regional topography. However, the disposition of the Karabakır Formation lacustrine deposits indicates that, on a local scale, vertical crustal motions have been more complex (e.g., Westaway & Arger 2001). Indeed, over significant parts of the region, eastward tilting is evident, the opposite effect to the overall westward decrease in altitude of the Anatolian Plateau. For instance, these deposits are found at altitudes of up to ~1480 m ~5 km east of Baskil at c. [DC 897 701] (Figure 4). However, ~12 km farther east around Yolçatı (c. [EC 019 650]), they are found no higher than ~1270 m (Figure 4). In this area these deposits are observed to be tilted gently northeastward (Tonbul 1987). At Elazığ, ~20 km farther NE these deposits reach ~1100 m a.s.l., whereas ~50 km farther east at Hacısam they are found no higher than ~900 m a.s.l. Throughout this area these deposits are quite thin, typically no more than tens of metres thick. In many localities around Elazığ anticlines formed in older rocks protrude above the level of the 'Karabakır' palaeo-lake (Figure 4); this folding has been thought to date from the mid-Cenozoic (i.e., Late Eocene to early Late Miocene) phase of crustal shortening (cf. Yazgan 1984), although some of it may possibly be
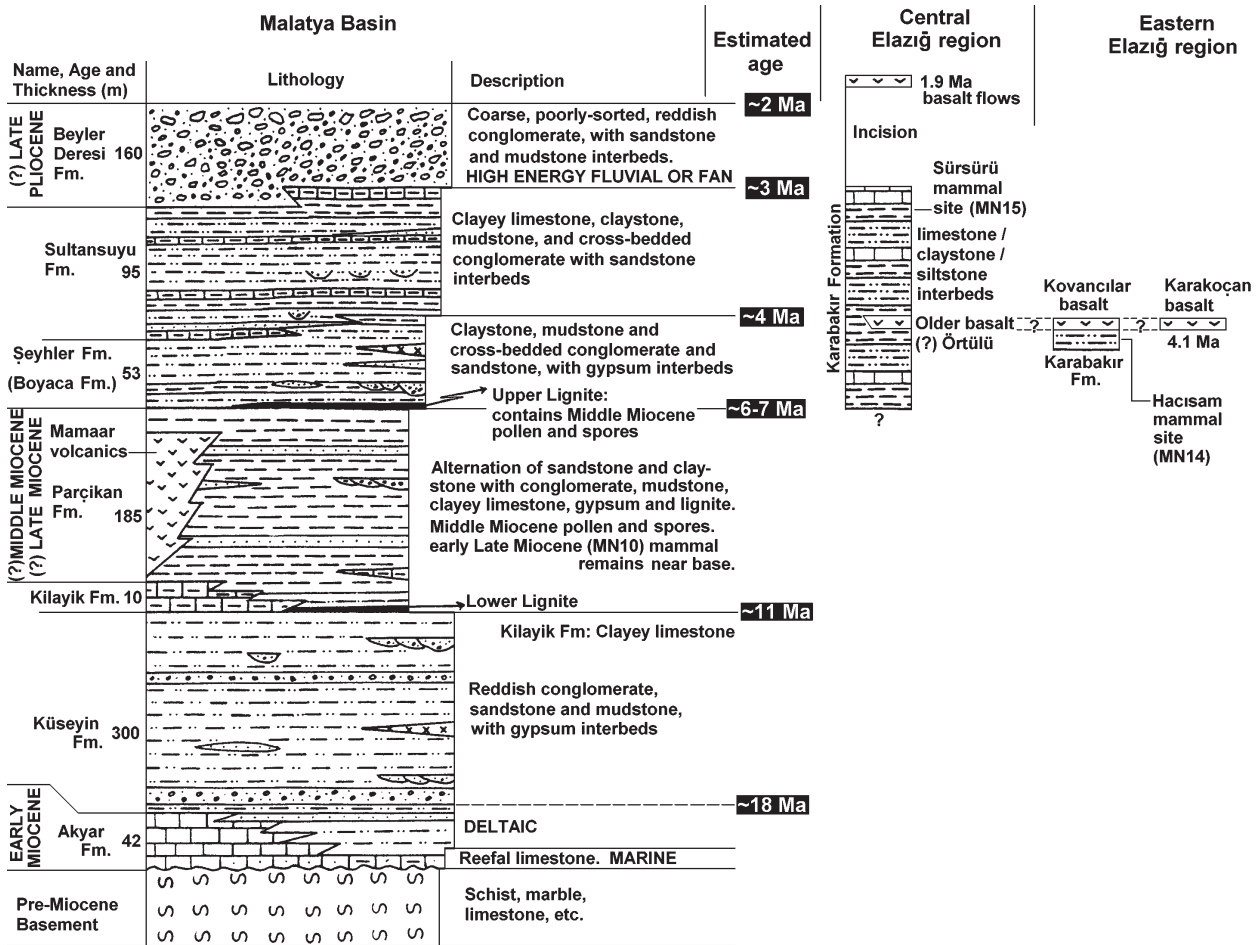
Figure 3. Comparison of Late Cenozoic lacustrine successions and associated volcanism in different parts of the present study region. Left part of Figure indicates schematic stratigraphic column (using standard notation for lithologies) for the stacked sequence of the southern Malatya Basin, based on Figure 2 of Önal (1995) with additional information from Önal (1997), and with suggested ages from the present study. Thicknesses indicated refer to type localities. Right part of the Figure indicates our tentative suggestions for how the successions in the central and eastern parts of the Elazığ region correlate with the Malatya Basin. Note the progressive eastward reduction in the span of time for lacustrine deposition. In the central Malatya Basin, Önal (1997) defined only the Boyaca Formation as overlying the Parçikan Formation, this being evidently a lateral equivalent of the Şeyhler Formation. The top of the Beyler Deresi Formation has been incised by modern rivers, such as the Sultansuyu (Figure 2) and the Beyler Deresi (Figure 6a), to create the modern dissected landscape in the Malatya Basin interior. Fluvial deposits that post-date the start of this incision are not shown. Except where other environments are indicated, the stacked succession is lacustrine or low-energy fluvial, the proportions of both types of input varying laterally and over time, as indicated by the lithologies. The Mamaar volcanics, depicted, in the central Malatya Basin are equivalent, according to Kaymakcı *et al.* (2006), to the Yamadağ volcanics farther north (Figure 2). The latter volcanism is Middle Miocene, given K-Ar dates of 18.7±0.5, 16.8±0.5 and 14.1±0.4 Ma (Leo *et al.* 1974), and of 15.9±0.4 and 15.2±0.5 Ma (Arger *et al.* 2000). As noted in the main text, this K-Ar interpretation and the pollen evidence (Önal 1995, 1997) for a Middle Miocene age for the Parçikan Formation is contradicted by mammalian biostratigraphic evidence from Kaymakcı *et al.* (2006), which requires the lower part of this deposit to be no older than the early Late Miocene. Kaymakcı *et al.* (2006) suggested using the name Sultansuyu Formation for terrace deposits of the Sultansuyu, Tohma and Kuru rivers that are inset into the stacked sequence of the Malatya Basin. However, this would be confusing, as the same name is already in use for older deposits in the region, as illustrated. Regarding the chronology, Önal (1995, 1997) proposed that the whole sequence above the Küseyin Formation is Middle Miocene, but provided no age-control above the Upper Lignite, which could be latest Middle Miocene. Kaymakcı *et al.* (2006) suggested that the low-energy sediments above the stratigraphic level of the Mamaar/Yamadağ volcanics, including the Upper Lignite, are Late Miocene, and the overlying coarse fluvial clastics are Early to Middle Pliocene, the latter age assignment based on a correlation with the lacustrine deposits at Sürsürü near Elazığ (see text, this Figure, and Figure 4). However, such a correlation seems most unlikely, as the lithologies in the two localities are very different. We tentatively infer that the deposits of the Beyler Deresi Formation are Late Pliocene, having aggraded after the Mid-Pliocene climatic optimum but before the regionl increase in uplift rates at ~2 Ma (see text).
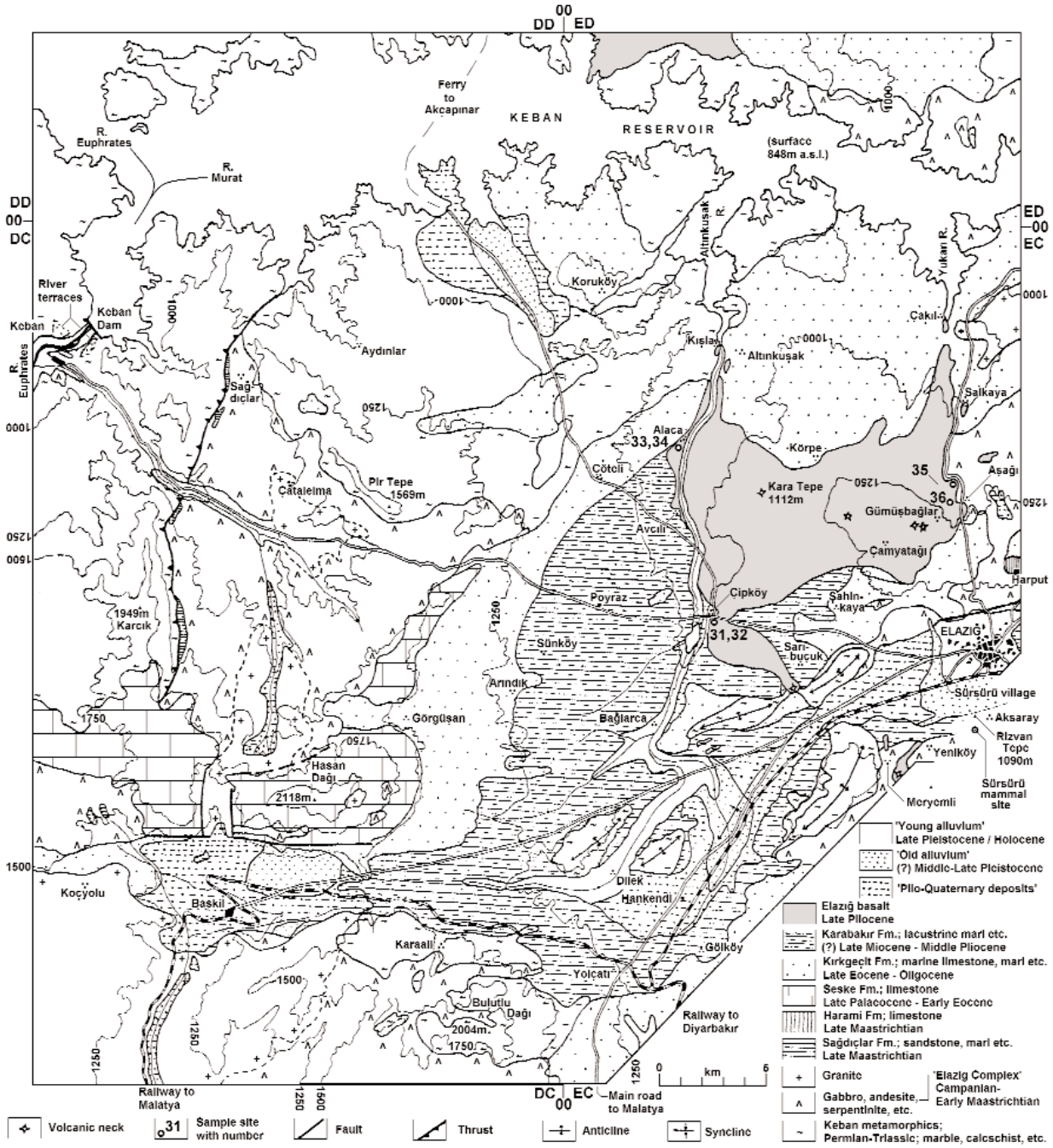
Figure 4. Geological map of the central part of the Elazığ region, after Tonbul (1987), with additional information from Bingöl (1984). The Sürsürü mammal site is in the position shown, c. [EC 189 774], adjoining the minor road between the villages of Aksaray and Yeniköy (~1 km SW of the former; ~2 km NE of the latter). This site was evidently named after the village of Sürsürü, although this is ~2.5 km away and thus has no particular connection with it.

younger and may indeed be associated with the observed gentle tilting of the Pliocene lacustrine deposits (see below).

As previously noted (Westaway & Arger 2001; Demir *et al.* 2004), at present the limit of this lacustrine sediment at Baskil coincides with a col (the Belhan Pass)

503

between the Altınkuşak river, which flows into the Murat near Elazığ, and a local south-flowing Euphrates tributary that joins this river near Kale near the SE margin of the Malatya Basin (Figures 2 & 4). Demir *et al.* (2004) suggested that this Belhan Pass marked the former drainage outlet from the Elazığ region into the Malatya Basin, at which the level of the 'Karabakır' palaeo-lake was regulated. They inferred that as a result of some combination of processes (the northward component of subsequent tilting? river capture?) this drainage was diverted to the modern course of the Murat farther north. Conversely, although the col between the Elazığ region and local drainage into the Malatya Basin south of Yolçatı at Günaçtı (c. [EC 017 588]) is much lower (~1280 m), there is no geomorphological evidence that it ever formed a drainage outlet from the Elazığ region.

The Sürsürü mammal site (Figure 4) is at ~1080 m a.s.l., ~10 m below the 1090 m a.s.l. summit flat of Rızvan Tepe ~500 m farther north. The mapping by Bingöl (1984) and Tonbul (1987) indicates that this ~1090 m a.s.l. level locally marks the top of the stacked sequence of the Karabakır Formation (Figure 4). Ünay & de Bruijn (1998) described the Karabakır Formation at this site as consisting of a fossil bed of brown claystone with abundant molluscs, interbedded within a sequence of grey limestone and green siltstone. Their rodent finds included *Mimomys occitanus*, *Occitanomys brailloni*, *Apodemus dominans*, *Mesocricetus* aff. *primitivus*, and other specimens not identified to species level. In their view, the most significant age-diagnostic taxon was *M. occitanus*, indicative of the Late Ruscinian (biozone MN15) mammal stage, with a numerical age in the range 4.2–3.2 Ma (cf. Agusti *et al.* 2001).

The Hacısam mammal site is at c. [EC 627 809], ~900 m a.s.l., in a cutting along the minor road linking Hacısam village to the Elazığ-Bingöl highway at Muratbağı (Figure 2) (~0.75 km SSE of the former village; ~3 km NNW of the latter), near where the River Murat leaves the north side of the EAFZ linear valley (Figure 2) via a narrow gorge. This area is now flooded to ~850 m a.s.l. by the Keban hydroelectric reservoir. The thin 'veneer' of Karabakır Formation deposits that blankets much of the landscape in this area, unconformably overlying the Kırkgeçit Formation, was missed by Altınlı (1961) and Bingöl (1984), but was later noted by Herece *et al.* (1992). At the Hacısam site these deposits reportedly consist of mollusc-bearing massive

lacustrine mudstone. Ünay & de Bruijn (1998) noted rodent finds including *Mimomys moldavicus*, *Apodemus* cf. *dominans*, and other specimens not identified to species level. In their view, the most significant age-diagnostic taxon was *M. moldavicus*, indicative of the Early Ruscinian (late biozone MN14) mammal stage. According to Agusti *et al.* (2001), biozone MN14 spanned 4.9–4.2 Ma. Since the Hacısam site has been placed late within this biozone, its probable age is close to 4.2 Ma.

The Elazığ Region; Basalts

Associated with the Karabakır Formation lacustrine deposits are widespread basalts (Figures 3 & 4), dating of which can constrain the ages of the sediments. Most of these basalts (e.g., those illustrated in Figures 2 and 4) have flowed over the surface of these lacustrine deposits or along river valleys incised into them. The individual flow units, in localities south of the Murat or west of the Euphrates, will be briefly described. Available geological maps (e.g., Altınlı 1961; Bingöl 1984; Asutay 1988) indicate that stratigraphically equivalent basalts also crop out north of the Murat, including the designated type locality of the Karabakır Formation, noted above, but have not yet been investigated by us.

The basalt at Çipköy, ~13 km west of Elazığ (Figure 4), was studied by Arger *et al.* (2000) using whole-rock K-Ar dating. They identified a lower rather altered flow, with a date of 1.47±0.18 Ma (±2σ), and an upper, fresher-looking flow with a date of 1.87±0.14 Ma (±2σ), which they considered more likely to be correct. They also suggested that Sanver's (1968) normal magnetic polarity in the basalt near Gümüşbağlar (~7 km N of Elazığ; Figure 4) probably denotes the Olduvai subchron, likewise indicating an age of ~1.9 Ma. East of Gümüşbağlar, more basalt with a similar disposition in the landscape is evident (e.g., Bingöl 1984; Figure 2); it flows northward from a neck at Karataş into the Murat valley around Beydalı. A similar disposition is evident around Ağın, where basalt from the Kara Dağ neck flowed eastward towards the Euphrates and southward towards the tributary valley of the Arapkir River (e.g., Asutay 1988; Figure 2). Other basalt flows in this region are illustrated in Figure 4 and discussed below.

In the easternmost part of the Elazığ region is the extensive young basaltic volcanism Sanver (1968) obtained a whole-rock K-Ar date of 4.10±0.64 Ma (±2σ) for basalt from ~10 km SE of Karakoçan (Figure 2),

around [ED 985 065], and showed it to be reverse-magnetised, indicating eruption during the Gilbert chron. However, this site is well east of localities where the Karabakır Formation lacustrine deposits have been identified. Some 25 km farther SW, ~55 km east of Elazığ, we have observed localised basalt capping hilltops in the vicinity of the easternmost part of the 'Karabakır' palaeo-lake, ~1 km SW of Kovancılar (c. [EC 735 845]; Figure 3).

The Gümüşbağlar basalt, already noted, crops out over a ~100 km^2 area centred ~10 km NW of Elazığ (Figure 4). As mapped by Tonbul (1987) it erupted from an E–W chain of necks in the modern interfluve between the Yukarı and Altınkuşak rivers, northward-flowing left-bank tributaries of the Murat. The main neck, in the east, reaches ~1430 m a.s.l. at c. [EC 154 866], between Gümüşbağlar and Çamyatağı (Figure 5a); Kara Tepe, ~7 km farther west at [EC 089 880], reaches no higher than 1112 m a.s.l. Basalt that probably originated from the main, eastern, neck flowed northward into the Yukarı valley (Figure 5b), then downstream past Salkaya to the ~850 m a.s.l. level of the Keban reservoir at Çakıl. Other basalt flowed initially westward into the Altınkuşak valley, then downstream past Alaca (Figure 5c) to the level of this reservoir at Kışla. Inspection of the map by Altınlı (1961), which pre-dates the Keban dam, indicates that both these basalt flows died out where they now adjoin the reservoir; no significant former basalt outcrop is now submerged. The reservoir is locally ~100 m deep; thus, no more than ~100 m of fluvial incision has occurred locally since these basalt eruptions.

We designate as the Sarıbuçuk basalt the flow unit that originates from a neck near the village of this name, at ~1180 m a.s.l. at c. [EC 104 791], and flows NW for ~5 km, dying out at ~1000 m a.s.l. in the eastern flank of the Altınkuşak river valley near Çipköy, c. [EC 063 819]. As illustrated in Figure 4, the distal end of this flow unit adjoins the SW limit of the Gümüşbağlar basalt. Although field relationships are unclear due to the limited exposure, we suspect that the upper flow unit exposed in the Çipköy highway cutting (cf. Arger *et al.* 2000) is the distal part of this Sarıbuçuk basalt, whereas the lower flow unit exposed in this cutting may instead be a distal part of the Gümüşbağlar basalt.

Two other small flow units are evident near Meryemli, ~6 km SW of Elazığ (Figure 4). The larger flow

originated at ~1250 m a.s.l. at c. [EC 155 750] and persisted NE for ~2 km to c. [EC 169 762], dying out at ~1150 m a.s.l. near Yeniköy. The smaller more westerly flow extends northward for ~600 m from c. [EC 151 758] at ~1200 m a.s.l. to c. [EC 151 764] at ~1150 m a.s.l., its distal end overlying the Karabakır Formation. Other basalt (also undated; not illustrated in Figure 4) is also evident in a quarry section (c. [EC 18950 77850) in the vicinity of (but stratigraphically below) the Sürsürü mammal site, overlain by the upper part of the lacustrine succession (Figure 3). The age of this older volcanism may be very tentatively estimated as ~4 Ma, making it possibly contemporaneous with the Karakoçan/Kovancılar basalt mentioned above.

Finally, farther west (Figure 2), there is the Örtülü basalt of Arger *et al.* (2000). This appears to have erupted from a neck in the vicinity of Karakez Dağ, which reaches 1523 m a.s.l. c. [DD 614 056]; it is preserved mainly eastward and southeastward of this point for distances of up to ~10 km. As mapped by Asutay (1988), this basalt reaches ~1475 m a.s.l. at Karakez, indicating that it is locally overlain by ~50 m of lacustine limestone, assigned to the Karabakır Formation; like the Sürsürü basalt it thus pre-dates the end of stacked deposition. The same mapping also indicates that this basalt is underlain by the marine Alibonca Formation, although earlier mapping by Baykal (1961) depicts the basalt as capping sediments considered as lateral equivalents of what is now known as the Karabakır Formation (i.e., lacustrine sediments). This basalt crops out for >5 km along the road from Keban to Arapkir at altitudes between ~1250 c. [DD 654 029] and ~1350 m a.s.l. c. [DD 620 073]. Its eastern distal part has been exposed by young incision in the flanks of the Kuru river valley (which flows eastward into the Arapkir river and thus into the Euphrates) around Yedibağ. According to the mapping by Asutay (1988), its base descends to ~1050 m a.s.l in the northern flank of this valley at c. [DD 698 059] and to ~1100 m a.s.l. in its southern flank at c. [DD 684 028].

The Malatya Basin

Lacustrine sediments of the Malatya Basin (Figure 3) can be traced for ~100 km in the NNE–SSW direction, parallel to the Malatya Fault (Figure 2). Lacustrine
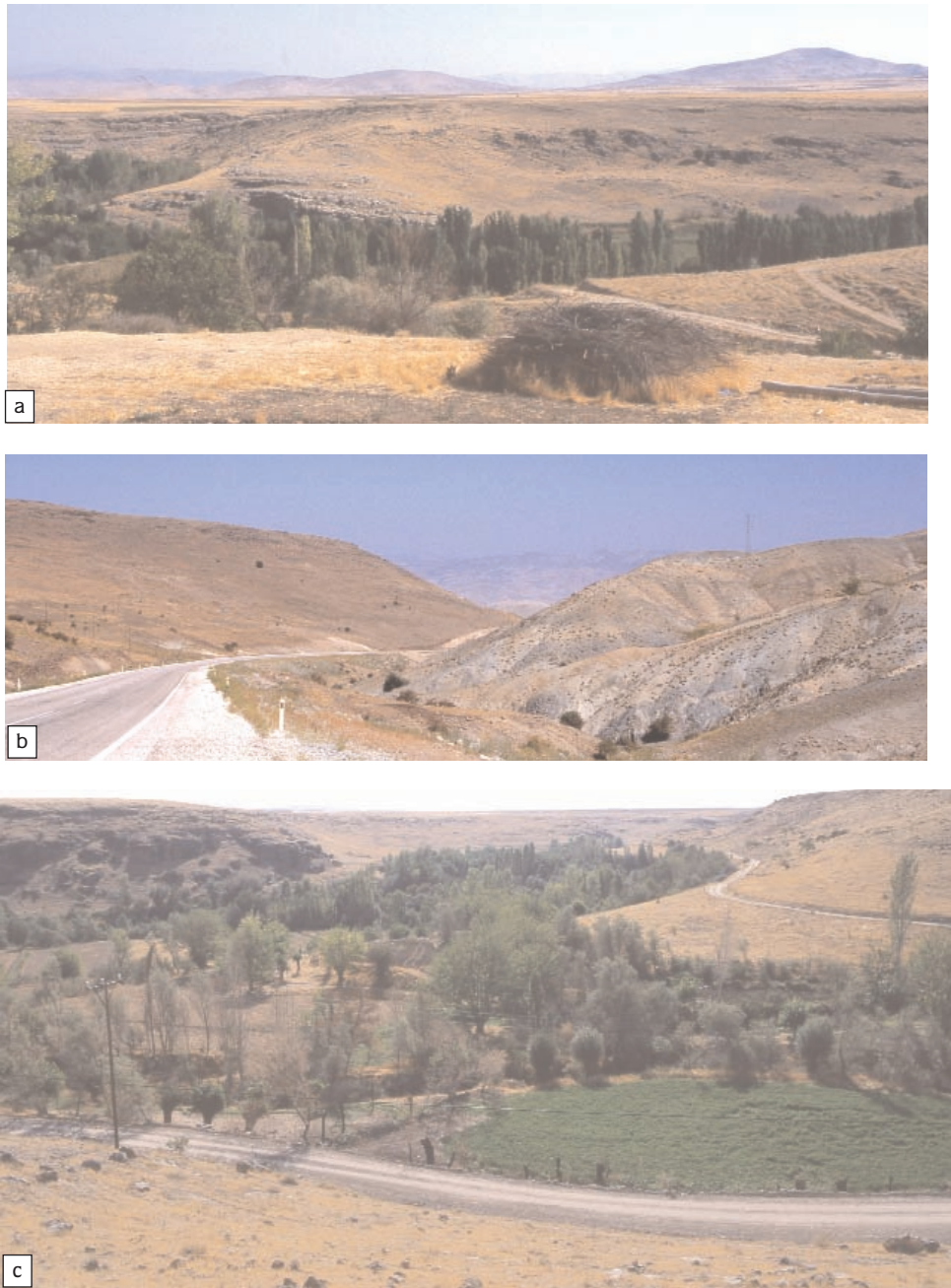
Figure 5. Elazığ region field photos. **(a)** View ENE from Avcılı, at [EC 05782 86780], looking across the Altınkuşak river gorge towards Körpe. In the left foreground, the gorge exposes an inlier of gently tilted limestone of the Kırkgeçit Formation. To the right, sandy deposits of the Karabakır Formation are banked against this inlier, although this is not clear in this view. These sediments are capped by the Gümüşbağlar basalt, flows of which are warped across the Kırkgeçit Formation inlier, indicating channelization by contemporaneous palaeo-relief. In the right background is the main neck, near Gümüşbağlar village, from which much of this basalt erupted (the Kara Tepe neck is almost directly in front of this and is thus diffict to identify). In the left background are small cuestas of Kırkgeçit Formation limestone, in the area around Körpe, rising to ~1300 m a.s.l., which prevented the flow of basalt in that direction. **(b)** View north looking down the Yukarı river gorge from [EC 17520 89390], a point ~2 km N of Aşağı and ~2.5 km S of Salkaya. The west flank of this gorge is capped by the main part of the flow unit of Gümüşbağlar basalt. A small outlier of the same basalt is present in its east flank, next to the electricity pylon. After basalt eruption this river has cut down into the underlying rocks of the Late Cretaceous subduction-related complex by ~50 m, keeping mostly (except for this outlier) beyond the eastern margin of the basalt. **(c)** View SE from Alaca at [EC 05249 89380], adjacent to the point where samples 02TR33 and 34 were collected, looking up the narrow Altınkuşak river gorge that is flanked by Gümüşbağlar basalt.

deposition seems to have begun in this area immediately after the region uplifted above sea-level, as the succession overlies Lower Miocene marine deposits (Figure 3). Önal (1995, 1997) designated the succession as consisting of four mainly lacustrine formations, known as the Küseyin, Parçikan, Boyaca (or Şeyhler), and Sultansuyu formations, in order of decreasing age. The latter deposit is overlain by the Beyler Deresi Formation, comprising fluvial conglomerate, forming the uppermost part of the stacked succession (Fig. 6a). As noted by Önal (1995, 1997), the typical extent of erosion of this succession increases northward. Thus, the Beyler Deresi Formation is only found in the southern part of the basin; farther north, erosion has typically removed progressively more of the succession so that only its basal part remains (Figure 6b).

The northern Malatya Basin adjoins the Örtülü area, the upper surface of the Karabakır Formation is at its highest, ~1500 m a.s.l., around Karakez, and – as noted by Asutay (1988) – slopes SE from this point to no higher than ~1280 m ~14 km farther SE near Bayındır, c. [DC 718 964], just north of the modern Euphrates gorge downstream of Keban (Figure 2). This gorge is ~600 m deep, cut mostly into the metamorphic basement (formed by the Palaeozoic / Mesozoic Keban Group), incising to a modern river level of ~690 m a.s.l. The Asutay (1988) mapping indicates that the Karabakır Formation lacustrine limestone is ~30 m thick around Bayındır. It has not been reported farther south, suggesting that the Bayındır area lay near the southern margin of the Karabakır palaeo-lake. This implies that – once fluvial incision began – the southward tilt of the landscape caused the Euphrates gorge to rapidly become 'locked' in the southern part of this former depocentre where the uplift rate was least. The amount of fluvial incision here is, nonetheless, much more than near Elazığ, where the top of the Karabakır Formation is ~1100 m a.s.l. (Figure 4) and the local level of the River Murat is ~750 m a.s.l., indicating ~350 m of post-Karabakır incision.

Farther SW, at a point ~5 km E of Yazıbaşı, ~10 km SSW of Taşdelen, and ~2 km N of the upstream end of the Karakaya reservoir on the Euphrates (at [DC 54319 92004]), the road from Malatya to Keban crosses the Söğütluçay river. This is a substantial right-bank tributary of the Euphrates, ~30 km long, which flows southward from the vicinity of Arapkir (Fig. 2). Along it, the land surface forms a succession of terrace flats, capped by

fluvial gravel, a notable example being around [DC 54387 92214], estimated at ~40 m above present river level (~730 m against ~690 m a.s.l.). These fluvial deposits are inset into sand, mapped by Asutay (1988) as the part of Lower Miocene marine Alibonca Formation. No lacustrine deposits assigned to either the Karabakır Formation or the Malatya Basin lacustrine succession are present in this area. However, it is evident that the land surface has locally been dissected by fluvial incision to a level well below that of the Karabakır Formation. Farther upstream, for instance c. [DD 530 010], the Söğütluçay river has cut its own ~350 m deep gorge (from ~1300 m to ~950 m a.s.l.) into the Keban metamorphics, similar to the main Euphrates gorge near Bayındır.

According to the mapping by Baykal (1961), the lacustrine succession (with interbedded lava flows) of the Malatya Basin is first encountered ~3.5 km west of the Söğütluçay valley, where the basal part of these deposits crops out above the marine succession at ~900 m a.s.l., c. [DC 501 908]. These deposits are found at progressively higher levels to the north and west, for instance reaching ~1300 m a.s.l. c. [DD 420 015]. The similarity in altitude range suggests that, before incision by the Söğütluçay river, this lacustrine succession passed continuously laterally into its Karabakır Formation counterpart ~15 km farther northeast in the Karakez/Bayındır area (Figure 2).

The only mammalian biostratigraphic control for the Malatya Basin succession is from Kaymakcı *et al.* (2006), who mentioned (without giving details) evidence of the ancestral mouse *Progonomys* sp. at their site 35, at [DC 41583 77639], near Karababa (formerly called Mamaar or Mamahar), adjoining the locality depicted in Figure 6c. Based on their co-ordinates and the mapping of the area by Önal (1997), we infer this site to be located near the base of the Parçikan Formation (Figure 3). According to Agusti *et al.* (2001), the first appearance of *Progonomys cathalai* is in mammal zone MN10, which spans 9.7–8.7 Ma. On this basis, this sediment can be no older than early Late Miocene, making it younger than the Middle Miocene age determined for the Parçikan Formation by Önal (1995, 1997) using pollen. The Mamaar volcanics crop out nearby, also around Karababa, for instance at [DC 42134 77155], where they interbed with sediments of the Parçikan Formation. These lavas have been described as typically andesitic (Önal 1997), thus similar to the Yamadağ volcanism farther north (Figure 2), with which

507
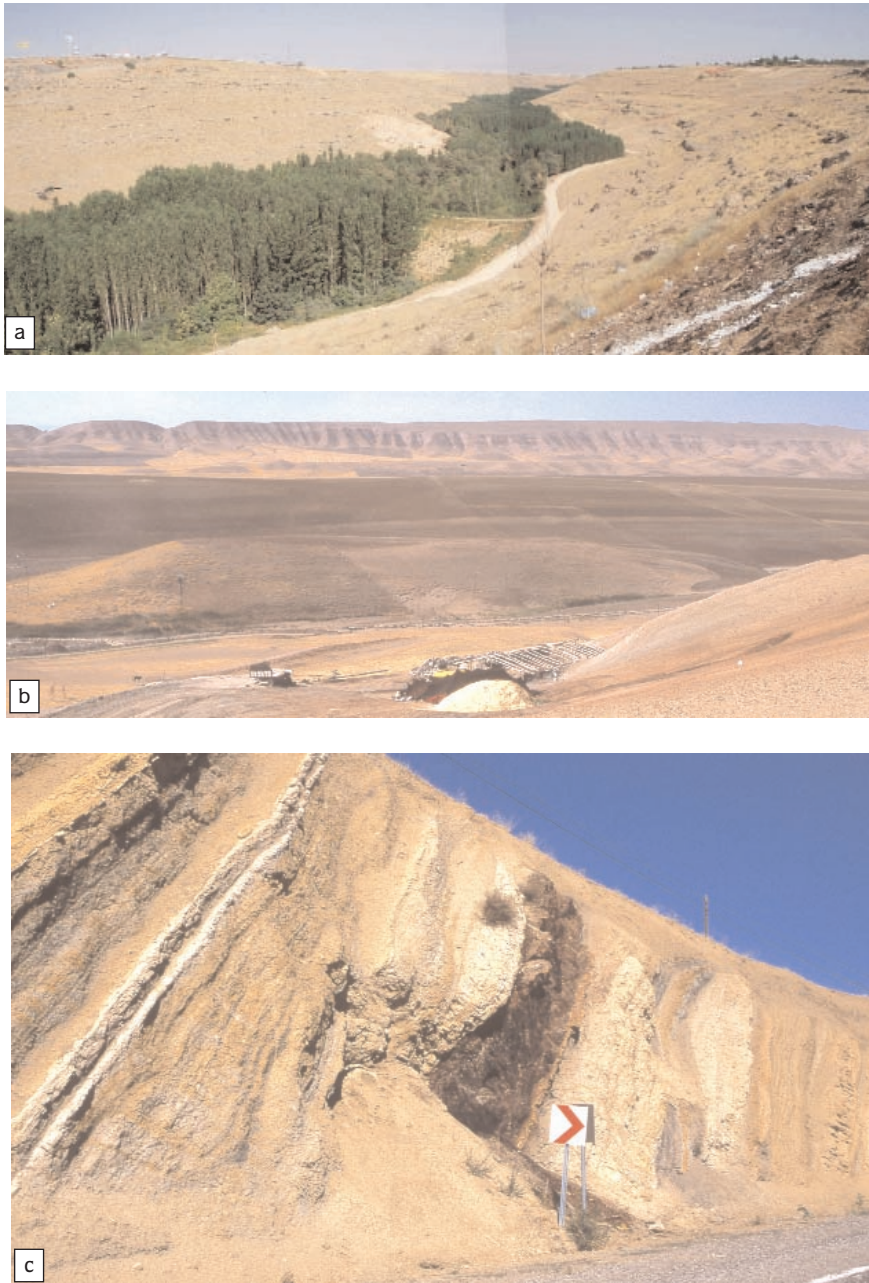
Figure 6. Malatya Basin field photos. **(a)** View northward, looking down the Beyler Deresi valley from [DC 31090 43362], ~5 km west of Malatya. The view illustrates coarse, poorly-sorted but well-stratified fluvial conglomerate of the Beyler Deresi Formation, which has been incised by ~70 m (locally, from ~900 m to ~830 m a.s.l.) to create the modern dissected fluvial landscape. Note the flat upper surface of the conglomerate, the top of the stacked sequence in the Malatya Basin, in the interfluves on both sides of the young river gorge. **(b)** View WSW from the E–W-trending ridge ~400 m N of Küseyin village, in deposits of the Küseyin Formation at [DC 36196 77724] looking across the Malatya Basin interior to the W–E-trending Arkaç Dağı ridge. The part of the Arkaç Dağı ridge illustrated is between ~3 km (to the left) and ~5 km away (to the right). The eroded top of the stacked succession of the Malatya Basin, the lacustrine Parçikan Formation, overlain by the lacustrine/fluvial Boyaca Formation in the Önal (1995, 1997) stratigraphic scheme, is overlain by up to a few tens of metres thickness, and no more than ~100 m of width, of sand and gravel, presumably deposited by the ancestral Kuru River at an early stage of its history of fluvial incision. This cap of relatively erosion-resistant material has locally preserved the underlying lake sediment, creating the observed topography. In the foreground (behind the farmer's shack) is a tell. **(c)** View of the west face of the cutting on highway 875 (Malatya–Keban) at [DC 37666 76675] in the central Malatya Basin, showing the lacustrine sequence (clay, silt, lignite, etc.) of the Parçikan Formation, mentioned in the text, tilted steeply to the south, apparently as a result of slip at depth on the underlying Aydınlar Thrust (see main text). The stratigraphic section illustrated is ~10 m thick.

they have been tentatively correlated (Kaymakcı *et al.* 2006). However, there has been no detailed work (e.g., involving dating or geochemical analyis), to substantiate such a correlation, and other mapping (e.g., that by Baykal 1961) depicts the Mamaar and Yamadağ lava flows as distinct phases of volcanism. K-Ar dating places the Yamadağ volcanism in the Middle Miocene (19–15 Ma; Leo *et al.* 1974; Arger *et al.* 2000), consistent with the dating of the Parçikan Formation by Önal (1995, 1997) (Figure 3) but inconsistent with the mammalian age from Kaymakcı *et al.* (2006). At this stage we merely note these difficulties over the chronology of the lacustrine succession of the Malatya Basin, resolution of these difficulties being beyond the scope of this study. From the available evidence, we consider it probable that lacustrine deposition in the Malatya Basin continued through the Middle and Late Miocene and Pliocene.

No biostratigraphic control thus exists for the upper part of the Malatya Basin succession. Deposition of the Beyler Deresi Formation (Figures 3 & 6a) evidently required an environment conducive to rapid erosion (in adjoining upland areas, such as the Malatya Mountains; Figure 2) and sediment transport. Pervasive vegetation cover will prevent such high rates of erosion and sediment transport. By analogy with adjoining regions (e.g., western Turkey and Bulgaria; Westaway *et al.* 2006c; Westaway 2006a), it is expected that such vegetation cover was present until, at the earliest, the end of the Mid-Pliocene climatic optimum. We thus consider it unlikely that an environment consistent with deposition of the Beyler Deresi Formation could have existed during or before this time. We thus infer that this sediment probably post-dates this time, suggesting an age for it in the range ~3–2 Ma; it is evidently younger than the upper part of the stacked lacustrine sequence at Elazığ, given that no analogous cap of coarse sediment is present in this area (see above). A similar succession, involving prolonged lacustrine deposition, then stacked deposition of coarse fluvial clastics, then fluvial incision, is evident elsewhere in eastern Turkey, such as around Diyarbakır in the northern Arabian Platform (e.g., Tolun 1951; Westaway *et al.* 2008; Figure 1), and may reflect the same chronology.

At the extreme SSW end of the Malatya Basin around Doğanşehir (c. [DC 015 170]), the upper part of its lacustrine sequence forms extensive flats at ~1280 m a.s.l., dissected by the upper reaches of the Sultansuyu River, for instance around [DC 040 217] and [DC 050 240]. These deposits persist as far south as the col, also at ~1280 m a.s.l. (at [DC 005 130]), which separates the Sultansuyu catchment from the Göksu catchment farther south (Figure 2). This evidence suggests that this col, rather than the modern Euphrates gorge (Figure 2), formed the drainage outlet of the Malatya Basin while a lake existed within it.

The modern Euphrates gorge leaves the Malatya Basin at Kale (Figure 2). Locally, it reaches a depth of ~800 m, for instance in the vicinity of the Karakaya Dam west of Çüngüş, c. [EC 118 311], where this gorge has become incised from ~1350 to ~550 m a.s.l.. As has been noted previously (e.g., Westaway & Arger 2001; Demir *et al.* 2004) this gorge is offset left-laterally across the EAFZ by much less distance than the total slip on this fault zone. At the SW end of the EAFZ (SW of Çelikhan; Figure 2) it is observed to have accommodated ~37 km of TR-AR relative motion: ~4 km across the Sürgü Fault; and ~33 km across the Göksu Fault and its southwestward continuations (Westaway *et al.* 2006b). In contrast, the main EAFZ strand offsets the Euphrates gorge at Doğanyol by 13 km, whereas farther south at Çüngüş the subsidiary en échelon Çüngüş Fault offsets this gorge by ~5 km (Figure 2). Recent kinematic models, from both geological and geodetic evidence, predict ~9–10 mm a^{-1} of slip on the EAFZ (e.g., McClusky *et al.* 2000; Westaway 2004a; Westaway *et al.* 2006b), making its age ~4 Ma (3.73±0.05 Ma was estimated by Westaway *et al.* 2006b). The ~18 km of EAFZ slip since the modern Euphrates gorge became established suggests that this gorge developed around 2 Ma. Capture of the Malatya Basin by this gorge would have caused rapid emptying of its lake and initiated the dissection of the underlying lacustrine sequence. However, the current lack of age-control evidence from the Malatya Basin itself prevents any direct confirmation of this inferred timing of the disruption of this lake basin.

Basalt Sampling and Analysis

Fieldwork

Basalt samples for geochemical analysis and Ar-Ar dating were collected from four localities around Elazığ, from Örtülü, Çipköy, Alaca and Gümüşbağlar.

Sample 02TR22 was collected from the Örtülü basalt at [DD 63688 05078], ~1200 m a.s.l., just below the contact with the overlying lacustrine limestone. Two basalt flows are locally visible in the landscape: a lower

flow that is vesicular and highly weathered, and an upper more massive flow that appears much less weathered. The sample was collected from a fresh section exposed in a ~3 m deep trench cut into this upper flow.

Sample 02TR31 was collected from the upper flow in the cutting on the Elazığ-Keban road at Çipköy, at [EC 06704 82031]. This flow consists of ~3 m of greyish basalt that appears only slightly altered. Sample 02TR32 was collected ~30 m farther west, where the cutting has descended to the level of the lower flow, at [EC 06669 82033]. This lower flow, of which up to ~1.5 m thickness is exposed, appears darker and more altered, and has a vesicular top, many vesicles having been infilled by calcite or silty material.

Samples 02TR33 and 02TR34 were collected farther down the Altınkuşak valley at Alaca, at [EC 05249 89380] (Figure 5b). The Gümüşbağlar basalt exposed here is ~10 m thick, its top ~950 m a.s.l.; it locally overlies the Kırkgeçit Formation. Since the eruption, the river has locally incised to ~880 m a.s.l., creating a ~70 m deep and ~200 m wide gorge (Figure 5b). Sample 02TR33 came from ~2 m below the top of the section, where the basalt is massive and shows no significant alteration. Sample 02TR34 came from the base of the exposed section, in what appears to be the same flow unit, but highly altered.

Sample 02TR35 was collected ~1200 m a.s.l. at [EC 18088 88361] from basalt exposed in a cutting on the west side of the road linking Elazığ to the ferry across Keban Reservoir to Pertek, ~1 km N of the Aşağı district of Gümüşbağlar village. This basalt, which presumably originated from the main Gümüşbağlar neck ~3 km to the SW, has backfilled a former river channel cut into rocks of the Elazığ Complex. We sampled the lowest flow exposed, in direct contact with the bedrock. The headwaters of the present Yukarı River have subsequently incised a new course ~300 m farther west, reaching a level ~50 m lower. Sample 02TR36 was collected ~1 km farther south, at [EC 17738 87300], also ~1200 m a.s.l., from what may be the same flow unit. This site is near the northern end of a flat land surface capped by basalt, on which Gümüşbağlar village has been built. A short distance farther north the basalt appears to cascade down a bluff into the Yukarı river valley. This flow unit is locally ~15 m thick, as indicated by the extent of fluvial incison; its upper part was sampled.

Analysis Procedures

Preparation for Ar-Ar dating involved initial screening by inspection of hand specimens and petrographic thin sections. Samples were then crushed, washed in deionized water and dilute hydrochloric acid, sieved to a 60–80 μm size fraction, and phenocrysts and xenocrysts were removed by magnetic separation and hand picking. This choice of grain size was determined by the desirability of excluding phenocryst material from the samples, given the tendency for excess, or 'inherited', argon to reside in phenocrysts (e.g., Lanphere & Dalrymple 1976; Kaneoka et al. 1983; Laughlin et al. 1994; Singer et al. 2004). On the other hand, sieving to too small a grain size would increase the logistical difficulties of picking out any phenocryst or xenocryst material, and would also increase the risk of obtaining incorrect ages due to effects of ^{39}Ar recoil during sample irradiation.

The basis of conventional K-Ar dating is the measurement of decay of ^{40}K into ^{40}Ar; however, this requires independent measurements of concentrations of potassium and of argon isotopes in each sample. In the Ar-Ar variant of the technique, irradiation in a nuclear reactor converts ^{39}K into ^{39}Ar. The resulting ^{39}Ar, a proxy for the potassium content in the sample, can then be measured at the same time as the other argon isotopes.

Irradiation of our multi-grain samples utilized the Cadmium-Lined, In-Core Irradiation Tube (CLICIT) facility within the Oregon State University TRIGA reactor in Corvallis, Oregon. Argon isotopes were subsequently measured in the microcrystalline groundmass at the Laboratory for Noble Gas Geochronology, Massachusetts Institute of Technology, and analyzed using procedures essentially the same as those described by Singer & Pringle (1996) and Harford et al. (2002). Argon release from each sample occurred in ten heating steps, as indicated in Figure 7. Four methods of age-determination are thus available for each sample (Tables 1 & 2). First, is the 'total fusion' age, using the total amounts released of ^{39}Ar and ^{40}Ar. Second is the 'weighted plateau' age, which uses only data from the heating steps that form a concordant age plateau (Figure 7). Finally, one may use the argon isotopes from the different step-heating splits to generate isochron plots for each sample. This can be done either as a 'normal' isochron, by plotting ^{40}Ar/^{36}Ar against ^{39}Ar/^{36}Ar, or as an 'inverse' isochron, by plotting ^{36}Ar/^{40}Ar against ^{39}Ar/^{40}Ar. Full documentation of this

(a)

(b)

(c)
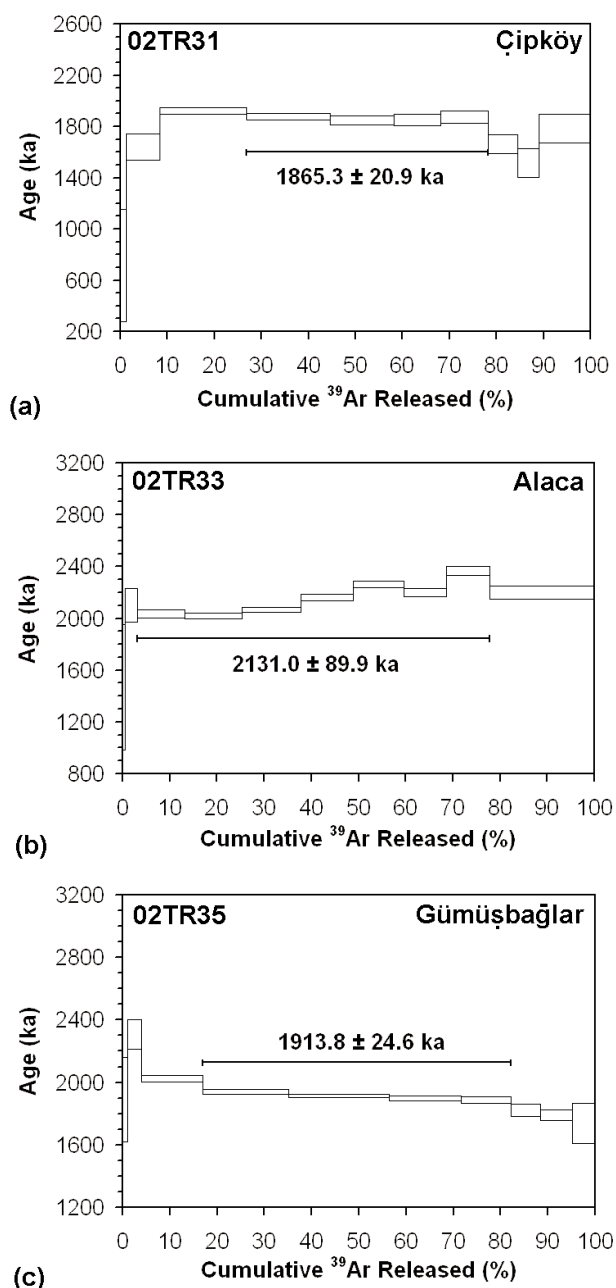
Figure 7. Graphs showing apparent Ar-Ar ages and their uncertainties for each heating step of each sample. The age range for each heating step spans a ±2σ margin of uncertainty. Horizontal bars indicate the splits that contribute to each of the "weighted plateau" age determinations in Tables 1 and 2.

procedure, including analyses of calibration blanks, temperatures of heating steps, concentrations of argon isotopes, and related graphs, are provided in the Appendix. Results are summarised in Tables 1 and 2 and Figures 7 and 8.

To facilitate geochemical classification, whole-rock samples were analysed using an automated ARL 8420 X-ray fluorescence spectrometer at the School of Earth Sciences and Geography, Keele University. Major oxide analyses used fused glass beads with a 1:5 ratio of sample powder and lithium metaborate flux; trace element analyses used pressed powder pellets. For analytic details see Floyd & Castillo (1992); for details of calibration see Yurtmen *et al.* (2002). Table 3 lists the results of this analysis.

On the basis of inspection of the samples in thin section, we anticipated that the principal constituent of the groundmass, and thus the mineral phase yielding the Ar-Ar dates, would be plagioclase. However, only the highest-temperature heating steps of the samples indicate low K/Ca ratios, characteristic of plagioclase (Figure 9). This suggests that the samples represent mixtures of mineral phases, which bears upon the interpretation of the dating results (see below).

Results

For sample 02TR31, from the upper basalt flow at Çipköy, the weighted plateau age and both isochron ages are in good agreement, ~1.9 Ma, somewhat greater than the total fusion age (Table 2). We thus adopt the weighted plateau age, of 1865±21 ka (±2σ), as our preferred age-determination for this sample. This confirms the validity of the Arger *et al.* (2000) whole-rock K-Ar date of 1870±140 ka (±2σ) for the same flow.

For sample 02TR35 from Gümüşbağlar, all four age determinations are in good agreement, ~1.9 Ma (Table 2). The weighted plateau age is associated with a high MSWD value (Table 2); however, Figure 7c indicates that this is because the individual step-heating splits have very narrow margins of uncertainty but their ages are slightly different; it is thus not a problem. We adopt this weighted plateau age, of 1914±25 ka (±2σ), as our preferred age-determination for this sample. This date lies within the Olduvai subchron, which spans marine oxygen isotope stage (MIS) 72 to MIS 64 or ~1950–1780 ka (e.g., Hilgen 1991). It thus confirms the deduction by Arger *et al.* (2000) that the normal geomagnetic polarity of this basalt indicates the Olduvai subchron (cf. Sanver 1968) and that this volcanism was essentially synchronous with that at Çipköy.

Table 1. Summary of Ar-Ar dating results.

Site	Sample	UTM	Lab. No.	$^{40}Ar(r) / {^{39}}Ar(k)$ (±2σ)	Age (ka) (±2σ)	$^{39}Ar(k)$ (%)	K/Ca (±2σ)
Çipköy	02TR31	EC 06704 82031	E21 RW5F041Q	2.9148±0.0275 (±0.94%)	1865.3±20.9 (±1.12%)	51.42	0.667±0.195
Alaca	02TR33	EC 05249 89380	E22 RW5F041R	3.3331±0.1392 (±4.18%)	2131.0±89.9 (±4.22%)	74.78	0.730±0.010
Gümüşbağlar	02TR35	EC 18088 88361	E23 RW5F041S	2.9982±0.0341 (±1.14%)	1913.8±24.6 (±1.28%)	65.31	1.540±0.020

All samples were of basaltic groundmass, separated as described in the text. $^{40}Ar(r) / {^{39}}Ar(k)$ is the measured ratio of the number of ^{40}Ar atoms produced by radioactive decay of the potassium in the sample to the number of ^{39}Ar atoms produced by irradiation of the potassium in the sample. Age is the weighted plateau age for each sample (see Table 2). $^{39}Ar(k)$ (%) is the percentage of the ^{39}Ar in the irradiated sample that is determined to have been produced by irradiation of potassium. K/Ca is the measured ratio of potassium to calcium atoms in the sample, which is used to correct the ^{39}Ar measurements for ^{39}Ar produced by irradiation of calcium. All ages have been calibrated relative to the U.S. Geological Survey Taylor Creek Rhyolite tcr-2a sanidine standard, as a neutron flux monitor during sample irradiation, with an assigned age of 28.34 Ma (after Renne *et al.* 1998). Calculations assume decay constants from Steiger & Jäger (1977), together with $^{40}Ar/{^{36}}Ar$ ratio for atmospheric argon of 295.5.

Table 2. Comparison of alternative Ar-Ar age-determinations.

Site	Sample	Total fusion age (ka)	Weighted plateau			Normal isochron		Inverse isochron	
			Age (ka)	n/N	MSWD	Age (ka)	MSWD	Age (ka)	MSWD
Çipköy	02TR31	1806.9±22.6	1865.3±20.9	4/10	0.75	1873.4±58.9	1.08	1874.3±58.1	1.07
Alaca	02TR33	2156.8±19.1	2131.0±89.9	7/10	80.52	1883.7±267.6	45.41	1877.3±255.7	44.20
Gümüşbağlar	02TR35	1916.7±15.1	1913.8±24.6	4/10	8.61	1929.8±80.7	11.11	1929.4±86.7	12.27

See Table 1 for site co-ordinates and other details. MSWD is the mean squared weighted deviation for each of the age determinations, a measure of the scatter between individual contributing data (age estimates for different heating steps, or sets of isotope ratios used to fit each of the isochrons). For the weighted plateau age, N is the total of heating steps measured; n is the number of these steps that were used for each age determination.

For sample 02TR33, the total fusion age and weighted plateau age (Figure 7b) are more than 200 ka older than the two isochron ages (Figure 8c, d)), which are ~1.9 Ma, albeit with high margins of uncertainty (Table 2). These isochron plots have y-intercepts that indicate $^{40}Ar/{^{36}}Ar$ ratios of ~380–390, well above the value for atmospheric argon (295.5). This implies that, despite the preparation steps taken to eliminate phenocryst material, the sample contains inherited radiogenic ^{40}Ar, causing the weighted plateau age to exceed its true age. As previously noted (McDougall & Harrison 1999, p. 114–116) the presence of inherited argon will mimic the effect, in the weighted plateau age calculation for this sample, of an atmospheric $^{40}Ar/{^{36}}Ar$ ratio of ~380–390 (Figure 8c, d). It would thus be possible, in principle, to re-run the calculation with this higher ratio, which would lead to an alternative weighted plateau age that would be similar to the isochron ages already determined for the sample. However, we prefer instead simply to adopt the inverse isochron age in Figure 8d, 1877±256 ka (±2σ) as our preferred age for this

sample, it being marginally the better constrained of the two isochron ages.

Four dates thus now exist for this volcanism: 1870±140 ka (±2σ) for the upper basalt flow at Çipköy, from Arger *et al.* (2000), and, from this study, 1865.3±20.9 ka (±2σ) for the same flow, 1877±256 ka (±2σ) for the basalt at Alaca, and 1913.8±24.6 ka (±2σ) for the Gümüşbağlar basalt. These dates are concordant at the ±2σ level, indicating no significant differences in age. The overall weighted mean for these four dates is 1885.4±15.8 ka (±2σ), within the Olduvai subchron, consistent with the palaeomagnetic evidence (Sanver 1968; see also above).

The potential outlier of this set of data, with the oldest apparent age, is the Gümüşbağlar basalt (sample 02TR35). As Figure 7c indicates, the majority of the splits of this sample indicate a trend of apparent age decreasing slightly with increasing heating temperature. In principle, such a trend might result from the effect of recoil of ^{39}Ar nuclei produced by irradiation of ^{39}K (e.g.,

Table 3. Geochemical analysis results.

Sample	UTM Co-ordinates	SiO2	TiO2	Al2O3	Fe2O3T	MnO	MgO	CaO	Na2O	K2O	P2O5	LOI	Total	Cr	Cu	Ga	Nb	Ni	Pb	Rb	Sr	Th	V	Y	Zn	Zr	Ba	Ce	La	Nd	Cl	S	Sc	Ba/La	Zr/Nb	Qz	Ol	Ne
							Major elements (wt%)											Trace elements (ppm)																	Ratios		Norms (wt%)		
Örtülü																																						
02TR22	Dd 63688 05078	46.75	1.68	16.50	10.58	0.14	9.11	8.80	2.50	0.41	0.23	3.80	100.48	243	77	19	8	152	1	15	1206	1	141	25	72	114	300	19	4	22	59	109		75.000	14.250	0.000	12.329	0.000
94-E3	Dd 628 065	47.65	1.376	16.25	10.33	0.147	7.85	8.98	3.07	0.54	0.198	3.02	99.41	228.3	50.7		7.3	111.8	3.9	11.2	306.1	3.9	153.3	24.7	80.0	117.4	164.2	34.9	16.1	15.6			21.9	10.199	16.082	0.000	14.001	0.000
94-E5	Dd 628 065	47.60	1.369	16.33	10.11	0.143	7.51	9.24	3.11	0.55	0.196	3.51	99.66	255.1	52.1		7.5	112.9	2.3	11.4	302.1	4.7	175.1	24.7	78.6	117.6	164.0	34.4	17.0	19.1			27.6	9.647	15.680	0.000	13.901	0.000
Çipköy																																						
02TR32	Ec 06669 82033	45.03	2.15	16.11	9.97	0.16	7.42	10.08	2.84	2.42	0.56	2.86	99.60	175	62	18	62	90	5	43	1031	1	171	28	81	231	399	41	40	17	435	278		9.975	3.726	0.000	14.761	7.472
94-E1	Ec 072 822	46.19	2.194	16.57	10.33	0.179	6.89	9.26	3.88	1.58	0.633	1.67	99.38	203.1	45.8		68.9	104.3	3.7	48.2	831.4	8.1	194.0	26.3	78.0	251.9	626.2	77.6	38.4	30.1			19.9	16.307	3.656	0.000	13.901	6.786
94-E2	Ec 072 822	46.41	2.121	16.24	10.00	0.171	6.84	8.79	3.95	2.83	0.617	1.34	99.31	196.7	46.2		69.4	93.8	4.3	61.3	803.9	6.4	179.3	26.2	80.2	250.0	603.0	83.4	39.5	34.7			19.3	15.266	3.602	0.000	14.040	11.496
Alaca																																						
02TR33	Ec 05249 88380	49.60	1.96	16.56	9.62	0.14	6.90	7.60	4.02	2.23	0.61	0.20	99.44	135	54	18	50	100	5	39	648	0	152	27	72	271	535	47	22	27	250	74		24.318	5.420	0.000	15.077	3.081
02TR34	Ec 05249 88380	47.94	2.08	17.35	10.23	0.16	7.05	8.51	3.18	1.44	0.65	1.46	100.04	151	55	19	52	96	4	13	793	0	140	27	67	260	544	53	30	19	106	69		18.133	5.000	0.000	16.279	0.000
Gümüşbağlar																																						
02TR35	Ec 18088 88361	49.29	1.99	17.47	9.64	0.14	6.06	7.32	3.23	2.38	0.78	1.38	99.70	115	49	20	63	88	0	40	864	1	146	27	71	309	525	67	33	30	101	71		15.909	4.905	0.000	10.719	0.000
02TR36	Ec 17738 87300	50.34	1.89	17.24	9.03	0.14	6.31	6.82	4.55	2.43	0.77	0.33	99.85	111	50	18	63	79	8	43	760	5	143	26	68	308	232	49	33	23	339	66		7.030	4.889	0.000	14.150	3.865

Samples prefixed 02, collected in 2002 and original to this study, were analyzed by x-ray fluorescence spectrometry at Keele University in 2004. Blank cells indicate that no measurement was determined; LOI means loss on ignition; Qz, Ol and Ne indicate normative quartz, olivine, and nepheline. Site co-ordinates for these samples were measured in the field to the nearest metre using a handheld GPS receiver. Due to an oversight, no analysis of sample 02TR31 was run. Those prefixed 94, collected in 1994, were analysed by x-ray fluorescence spectrometry at Edinburgh University in 1996; for analytic details see Arger *et al.* (2000). Site co-ordinates for these samples were measured to a nominal precision of 100 m using available 1:100,000 and 1:500,000 scale topographic maps. The 2002 Çipköy samples came from essentially the same place as their 1994 counterparts; 94-E1 and 02TR32 came from the lower basalt flow at Çipköy and 94-E2 and 02TR31 came from the upper flow. The 2002 Örtülü sample came from a more proximal part of the flow unit, a few hundred metres west and north of its 1994 counterparts. Norm calculations assume a Fe2O3/FeO wt% ratio of 0.2 for most samples, with 0.3 for hawaiites (94E1, 02TR33 and 02TR35) and 0.35 for the mugearite (02TR36), after Middlemost (1989).
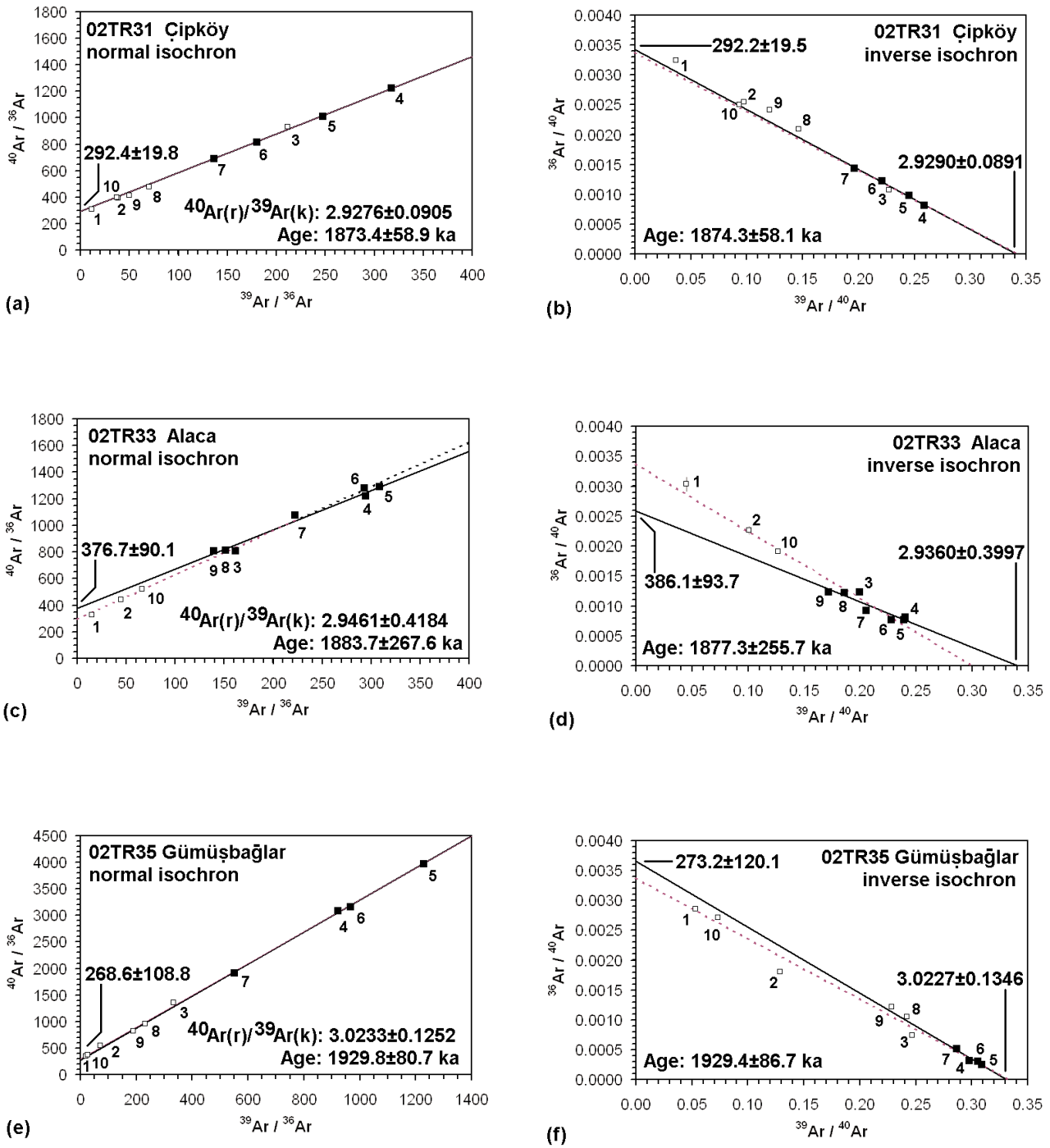
Figure 8. Graphs of isochron ages for each of our samples, as summarized in Table 2. Solid lines are isochron lines of best fit, fitted through the data points marked with solid symbols. Open symbols are data points that are not used in fitting the isochrons, these being the same points as are excluded from the weighted plateau age determinations (Figure 7). Dashed lines are isochrons that are fitted, for comparison, through a y-intercept corresponding to the modern ratio of $^{40}Ar/^{36}Ar$ in the atmosphere (295.5). Solid and open symbols are labelled to indicate their order of release by step-heating, for comparison with graphs in Figure 7 and data tables in the appendix. Key argon isotope ratios dewtermined from the graphs are labelled, those for the inverse isochron graphs being expressed as reciprocals to facilitate comparison with the normal isochron graphs. All margins of uncertainty are ±2σ. See text for discussion.

(a) 02TR31
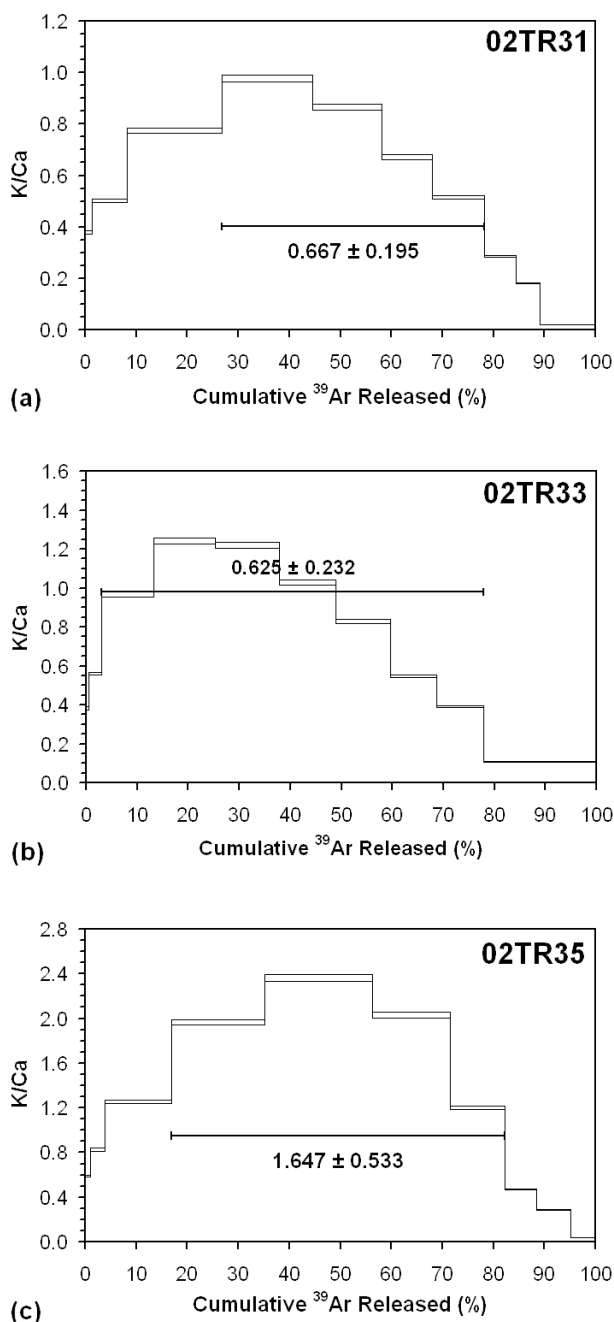
0.667 ± 0.195

(b) 02TR33

0.625 ± 0.232

(c) 02TR35

1.647 ± 0.533

Figure 9. Graphs of the K/Ca ratio (±2σ) in each of the step-heating splits of each of our samples, calculated from the measured concentrations of argon isotopes (tabulated in the appendix) after Singer & Pringle (1996) and Harford *et al.* (2002). See text for discussion.

Turner & Cadogan 1974; Hess & Lippolt 1986). Such recoil will result in partial loss of the ^{39}Ar, the loss being greatest from near the edges of mineral grains, which release argon early in the step-heating sequence. Since

^{39}Ar is a proxy for ^{39}K, such an effect would result in apparent ages that would be too old; one would thus expect to see a decrease in apparent age with step-heating temperature, as is indeed observed for sample 02TR35 (Figure 7c). However, ^{39}Ar recoil is not expected to be a significant problem for samples with grain size as large as ours (60–80 μm); it is only expected to become significant at much smaller grain sizes (e.g., Paine *et al.* 2006; Jourdan *et al.* 2007). Nonetheless it is impracticable to correct any of our apparent ages for loss of ^{39}Ar by recoil, using the equations derived by Jourdan *et al.* (2007), because they require information (such as, the typical shape of the grains) that was not measured during the analysis of our samples.

In any case, for sample 02TR35, the trend of decreasing apparent age with step-heating temperature correlates with a trend of decreasing K/Ca ratio with step-heating temperature (Figure 9c), the latter trend suggesting (as noted above) that a mixture of mineral phases is present. The trend in apparent age may thus be unrelated to ^{39}Ar recoil; it could simply indicate that the different mineral phases yield slightly different apparent ages, the low-K/Ca phase that is most concentrated in the highest-temperature splits giving a lower apparent age than the other phase. However, regardless of the correct interpretation of the data in Figure 7c, the trend in apparent age introduces some doubt as to the true age of the sample. We have therefore recalculated the age of sample 02TR35 using the three highest-teperature splits, which yield apparent ages (all ±2σ) of 1822.4±37.3 ka, 1790.2±32.8 ka, and 1739.3±128.1 ka, obtaining a weighted mean value of 1801.9±24.2 ka (±2σ). The weighted mean of this date and the dates of the three Çipköy and Alaca samples can be determined as 1838.8±15.7 ka (±2σ). Both this alternative age for sample 02TR35 and the resulting overall weighted mean age fall within the Olduvai subchron, consistent with the palaeomagnetism (Sanver 1968); thus, like the first set of calculations, this alternative set of results is consistent with the available evidence, and is thus a tenable age assignment.

Another alternative method of determining the age of sample 02TR35 would be to fit a new inverse isochron (cf. Figure 8f), weighted to fit the trend through step-heating splits 8, 9 and 10. As can be seen by inspection of Figure 8f, such an isochron would intersect the ^{36}Ar/^{40}Ar axis close to the modern atmospheric ^{40}Ar/^{36}Ar
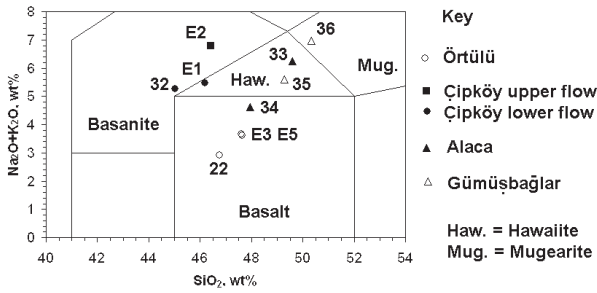
515

Figure 10. Total alkali (Na$_2$O+K$_2$O) versus SiO$_2$ diagram for Elazığ basalts (after Le Bas *et al.* 1986).

ratio (295.5), and would also intersect the ^{36}Ar/^{40}Ar axis slightly to the right of the marked intercept, which would indicate a slightly lower ratio of radiogenic ^{40}Ar to ^{39}Ar produced by the irradiation of the sample, and so would indicate a slightly lower age of the sample, in agreement with our deduction from reanalysis of the age spectrum graph (Figure 7c).

We also hoped to date sample 02TR22 of the Örtülü basalt. Arger *et al.* (2000) had previously collected two samples of this basalt for dating, but these were rejected as too altered. Despite the careful selection in the field, sample 02TR22 was likewise rejected; as a result, the Örtülü basalt remains undated. This basalt evidently erupted into the Karabakır palaeo-lake; its alteration thus presumably reflects a hydrothermal effect at the time of eruption rather than subsequent chemical weathering. It pre-dates the local end of lacustrine deposition, but whether it is Late Miocene, as was tentatively suggested by Asutay (1988) or Pliocene (cf. Arger *et al.* 2000; possibly contemporaneous with the Karakoçan/Kovancılar basalt already discussed) still cannot be resolved.

To supplement the results of our geochemical analysis, we add those from Arger *et al.* (2000) for the Örtülü and Çipköy localities (Table 3). As Figure 10 indicates, using total alkali versus silica this set of samples is quite diverse, comprising basalts (sensu stricto), basanites, hawaiites and a mugearite. On the basis of normative composition (Table 3), all samples classify as alkali basalt due to the presence of normative olivine and the absence of normative quartz. All three samples analysed from Çipköy and two others – 02TR33 from Alaca and 02TR36 from Gümüşbağlar – contain normative nepheline. From its position in the landscape (Figure 4) the Alaca basalt could be a distal part of either the Çipköy (Sarıbuçuk) or Gümüşbağlar flows. On the

basis of geochemistry (Figure 10) it seems more likely to correspond to the Gümüşbağlar flow. However, the volcanism at all three localities was essentially synchronous, as already noted.

It is evident that many characteristics of these basalts (Table 3) are complex and no single petrogenetic process can explain them. Most samples have low ratios of Zr/Nb (~4), suggesting that thay have formed as a result of small-degree partial melting of mantle material. However, some have Ba/La ratios of >>10, suggesting some input of crustal contamination. The Zr/Nb ratio measures the degree of partial melting, primarily because Nb becomes concentrated in the melt to a greater extent than Zr (e.g., Johnson *et al.* 1989; Camp & Roobol 1992). A Ba/La ratio of 10.2 is expected for primitive mantle (Sun & McDonough 1989); a ratio >>10 thus indicates crustal contamination.

Following Pearce *et al.* (1990), we assess the relative importance of partial melting and fractional crystallisation in the formation of these basalts using a plot of the abundances of Cr against Y (Figure 11). The incompatible element Y becomes strongly concentrated in small-degree partial melt and is not readily taken up during any subsequent fractional crystallization. The compatible element Cr exhibits the opposite behaviour: its tendency to remain bound within silicate crystal lattices means that it is strongly depleted in partial melt and becomes even more depleted in the residual melt left after any fractional crystallization. Figure 11 suggests that the measured abundances of Cr and Y indicate that small-degree partial melting of the asthenosphere at a temperature of ~1225 °C was followed by significant differentiation by fractional crystallization. The samples indeed all plot along the same fractional crystallisation trend, suggesting that the Örtülü basalts have experienced the least differentiation as a result of fractional crystallization and those from Gümüşbağlar the most.

Discussion

Evolution of Fluvial and Lacustrine Systems

As already discussed, it seems probable that a lake basin existed in the Malatya area from the time this region rose above sea-level – in the Early Miocene – onward. For much of this time, this deposition was evidently unrelated to the motions of adjoining plates, and presumably took place simply because this region acted as a sediment trap or sag basin. This palaeo-lake basin may well have
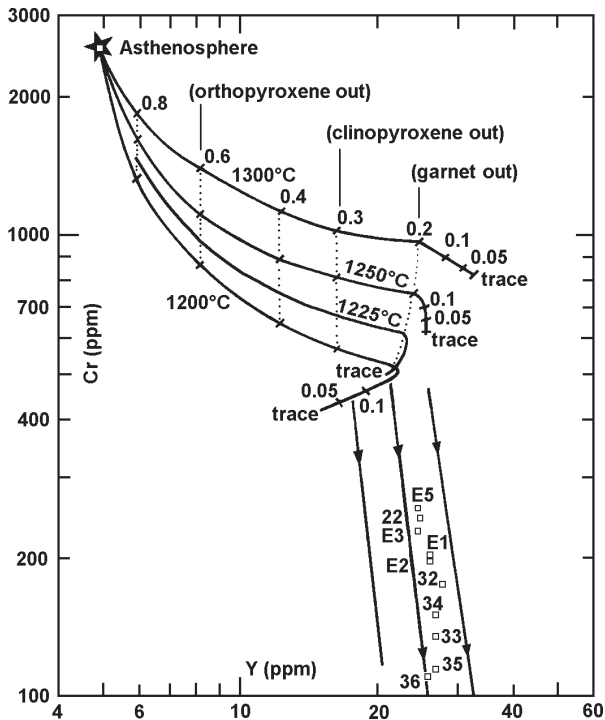
Figure 11. Cr versus Y diagram highlighting the roles of partial melting and fractional crystallization in the formation of the basalts in the study region. Solid lines are partial melting trends, calculated by Pearce *et al.* (1990) for garnet lherzolite (55% olivine, 20% orthopyroxene, 12.5% clinopyroxene, and 12.5% garnet) at 1200°C, 1250°C, and 1300°C, with each solid phase disappearing at the indicated degree of partial melting. See Pearce *et al.* (1990) for the values of the partition coefficients used and for sources of data. The line for 1225°C is estimated in this study by interpolation. Barbed lines indicate mafic crystallization trends, also from Pearce *et al.* (1990). See text for discussion.

extended well to the west of the line along which the Malatya Fault later developed, as depicted schematically in Figure 12a on the basis of the fragmentary local evidence of terrestrial sediment.

At this time, before any of the Late Cenozoic strike-slip fault systems developed, eastern Anatolia accommodated the NNW convergence between the Arabia and Eurasian plates by crustal shortening. The stratigraphic evidence noted by Kaymakcı *et al.* (2006) suggests that the major sediment influx into the Malatya Basin was from the east, consistent with fluvial input from the ancestral River Murat across the Belhan col near Baskil (Figures 2, 4 & 12a). We tentatively suggest that the Küseyin and Parçikan formations (Figure 3) date from this time.

Around 7 Ma, we estimate, the MOFZ became active (cf. Westaway 2003, 2004a; Westaway *et al.* 2005). We infer that the component of local subsidence east of the Malatya Fault created accommodation space for further lacustrine sedimentation in the Malatya Basin, resulting in the accumulation of the thick sequence in this basin. In contrast, the associated relative uplift of the area west of this fault would have rapidly brought lacustrine sedimentation to an end. Reworking of material by rivers flowing through the Malatya Fault escarpment, such as the Tohma and Kuru (Figure 2), may have redistributed much of the sediment formerly deposited in this area into the Malatya Basin. Notwithstanding the uncertainties already discussed in the dating of the Malatya Basin succession, we consider it probable that the Boyaca/Şeyhler Formation was deposited while the Malatya Fault was active, as this part of the sequence thickens strongly towards the Malatya Fault in a manner consistent with localised subsidence associated with slip on this fault (cf. Kaymakcı *et al.* 2006).

It can be presumed that the loading of the crust by this thickness of sediment in turn affected the isostatic balance, locally depressing the crust (or partly cancelling the regional uplift that would otherwise have occurred) and also causing the land surface ESE of the Malatya Basin to tilt towards the WNW. We presume that this combination of processes led to the abandonment by the ancestral River Murat of its former Baskil course and its deflection northward, together with the gradual northward and eastward expansion of the palaeo-lake to encompass the Karabakır Formation localities in the Elazığ region. In contrast, the much greater stability of the Doğanşehir outlet col implies greater local crustal stability, possibly related to the proximity of the Neotethys suture (Figure 2) and the nearby presence of much stronger crust of the Arabian Platform (see below). Figure 12b shows a schematic illustration of the inferred palaeo-geography at ~4 Ma, shortly before slip on the MOFZ ended. The palaeo-lake system seems to have reached its greatest extent around this time, as evidenced by the thin lacustrine sediments in the Palu area, dated at Hacısam (Figure 2) to >~4 Ma by mammalian biostratigraphy.

We presume that significant transtension on the Malatya Fault ended with the adjustment of the TR-AR plate boundary from the MOFZ to the EAFZ around 4 Ma. The end of creation of accommodation space by this local
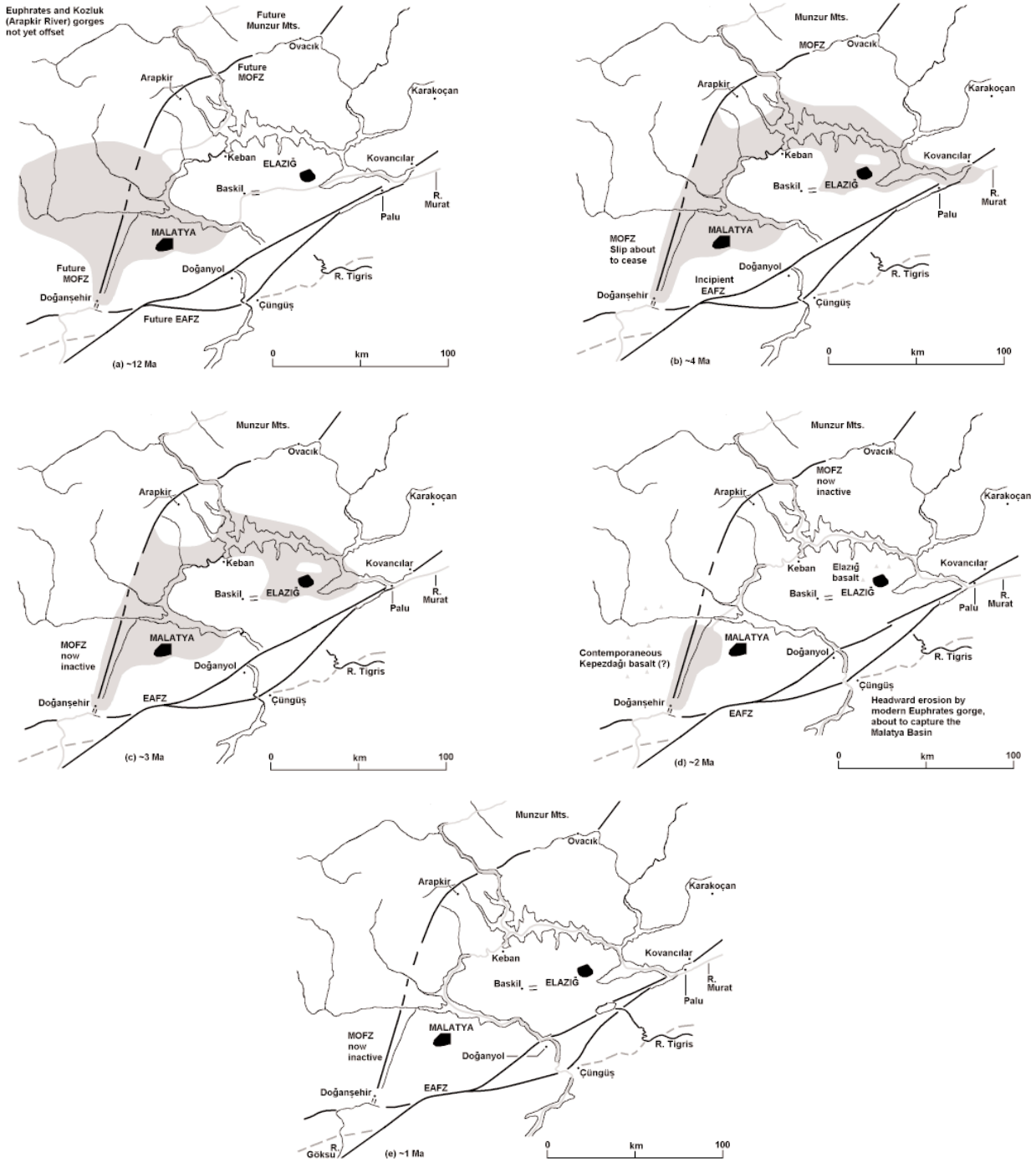
Figure 12. Cartoons indicating schematically the history of river system development and lacustrine sedimentation in the Malatya-Elazığ area. Grey shading indicates palaeo-rivers and lake basins that are inferred to have existed at each stage. The black background is taken from Figure 2. Post ~4 Ma slip on the EAFZ has been restored assuming that slip on the Çüngüş Fault began at ~2 Ma and its ~5 km of subsequent slip has occurred at a uniform rate of ~2.5 mm a^{-1}. It follows that the main NAFZ strand in this area has slipped ~30 km of which 13 km has occurred since 2 Ma at a uniform rate of ~6.5 mm a^{-1}, and the remainder occurred beforehand at a uniform rate of ~9 mm a^{-1}. Other solutions are also possible. Slip on the Sürgü Fault has not been restored. Likewise, other than to restore the offsets of the Euphrates and Arapkir (Kozluk) gorges the strike-slip and normal slip on the MOFZ have not been restored. All these minor displacements would be difficult to show clearly on a diagram covering a region of this size.

component of downthrow presumably meant that this lake basin no longer acted as such an effective sediment trap; from this time onward the sediment flux through the Doğanşehir outlet col is thus expected to have increased significantly. At the same time, the general eastward increase in regional uplift across Anatolia, combined with the stability of the outlet col, required – given the need for the lake surface to maintain its own level – the eastern margin of this lake to retreat progressively westward. We tentatively suggest that the Sultansuyu Formation (Figure 3) marks the deposition occurring within the Malatya Basin at this time. The mammalian biostratigraphy at the Sürsürü site near Elazığ (Figure 4) indicates that lacustrine deposition ceased locally at or shortly before 3 Ma. Figure 12c illustrates the palaeo-geography thus deduced around this time.

We infer that continued westward regional tilting led to further progressive westward retreat of the lake basin, such that by ~2 Ma it may have been quite small, possibly confined to the southern Malatya Basin as shown schematically in Figure 12d. As already noted, we infer that the Beyler Deresi Formation (Figure 3), in the south of the Malatya Basin, marks the deposition around this time. Shortly afterwards, as already noted, headward incision by the modern Euphrates gorge around Doğanyol captured the Malatya Basin, causing the abandonment of its former Doğanşehir outlet col and initiating the rapid dissection of the lacustrine sequence. Thus, at ~1 Ma we infer that a situation similar to that at present already existed, although with smaller-than-present offsets of river gorges by the EAFZ strands (Figure 12e).

One complicating factor regarding such an interpretation concerns the possible role of localized faulting, as opposed to regional uplift, in causing some of the vertical crustal motions in the study region. East of the Malatya Basin is a north-dipping reverse-fault zone known as the Aydınlar thrust (e.g., Kaymakcı *et al.* 2006; Figure 2). This structure continues westward across the Malatya Basin, slip on it being thought responsible (e.g., by Kaymakcı *et al.* 2006) for localized deformation of the basin succession (as in Figure 6c). At its eastern end this structure seems to pass end-on into the WNW-dipping Piran thrust (Figures 2 & 4), along which the Keban Group metamorphic rocks have been overthrust onto rocks of the Elazığ Complex. Farther east, there is another ENE-trending mountain range, passing north of

Elazığ through Harput (Figure 4), which we call the Harput Fault. All these structures have hitherto been thought to be related to Late Cretaceous or Mid-Cenozoic crustal deformation, pre-dating the modern tectonic regime (e.g., Bingöl 1984; Yazgan 1984; Kaymakcı *et al.* 2006). For instance, in Figure 4 part of the Piran Thrust has been mapped as 'sealed' by Lower Cenozoic marine limestone, implying that it has not slipped since the Late Cretaceous. However, a variety of forms of evidence suggests the possibility of continued activity on such structures. For instance, west of Elazığ the Mid-Pliocene deposits of the Karabakır Formation reach ~1200 m a.s.l. around Şahinkaya, in the hanging-wall of the Harput Fault, more than 100 m higher than their upper limit nearby (at Rizvan Tepe) in its footwall (Figure 4). Likewise, the hanging-wall of the Piran/Aydınlar thrust has been recognized (e.g., by Tonbul 1987) as an area of dramatic fluvial incision, as has indeed been noted in the present study, such as may be expected if it is uplifting faster than its surroundings on the other side of this fault. Such an effect may possibly relate to reverse slip on this fault at depth but not at the Earth's surface (i.e., it is a 'blind' reverse fault). The deformation in the Malatya Basin (Figure 6c) is evidently younger than the whole sedimentary section preserved in the area, but whether it stopped at some point in the latest Miocene or Pliocene (as suggested by Kaymakcı *et al.* 2006) or continues to the present-day cannot be resolved from the available evidence. The available GPS evidence (e.g., McClusky *et al.* 2000) cannot resolve horizontal motions comparable in rate to the rates implied by these observations of vertical motion (i.e., by no more than hundreds of metres in millions of years, or of the order of a tenth of a millimetre per year).

Separating out regional-scale vertical crustal motions from local effects of faulting in Turkey and adjoining regions is well-known to be a difficult question (e.g., Westaway 2003, 2006a; Westaway *et al.* 2004, 2006c; Demir *et al.* 2007), as is trying to resolve whether vertical crustal motions in plate boundary zones (such as the present study region) are caused directly by the plate motions or are induced by climate, via the isostatic consequences of surface processes (e.g., Bridgland & Westaway 2008). As Demir *et al.* (2007) have noted, resolving possible contributions to vertical crustal motion from blind reverse faults requires detailed survey work, and is thus beyond the scope of the present study. Below,

we discuss possible mechanisms that may relate to deformation of the study region, caused by induced flow in the lower continental crust. It should be noted that such arguments are unaffected by whether the induced vertical motions occur gradually (i.e., involve only tilting of the upper crust), or whether the stresses induced by the moving lower crust are sufficient to reactivate segments of pre-existing faults (cf. Westaway 2006b).

Relationship to Crustal Properties

The maximum crustal thickness beneath eastern Anatolia is now tightly constrained at 50 km from travel times of seismic waves (Zor *et al*. 2003). This crust is thus not much thicker than that beneath the Arabian Platform (~40 km thick; see below), and yet is overlain by high topography, ≥2 km above sea-level, whereas most of Arabia is within ~500 m of sea-level. This situation has been seen as anomalous, and has led to the recent development of ad hoc models for the Late Cenozoic uplift of eastern Anatolia, in terms of the isostatic response to delamination of the underlying mantle lithosphere (e.g., Keskin 2003; Şengör *et al*. 2003; Barazangi *et al*. 2006). Elsewhere, notably in Europe, modern explanations for Late Cenozoic epeirogenic uplift, in terms of coupling between surface processes and induced lower-crustal flow, have removed the need for this and other ad hoc local explanations that were formerly prevalent (e.g., Westaway 2001, 2002a, b; Bridgland & Westaway 2008).

The surface heat flow in the Arabian Platform is low, being ~45–50 mW m^{-2} (e.g., Tezcan 1995; Medaris & Syada 1999; Al-Mishwat & Nasir 2004). Geobarometric, seismic and gravity studies indicate that this crust is ~40 km thick (e.g., Best *et al*. 1990; Nasir & Safarjalani 2000), but is thought to include a layer of mafic underplating at least ~10 km thick (e.g., Nasir & Safarjalani 2000; Al-Mishwat & Nasir 2004), which will not flow and thus forms the lower boundary to the overlying mobile layer (cf. Westaway 2001). Numerical modelling of Late Cenozoic uplift histories, derived from trerrace staircases of the River Euphrates in the Arabian Platform in SE Turkey and farther downstream (Demir *et al*. 2007), indicate that this mobile layer is locally no more than ~5 km thick. We thus infer that the local ~40 km thickness of crust consists of an upper brittle layer may be ~25 km thick, with this ~5 km mobile layer and a ~10 km mafic basal layer. The presence of this mafic

layer, in combination with the low heat flow, appears to be the main reason why the mobile lower crust is so thin in this region.

Taking the base of the upper-crustal brittle layer as marking the 350 °C isotherm, as in previous studies (e.g., Sibson 1983), and assuming a 10 °C km^{-1} geothermal gradient in the lower crust, we tentatively estimate temperatures of ~400 °C at the base of the mobile lower-crustal layer and ~500 °C at the Moho. Using the Westaway (1998) calibration, a temperature as low as ~400 °C at the base of the mobile lower-crust indicates an effective viscosity η_e for the lower-crustal layer in excess of ~10^{22} Pa s. For comparison, in the Kula area of western Anatolia (Figure 1) where the crust is ~30 km thick, the Moho temperatuire is estimated as ~660 °C, with η_e (again, using the Westaway 1998 calibration) of the order of 2×10^{18} Pa s (Westaway *et al*. 2004, 2006c).

Other modelling of the thermal state of the crust in western Anatolia (Westaway 2006c), where the surface heat flow reaches ~120 mW m^{-2}, suggests that the lithosphere is locally no more than ~60 km thick, comprising ~30 km thick crust overlying ~30 km thick mantle lithosphere. The station-spacing in the Zor *et al*. (2003) seismic tomography study was rather coarse to image such thin mantle lithosphere, raising the possibility that they have mistaken a situation with similarly thin mantle lithosphere for one where no mantle lithosphere is present. If the lithosphere of eastern Anatolia is instead represented by 50 km of crust overlying 30 km of mantle lithosphere, then – even neglecting any contribution from radiogenic heating in the crust – the Moho temperature can be estimated as ~875 °C, making η_e for the lower-crustal layer (again using the Westaway 1998, calibration) no greater than ~2×10^{16} Pa s. A dramatic contrast in effective viscosity of the lower crust, by more than five orders-of-magnitude, is thus inferred to exist between Arabia and eastern Anatolia.

This much greater mobility of the lower crust beneath Anatolia, causing the lithosphere of Arabia to be far stronger, is presumably the main reason why their Cenozoic continental collision has resulted in much greater deformation of the former than of the latter. It also explains how it is possible for the crust of eastern Anatolia with much higher topography (~2–3 km) to co-exist in isostatic equilibrium adjacent to Arabia: the lower crust of Arabia is so stiff that rates of outflow of lower-

crustal material from beneath Anatolia are limited. This situation thus provides a smaller-scale analogue to the continental collision between India and Eurasia farther east, where the higher topography of Tibet than of India is dynamically maintained by the contrast in rheology between the Archaean craton of peninsular India and the much younger and hotter lithosphere of Tibet (e.g., Westaway 1995). This effect was also formerly explained as a consequence of delamination of the mantle lithosphere beneath Tibet (cf. Molnar *et al.* 1993).

The predicted extreme mobility of the lower crust beneath eastern Anatolia means that the application of any local surface load (such as water or sediment in a lake basin) or of any negative load caused by local erosion, leads to significant outflow or inflow, respectively, of lower crust being induced. Extrapolating from what is observed in regions of less mobile lower crust (e.g., Westaway 2002c; Westaway *et al.* 2004), it is anticipated that the local addition at any point of a layer of rock at the Earth's surface will displace a significantly greater layer of lower crust at depth. This effect can readily explain the observations, by Westaway & Arger (2001) and in the present study, that amounts of surface uplift in the study region (revealed, for instance, by fluvial incision) show such dramatic local variations. In contrast, in localities with significantly less mobile lower crust, rates and amounts of surface uplift stay roughly constant across broad regions (e.g., Westaway 2001, 2002a, 2002b, 2004b; Westaway *et al.* 2002, 2006a). It means that the history of vertical crustal motion at each locality in the present study region is extremely sensitive to details of the histories of sedimentation and erosion both in that locality and in its immediate surroundings. An example of this complexity is the inference that sediment loading in the Malatya Basin palaeo-lake deflected the crust downward in a manner than enabled a narrow arm of this lake basin to extend eastward by more than 100 km (Figure 12b). In a region of much less mobile lower crust this would not have occurred, due to the much greater stiffness of the isostatic response to surface loading.

The Synchronous Elazığ Volcanism and Dissection of the Malatya Basin

Our dating (Gümüşbağlar) confirms and strengthens the earlier view (Arger *et al.* 2000) that the Elazığ volcanism occurred at 1.8–1.9 Ma. This timing has no obvious

relationship to any change in the regional kinematics, so potential explanations for it as a consequence of slip on the EAFZ are not favoured. In contrast, previous discussion suggested that the modern Euphrates gorge past Doğanyol (Figure 2) developed, and the resulting dissection of the Malatya Basin began, at ~2 Ma. We suspect that this similarity in timing is not coincidental, but instead raises the possibility of a cause-and-effect connection.

In western Europe, the time around ~2–1.9 Ma is known as the Tiglian C stage (e.g., Zagwijn 1992). As many studies (e.g., Shackleton *et al.* 1990; Hilgen 1991) now confirm, this was a time of significant climate instability at the 40 ka Milankovitch periodicity, reflected in the formation of contemporaneous terraces in many European rivers. A notable example, which is dated to the contemporaneous Olduvai subchron by magneto-stratigraphy, is provided by the Stoke Row terrace of the River Thames in SE England (e.g., Whiteman & Rose 1992; Rose *et al.* 1999; Westaway *et al.* 2002) and associated marine deposits that are magnetostratigraphically dated to the Olduvai subchron (Zalasiewicz *et al.* 1991). Periglacial conditions were thus widespread in western Europe during cold stages at this time (e.g., Kasse & Bohncke 2001), whereas in eastern Europe (where this part of the geological record is known as the Late Akchagyl stage) during cold stages an ice sheet is thought to have covered much of European Russia (e.g., Moskvitin 1961; Grichuk & Moskvitin 1968). Periglacial conditions can thus be anticipated in Turkey during cold stages at this time, as is indicated by the presence of successive Early Pleistocene river terraces reflecting this 40 ka Milankovitch periodicity (on the Gediz River around Kula, Figure 1; Maddy *et al.* 2005; Westaway *et al.* 2006c). Such cyclic patterns of climate instability promote alternations of fluvial incision and aggradation, strong incision often occurring during warming transitions (e.g., Bridgland 2000). In a region that is uplifting, rivers will thus cut to successively lower levels (relative to the rock column) during successive climate cycles. Eastern Turkey was already uplifting before ~2 Ma (e.g., Arger *et al.* 2000; Demir *et al.* 2007), but an increase in uplift rates at this time can be expected as the isostatic response to increased rates of erosion (cf. Westaway *et al.* 2004), inducing further fluvial incision. It is thus not surprising that the ancestral headwaters of the Lower Euphrates incised significantly

in the Çüngüş-Doğanyol area and thus cut headward at this time, enabling them to capture the Malatya Basin. Recent investigations of the northern Arabian Platform, comprising the reaches of the River Euphrates in Syria (e.g., Demir *et al*. 2007) and SE Turkey (Demir *et al*. 2008) and the reach of the River Tigris around Diyarbakır (Westaway *et al*. 2008), indicate a significant increase in incision rates at ~2 Ma that is presumed to mark a regional increase in erosion rates associated with climate change. A corresponding increase in rates of uplift and fluvial incision can be expected in the present study region, and can be expected to be more dramatic due to the higher relief and stronger isostatic response associated with the more mobile lower-crustal layer that is thought to be present.

The dissection of the lacustrine sequence in the Malatya Basin that is expected to have followed this capture process would have led to the rapid removal of much of this former sediment load and its downstream transport by the Euphrates. The resulting unloading of the crust in the Malatya Basin would have reduced the local pressure at the base of the upper-crustal brittle layer. This would have set up a lateral pressure gradient that acted to drive mobile lower-crust to beneath the Malatya Basin from beneath its surroundings. Since the lower crust in this region is expected to be highly mobile (see above), the resulting induced flow can be expected to have been vigorous, such that (by analogy with the behaviour of other analogous coupled systems; cf. Westaway 2002c; Westaway *et al*. 2004, 2006c) the influx of lower crust may well have exceeded the loss of material by erosion at the surface. The corresponding loss of lower-crustal material from surrounding regions, such as the Elazığ region, would be expected to reduce the local pressure in the underlying mantle lithosphere, adjusting conditions there towards the solidus of previously-frozen basaltic melt. The existence of earlier volcanism in these surrounding regions suggests that conditions were already close to the threshold for re-melting; thus, it is possible that even a relatively small pressure reduction may have been sufficient to 'trigger' the basaltic volcanism around 1.9 Ma.

We thus infer that the low-degree partial melting of the athenosphere that originally created the basaltic magmas that we have analysed (Table 3) occurred gradually in the ancient geological past. Since such small-volume melting results in negligible upward heat

transport, this material froze, and thus progressively accumulated, in the mantle lithosphere, but presumably remained at conditions close to the threshold for re-melting. It was thus feasible for any subsequent decrease in pressure, possibly for the reason described above, to trigger renewed melting. This potential explanation, which is similar in principle to explanations suggested for other instances of Late Cenozoic small-volume basaltic volcanism elsewhere in Turkey (e.g., Arger *et al*. 2000; Yurtmen *et al*. 2002; Westaway *et al*. 2004, 2005) is thus incompatible with the views of others (e.g., Keskin 2003; Şengör *et al*. 2003) that no mantle lithosphere is present beneath eastern Anatolia.

The nature of the melting process responsible for the production of basaltic magmas has long been debated. Many years ago, it was thought that complete or near-complete melting of amphibolite would produce hydrous basaltic magma (e.g., Yoder & Tilley 1962; Green & Ringwood 1967). The view subsequently developed that complete melting of any source rock is unfeasible; for instance, one modern textbook (Best & Christiansen 2001) states that 'Before total melting might occur, either the buoyant melt separates and moves out of the source or the partially melted rock becomes sufficiently buoyant to rise en masse, perhaps as a diapir, out of the source region and away from the perturbing changes'. If so, then re-melting of frozen basaltic melt would result in melt of much less mafic composition, invalidating the potential explanation for the basaltic volcanism of the study region that we proposed earlier. However, recent ideas about the rheology of basaltic melts (e.g., Hoover *et al*. 2001; Jerram *et al*. 2003; Cheadle *et al*. 2004) recognize that 'freezing' involves the development of a framework of crystals. When the volume of this framework reaches a threshold, which is of the order of 1/3 of the total volume (the proportion depends on factors such as the shape of the individual crystals), the residual melt can no longer percolate between these crystals. The aggregate thus develops a finite yield strength, i.e., effectively begins to behave as a solid. It follows that, on re-melting, the material will continue to behave as a solid until the proportion of melt exceeds ~2/3, after which the framework of crystals breaks down and the material behaves as a liquid. The remaining crystals will then be entrained within the moving melt and form phenocrysts in the basalt that is ultimately produced. It follows that basaltic melts may indeed freeze

and then re-melt, maintaining their original composition (i.e., without chemical differentiation by partial melting to form less mafic melts), consistent with the potential explanation, given above, for the basalts in the present study region.

This process also provides a natural explanation for the limited incision – no more than ~100 m – by the River Murat and its tributaries around Elazığ since ~2 Ma. The effective removal of a layer of lower crust from beneath this region by the sequence of processes described above has partly cancelled the crustal thickening (sustained by inflow of lower crust) that would have otherwise occurred. River gorges elsewhere in eastern Anatolia are notably much more dramatically incised, as is illustrated by examples discussed in this study and others noted by Westaway & Arger (2001).

Such effects are, however, difficult to quantify, because of the issue of converting incision in this upper part of the Euphrates system to uplift. If a river maintains a uniform downstream channel gradient, creates a staircase of terraces disposed subparallel to this gradient, and the downstream distance to the coastline does not change systematically over time, then incision can serve as a good proxy for uplift (e.g., Westaway *et al.* 2002). However, in the case of the Euphrates, first, it is evident that the coastline has retreated dramatically in the Late Cenozoic, which will cause the observed incision to underestimate the associated uplift. Second, it is evident that the channel gradient of the Euphrates increases significantly in the upstream direction; it is ~0.3 m km^{-1} in NE Syria (Demir *et al.* 2007), increasing to ~0.6 m km^{-1} in the reach between Atatürk Dam and Birecik (Demir *et al.* 2008), and (judging from topographic contours on old maps) as high as ~1.5–2.0 m km^{-1} in the reaches of the Euphrates and Murat that are now flooded by the Keban Reservoir. Such a variation will also result in incision underestimating the corresponding uplift by a progrsssively greater extent as one moves upstream through the system. It follows that the uplift in the Elazığ area since ~2 Ma may well be much greater than the ~100 m of fluvial incision. However, the same (potentially quite large) correction will also be applicable elsewhere in the region to convert uplift to incision; the smaller amount of incision around Elazığ thus implies less uplift than in other more deply-incised reaches of the upper Euphrates system.

Some previous studies (e.g., Kennett & Thunell 1975) have argued for a global increase in volcanic activity in the Quaternary. This point of view requires a cause-and-effect mechanism linking climate change to magmatic processes in the Earth's interior, which seems *a priori* unlikely. This Malatya-Elazığ example nonetheless indicates a sequence of processes whereby such a cause-and-effect relationship can arise indirectly: climate change triggers erosion, which induces lower-crustal flow, which triggers volcanism through decompression melting. In principle, this sequence of processes can be modelled quantitatively using software systems developed by one of us (R.W.). Although we present no numerical modelling of this effect at this stage, the above explanation is consistent with the behaviour of such coupled models, incorporating the non-steady response to increased rates of erosion and the associated induced lower-crustal flow, such as have been applied elsewhere in Turkey (e.g., Westaway *et al.* 2004, 2006c). However, having established the potential significance of this study region for demonstrating such a chain of cause and effect in this pilot study, we prefer to postpone quantitative modelling until more data pertaining to age-control has been collected.

Although less well constrained, an analogous cause-and-effect explanation may be applicable for the ~4.5–4.2 Ma end of lacustrine deposition in the eastern part of the Elazığ region (evidenced from the mammalian evidence at Hacısam) and the ~4.1 Ma volcanism in the adjacent Karakoçan area (Sanver 1968), or indeed to the early Middle Miocene Yamadağ volcanism (see above; also Leo *et al.* 1974; Arger *et al.* 2000) following the start of erosion accompanying the emergence of the region above sea-level.

Potential Alternative Explanations for the Surface Uplift and Volcanism in the Study Region

Regarding the question of whether the vertical crustal motions in eastern Anatolia are being caused by plate motions or by surface processes, we note the following observations. First, there is no reason why the present geometry of plate motions should cause uplift in this region. The EAFZ and eastern NAFZ are well-known to be good approximations to transform fault zones, slip on which requires no vertical crustal motion. The left-lateral EAFZ steps to the right in the vicinity of Çelikhan, which

requires localized transpression and thus a localized component of surface uplift, but this area is ~100 km away from the Elazığ volcanism (Figure 2). This volcanism is indeed located ~40 km or more from the nearest point on the EAFZ (Figure 2); thus, any direct cause-and-effect connection between this faulting and the volcanism seems unlikely. Second, as has already been noted, recent studies (e.g., Keskin 2003; Şengör *et al.* 2003; Barazangi *et al.* 2006) have argued that delamination of the mantle lithosphere can explain the uplift of eastern Anatolia. However, again as already noted, such an arbitrary explanation is difficult to test; in addition, it is evident (again from earlier discussion) that to explain the geochemistry of the Elazığ basalts requires the presence of mantle lithosphere beneath the region. Furthermore, the topography of eastern Anatolia is roughly as expected for continental crust of the observed thickness in isostatic equilibrium, and thus provides no basis for inferring that delamination has occurred. Second, it is now evident from recent detailed studies, at Diyarbakır (Bridgland *et al.* 2007; Westaway *et al.* 2008) and Birecik (Demir *et al.* 2008) in southeast Turkey and in the Raqqa-Deir ez Zor area of NE Syria (Demir *et al.* 2007), that the Arabian Platform is experiencing regional surface uplift. As Demir *et al.* (2007) argued, it is thus reasonable to conclude that eastern Anatolia is also experiencing regional uplift. It is, however, difficult to test this hypothesis by numerical modelling (as has been done in the Arabian Platform and in western Anatolia) due to a lack of suitably detailed evidence. The present study indeed forms part of the process of gathering the necessary evidence to undertake such a test for eastern Anatolia in future. Third, it has recently become apparent that the uplift histories of many other localities in and around the Mediterranean region are better explained in terms of the isostatic consequences of erosion than in terms of plate motions (e.g., Champagnac *et al.* 2007; Westaway & Bridgland 2007; Bridgland & Westaway 2008). There is no reason to assume that eastern Anatolia is any different, but (as noted above) the evidence required to demonstrate this is currently unavailable.

Likewise, by analogy with other regions, alternative explanations for the Elazığ volcanism could in principle be proposed, in terms of either decompression melting of the mantle lithosphere associated with transtension (e.g., Rocchi *et al.* 2003; Putirka & Busby 2007) or heating as a result of partial delamination of the mantle lithosphere

(e.g., Trua *et al.* 2006; Azzouni-Sekkal *et al.* 2007). Some studies (e.g., Cooper *et al.* 2002; Putirka & Busby 2007) have indeed noted that either of these explanations could in principle explain the basaltic volcanism in a given locality. However, the first of these potential explanations can be excluded for the present study region, given that the EAFZ is not transtensional; plus, as noted above, the distance between it and the Elazığ volcanic field would seem to preclude any direct cause-and-effect connection.

Although complete loss of the mantle lithosphere can also be excluded as a viable explanation of this volcanism (see above), thinning of it, whether by partial delamination or as a result of the loading by the thickened continental crust 'squeezing' part of it outward from beneath the thickened region, warrants careful consideration. Thinning of the mantle lithosphere will (like thickening of the continental crust) act to increase the temperature within the remaining mantle lithosphere. Thinning of the mantle lithosphere will also result in a decrease in pressure at mantle depths, relative to the pressure that would exist following crustal thickening alone. Thinning of the mantle lithosphere will thus result in conditions more conducive to re-melting of material from within the mantle lithosphere, and thus will enhance the feasibility of the proposed explanation for the Elazığ volcanism. However, the key problem with such an explanation is that no evidence exists to prove that the mantle lithosphere beneath eastern Anatolia has indeed thinned during the Late Cenozoic.

In a recent modelling study, Seyrek *et al.* (2008) have investigated the crustal and lithospheric conditions that have led to the development, since the Mid-Pliocene, of the topography of the northern Amanos Mountains in the area of southern Turkey SW of Kahramanmaraş (Figure 1), where small-scale basaltic volcanism, petrologically and geochemically similar to that in the Elazığ area, has erupted in and around the valley of the River Ceyhan. The crust of the Amanos Mountains was inferred by Seyrek *et al.* (2008) to have thickened as a result of transpression along the northern Dead Sea Fault Zone, but the isostatic response within the mantle lithosphere in this region is not a priori clear. Seyrek *et al.* (2008) thus considered two sets of modelling solutions, both consistent with the available constraints (e.g., from gravity anomalies). In one set of solutions it was assumed that the Moho maintained a constant depth, the mantle lithosphere thickening through the development of a root; in the

other set of solutions it was assumed that the base of the lithosphere maintained a constant depth and the mantle lithosphere thickened by deflecting the Moho upward. The second set of solutions thus involved much less thickening of the mantle lithosphere than the first. However, the observational consequences of these two fundamentally different assumptions about the nature of isostatic equilibrium within the mantle lithosphere were shown by Seyrek *et al.* (2008) to be minimal; the faster uplift predicted for a given set of parameters in any solution of the second type could be replicated, within the limits of precision imposed by the data, by a solution of the first type but with one model parameter (say, Moho temperature, and thus, the effective viscosity of the lower continental crust) adjusted to a slightly different value. By analogy, it is likely to be very difficult to establish in future, by modelling of this type, whether the mantle lithosphere beneath eastern Anatolia has thinned or not.

Conclusions

As the first stage of a programme of research aimed at improving understanding of the interrelationships between vertical crustal motions, regional kinematics, and landscape evolution in eastern Anatolia during the Late Cenozoic, we have undertaken a pilot project to date some of the Plio–Pleistocene basalt flows associated with lacustrine deposits of the Karabakır Formation in the Elazığ region, together with a reappraisal of the history of lacustrine sedimentation in the adjacent Malatya Basin. The Malatya Basin experienced a prolonged history of lacustrine deposition, probably spanning the Middle–Late Miocene and much of the Pliocene. This lacustrine system expanded eastward across the Elazığ region, reaching its maximum extent at ~4 Ma, dated using mammalian biostratigraphy. The eastern margin of this lake basin subsequently retreated westward, consistent with overall westward tilting of the landscape. We suggest that a remnant of it persisted in the Malatya Basin until ~2 Ma, but subsequently became abruptly dissected following capture of this area by the modern gorge of the River Euphrates that crosses the East Anatolian Fault Zone (the modern boundary between the Turkish and Arabian plates that came into being at ~4 Ma). Using the Ar-Ar technique, we have dated the Elazığ volcanism to 1.8–1.9 Ma, suggesting that it immediately post-dates this disruption of the Malatya lake basin. We suggest that the abrupt erosion of this lake basin was isostatically compensated by inflow of mobile lower crust from beneath its surroundings, including the Elazığ region. This loss of material resulted in local crustal thinning in these regions, decompressing the underlying mantle and – we suggest – inducing the local volcanism. This effect, like other aspects of this region's geomorphic evolution including the observed abrupt lateral variations in depths of incision along river gorges, requires highly mobile lower crust, such as may be expected from the estimated local Moho temperature of no less than ~875 °C. Moreover, the evidence suggests a cause-and-effect relationship between climate change and volcanism, although this relationship is indirect: climate change around 2 Ma caused fluvial incision, which led to wider-scale erosion, which induced lower-crustal flow, which triggered volcanism.

Acknowledgments

References

AGUSTI, J., CABRERA, L., GARCES, M., KRIJGSMAN, W., OMS, O. & PARES, J.M. 2001. A calibrated mammal scale for the Neogene of western Europe: state of the art. *Earth-Science Reviews* **52**, 247–260.

AKTAŞ, G. & ROBERTSON, A.H.F. 1984. The Maden complex, SE Turkey: Evolution of a Neotethyan active margin. *In:* DIXON, J.E. & ROBERTSON, A.H.F. (eds), *The Geological Evolution of the Eastern Mediterranean*. Geological Society, London, Special Publications **17**, 375–402.

AL-MISHWAT, A.T. & NASIR, S.J. 2004. Composition of the lower crust of the Arabian Plate; a xenolith perspective. *Lithos* **72**, 45–72.

ALTINLI, İ.E. 1961. *Erzurum Sheet of the Geological Map of Turkey, 1:500,000 Scale*. General Directorate of Mineral Research and Exploration (MTA) Publications.

ARGER, J., MITCHELL, J. & WESTAWAY, R. 2000. Neogene and Quaternary volcanism of south-eastern Turkey. *In:* BOZKURT, E., WINCHESTER, J.A. & PIPER, J.D.A. (eds), *Tectonics and Magmatism of Turkey and the Surrounding Area*. Geological Society, London, Special Publications **173**, 459–487.

ASUTAY, H.J. 1988. *Geological Map of the Malatya-H27 Quadrangle, 1:100,000 Scale, and Accompanying 12 Page Explanatory Booklet*. General Directorate of Mineral Research and Exploration (MTA) Publications [in Turkish].

ATEŞ, A., KEAREY, P. & TUFAN, S. 1999. New gravity and magnetic anomaly maps of Turkey. *Geophysical Journal International* **136**, 499–502.

AZZOUNI-SEKKAL, A., BONIN, B., BENHALLOU, A., YAHIAOUI, R. & LIEGEOIS, J.-P. 2007. Cenozoic alkaline volcanism of the Atakor Massif, Hoggar, Algeria. *In:* BECCALUVA, L., BIANCHINI, G. & WILSON, M. (eds), *Cenozoic Volcanism in the Mediterranean Area*. Geological Society of America Special Paper **418**, 321–340.

BARAZANGI, M., SANDVOL, E. & SEBER, D. 2006. Structure and tectonic evolution of the Anatolian Plateau in eastern Turkey. In: DILEK, Y. & PAVLIDES, S. (eds), *Postcollisional Tectonics and Magmatism in the Mediterranean Region and Asia*. Geological Society of America Special Paper **409**, 463–473.

BAYKAL, F. 1961. *Sivas Sheet of the Geological Map of Turkey, 1:500,000 Scale*. General Directorate of Mineral Research and Exploration (MTA) Publications.

BEST, J.A., BARAZANGI, M., AL-SAAD, D., SAWAF, T. & GEBRAN, A. 1990. Bouguer gravity trends and crustal struc Nasir ture of the Palmyride mountain belt and surrounding northern Arabian platform in Syria. *Geology* **18**, 1235–1239.

BEST, M.G. & CHRISTIANSEN, E.H. 2001. *Igneous Petrology*. Blackwell Science, Oxford.

BİNGÖL, A.F. 1984. Geology of the Elazığ area in the Eastern Taurus region. *In:* TEKELİ, O., GÖNCÜOĞLU, M.C. (eds), *Geology of the Taurus Belt, Proceedings of the 1983 Ankara Symposium*. General Directorate of Mineral Research and Exploration (MTA) Publications, 209–216.

BRIDGLAND, D.R. 2000. River terrace systems in north-west Europe: an archive of environmental change, uplift, and early human occupation. *Quaternary Science Reviews* **19**, 1293–1303.

BRIDGLAND, D.R. & WESTAWAY, R. 2008. Preservation patterns of Late Cenozoic fluvial deposits and their implications: results from IGCP 449. *Quaternary International*, in press.

BRIDGLAND D.R., DEMİR, T., SEYREK, A., PRINGLE, M., WESTAWAY, R., BECK, A.R., ROWBOTHAM, G. & YURTMEN, S. 2007. Dating Quaternary volcanism and incision by the River Tigris at Diyarbakır, SE Turkey. *Journal of Quaternary Science* **22**, 387–393.

CAMP, V.E. & ROOBOL, M.J. 1992. Upwelling asthenosphere beneath western Arabia and its regional implications. *Journal of Geophysical Research* **97**, 15255–15271.

CHAMPAGNAC, J.D., MOLNAR, P., ANDERSON, R.S., SUE, C. & DELACOU, B. 2007. Quaternary erosion-induced isostatic rebound in the western Alps. *Geology* **35**, 195–198.

CHEADLE, M.J., ELLIOTT, M.T. & McKENZIE, D. 2004. Percolation threshold and permeability of crystallizing igneous rocks; the importance of textural equilibrium. *Geology* **32**, 757–760.

COOPER, K.M., REID, M.R., DUNBAR, N.W. & McINTOSH, W.C. 2002. Origin of mafic magmas beneath northwestern Tibet; constraints from ^{230}Th-^{238}U disequilibria. *Geochemistry, Geophysics, Geosystems* **3** (11), 1065 [published online; doi: 10.1029/2002GC000332].

CRONIN, B.T., HARTLEY, A.J., ÇELİK, H., HURST, A., TÜRKMEN, I. & KEREY, E. 2000. Equilibrum profile development in graded deep-water slopes: Eocene, Eastern Turkey. *Journal of the Geological Society, London* **157**, 943–955.

DEMİR, T., SEYREK, A., WESTAWAY, R., BRIDGLAND, D. & BECK, A. 2008. Late Cenozoic surface uplift revealed by incision by the River Euphrates at Birecik, southeast Turkey. *Quaternary International*, in press.

DEMİR, T., WESTAWAY, R., BRIDGLAND, D., PRINGLE, M., YURTMEN, S., BECK, A. & ROWBOTHAM, G. 2007. Ar-Ar dating of Late Cenozoic basaltic volcanism in northern Syria: implications for the history of incision by the River Euphrates and uplift of the northern Arabian Platform. *Tectonics* **26**, 3012 [published online: doi: 10.1029/2006TC001959].

DEMİR, T., YEŞİLNACAR, İ. & WESTAWAY, R. 2004. River terrace sequences in Turkey: sources of evidence for lateral variations in regional uplift. *Proceedings of the Geologists' Association* **115**, 289–311.

FLOYD, P.A. & CASTILLO, P.R. 1992. Geochemistry and petrogenesis of Jurassic ocean crust basalts, ODP Leg 129, Site 801. *Proceedings of the Ocean Drilling Program, Scientific Results* **129**, 361–388.

GREEN, D.H. & RINGWOOD, A.E. 1967. The genesis of basaltic magmas. *Contributions to Mineralogy and Petrology* **15**, 103–190.

GRICHUK, M.P. & MOSKVITIN, A.I. 1968. K voprosu o klimate yuga Russkoy ravniny v nachale pleystotsena [The climate of the southern part of the Russian plain at the beginning of the Pleistocene]. *Doklady Akademii Nauk SSSR* **178**, 1157–1159.

HARFORD, C.L., PRINGLE, M.S., SPARKS, R.S.J. & YOUNG, S.R. 2002. The volcanic evolution of Montserrat using ^{40}Ar/^{39}Ar geochronology. *In:* DRUITT, T.H. & KOJKELAAR, B.P. (eds), *The Eruption of the Soufrière Hills Volcano, Montserrat, From 1995 to 1999*. Geological Society, London, Memoirs **21**, 93–113.

HERECE, E., AKAY, E., KÜÇÜMEN, Ö. & SARIASLAN, M. 1992. *Elazığ, Sivrice, Palu Dolayının Jeolojisi [Geology of Elazığ, Sivrice and Palu Region]*. General Directorate of Mineral Research and Exploration (MTA) Report no: **9634** [in Turkish, unpublished].

HESS, J.C. & LIPPOLT, H.J. 1986. Kinetics of Ar isotopes during neutron-irradiation: Ar-39 loss from minerals as a source of error in Ar-40/Ar-39 dating. *Chemical Geology* **59**, 223–236.

HILGEN, F.J. 1991. Astronomical calibration of Gauss to Matuyama sapropels in the Mediterranean and implications for the Geomagnetic Polarity Time Scale. *Earth and Planetary Science Letters* **104**, 226–244.

HOOVER, S.R., CASHMAN, K.V. & MANGA, M. 2001. The yield strength of subliquidus basalts – experimental results. *Journal of Volcanology and Geothermal Research* **107**, 1–18.

HUNTINGTON, E. 1902. The valley of the upper Euphrates River and its people. *Bulletin of the American Geographical Society* **34**, 301–318 and 384–393.

JERRAM, D.A., CHEADLE, M.J. & PHILPOTTS, A.R. 2003. Quantifying the building blocks of igneous rocks: are clustered crystal frameworks the foundation? *Journal of Petrology* **44**, 2033–2051.

JOHNSON, R.W., KNUTSON, J. & TAYLOR, S.R. 1989. *Intraplate Volcanism in Eastern Australia and New Zealand*. Cambridge University Press, Cambridge.

JOURDAN, F., MATZEL, J.P. & RENNE, P.R. 2007. ^{39}Ar and ^{37}Ar recoil loss during neutron irradiation of sanidine and plagioclase. *Geochimica et Cosmochimica Acta* **71**, 2791–2808.

KANEOKA, I., TAKAOKA, N. & CLAGUE, D.A. 1983. Noble gas systematics for coexisting glass and olivine crystals in basalts and dunite xenoliths from Loihi Seamount. *Earth and Planetary Science Letters* **66**, 427–437.

KASSE, K. & BOHNCKE, S. 2001. Early Pleistocene fluvial and estuarine records of climate change in the southern Netherlands and northern Belgium. *In*: MADDY, D., MACKLIN, M.G. & WOODWARD, J.C. (eds), *River Basin Sediment Systems: Archives of Environmental Change*. Balkema, Rotterdam, 171–193.

KAYMAKCI, N., İNCEÖZ, M. & ERTEPINAR, P. 2006. 3D architecture and Neogene evolution of the Malatya Basin: inferences for the kinematics of the Malatya and the Ovacık fault zones. *Turkish Journal of Earth Sciences* **15**, 123–154.

KENNETT, J.P. & THUNELL, R.C. 1975. Global increase in Quaternary explosive volcanism. *Science* **187**, 497–503.

KEREY, İ.E. & TÜRKMEN, I. 1991. Sedimentological aspects of Palu formation (Plio–Quaternary), the east of Elazığ, Turkey. *Bulletin of the Geological Society of Turkey* **34**, 21–26 [in Turkish with English summary].

KESKİN, M. 2003. Magma generation by slab steepening and breakoff beneath a subduction-accretion complex; an alternative model for collision-related volcanism in eastern Anatolia, Turkey. *Geophysical Research Letters* **30**, 8046 [published online; doi: 10.1029/2003GL018019].

LANPHERE, M.A. & DALRYMPLE, G.B. 1976. Identification of excess ^{40}Ar by the ^{40}Ar/^{39}Ar age spectrum technique. *Earth and Planetary Science Letters* **32**, 141–148.

LAUGHLIN, A.W., POTHS, J., HEALEY, H.A., RENEAU, S. & WOLDEGABRIEL, G. 1994. Dating of Quaternary basalts using the cosmogenic ^{3}He and ^{14}C methods with implications for excess ^{40}Ar. *Geology* **22**, 135–138.

LE BAS, M.J., LE MAITRE, R.W., STRECKEISEN, A. & ZANETTIN, B. 1986. A chemical classification of volcanic rocks based on the total alkali – silica diagram. *Journal of Petrology* **27**, 745–750.

LEO, G.W., MARVIN, R.F. & MEHNERT, H.H. 1974. Geologic framework of the Kuluncak-Sofular area, east-central Turkey, and K-Ar Ages of igneous rocks. *Geological Society of America Bulletin* **85**, 1785–1788.

MCCLUSKY, S., BALASSANIAN, S., BARKA, A.A., DEMIR, C., ERGINTAV, S., GEORGIEV, I., GÜRKAN, O., HAMBURGER, M., HURST, K., KAHLE, H.G., KASTENS, K., KEKELIDZE, G., KING, R., KOTZEV, V., LENK, O., MAHMOUD, S., MISHIN, A., NADARIYA, M., OUZOUNIS, A., PARADISSIS, D., PETER, Y., PRILEPIN, M., REILINGER, R.E., SANLI, İ., SEEGER, H., TEALEB, A., TOKSÖZ, M.N. & VEIS, G. 2000. Global Positioning System constraints on plate kinematics and dynamics in the Eastern Mediterranean and Caucasus. *Journal of Geophysical Research* **105**, 5695–720.

MCDOUGALL, I. & HARRISON, T.M. 1999. *Geochronology and Thermochronology by the ^{40}Ar/^{39}Ar Method*. Oxford University Press, Oxford.

MADDY, D., DEMİR, T., BRIDGLAND, D., VELDKAMP, A., STEMERDINK, C., VAN DER SCHRIEK, T. & WESTAWAY, R. 2005. An obliquity-controlled Early Pleistocene river terrace record from western Turkey? *Quaternary Research* **63**, 339–346.

MEDARIS, L.G., JR. & SYADA, G. 1999. Pyroxenite xenoliths from Al Ashaer Volcano, Syria; constraints on the thermal state of the subcontinental Arabian lithosphere. *International Geology Review* **41**, 895–905.

MIDDLEMOST, E.A.K. 1989. Iron oxidation ratios, norms, and the classification of volcanic rocks. *Chemical Geology* **77**, 19–26.

MOLNAR, P., ENGLAND, P. & MARTINOD, J. 1993. Mantle dynamics, the uplift of the Tibetan Plateau, and the Indian monsoon. *Reviews of Geophysics* **31**, 357–396.

MOSKVITIN, A.I. 1961. The flood-plain terraces of the Volga and early Caspian transgressions as related to glaciation. *Doklady of the Academy of Sciences of the USSR, Earth Sciences, English Translation* **136**, 76–78 [Russian original: *Doklady Akademii Nauk SSSR* **136**, 689].

NASIR, S. & SAFARJALANI, A. 2000. Lithospheric petrology beneath the northern part of the Arabian Plate in Syria; evidence from xenoliths in alkali basalts. *Journal of African Earth Sciences* **30**, 149–168.

ÖNAL, M. 1995. Miocene stratigraphy and lignite potential of the northern part of the Malatya graben basin, East Anatolia-Turkey. *In: Proceedings of the International Earth Sciences Colloquium on the Aegean region (IESCA-1995), İzmir*, 607–621.

ÖNAL, M. 1997. Malatya Graben havzası güney bölümünün stratigrafisi ve depolanma ortamları [Stratigraphy of the southern part of Malatya graben and their depositional settings]. *Cumhuriyet Üniversitesi Mühendislik Fakültesi Dergisi, Series A* **14**, 1–12, Sivas [in Turkish with English abstract].

PAINE, J.H., NOMADE, S. & RENNE, P.R. 2006. Quantification of ^{39}Ar recoil ejection from GA1550 biotite during neutron irradiation as a function of grain dimensions. *Geochimica et Cosmochimica Acta* **70**, 1507–1517.

PEARCE, J.A., BENDER, J.F., DE LONG, S.E., KIDD, W.S.F., LOW, P.J., GÜNER, Y., ŞAROĞLU, F., YILMAZ, Y., MOORBATH, S. & MITCHELL, J.G. 1990. Genesis of collision volcanism in eastern Anatolia, Turkey. *Journal of Volcanology and Geothermal Research* **44**, 181–198.

PERİNÇEK, D. & KOZLU, H. 1984. Stratigraphy and structural units of the Afşin-Elbistan-Doğanşehir region (Eastern Taurus). *In:* TEKELİ, O. & GÖNCÜOĞLU, M.C. (eds), *Geology of the Taurus Belt, Proceedings of the 1983 Ankara Symposium*. General Directorate of Mineral Research and Exploration (MTA) Publications, 181–198.

PUTIRKA, K. & BUSBY, C.J. 2007. The tectonic significance of high-K_2O volcanism in the Sierra Nevada, California. *Geology* **35**, 923–926.

RENNE, P.R., SWISHER, C.C., DEINO, A.L., KARNER, D.B., OWENS, T.L. & DEPAOLO, D.J. 1998. Intercalibration of standards, absolute ages and uncertainties in ^{40}Ar/^{39}Ar dating. *Chemical Geology* **145**, 117–152.

RIZAOĞLU, T., PARLAK, O., HOECK, V. & İŞLER, F. 2006. Nature and significance of Late Cretaceous ophiolitic rocks and their relation to the Baskil granitic intrusions of the Elazığ region, SE Turkey. In: ROBERTSON, A.H.F. & MOUNTRAKIS, D. (eds), Tectonic Development of the Eastern Mediterranean Region. Geological Society, London, Special Publications 260, 327–350.

ROBERTSON, A.H.F., PARLAK, O., RIZAOĞLU, T., ÜNLÜGENÇ, Ü, İNAN, N., TASLI, K. & USTAÖMER, T. 2007. Tectonic evolution of the South Tethyan ocean: evidence from the Eastern Taurus Mountains (Elazığ region, SE Turkey). In: REES, A.C., BUTLER, R.W.H. & GRAHAM, R.H. (eds), Deformation of the Continental Crust: The Legacy of Mike Coward. Geological Society, London, Special Publications 272, 231–270.

ROCCHI, S., STORTI, F., DI VINCENZO, G. & ROSSETTI, F. 2003. Intraplate strike-slip tectonics as an alternative to mantle plume activity for the Cenozoic rift magmatism in the Ross Sea region, Antarctica. In: STORTI, F., HOLDSWORTH, R.E. & SALVINI, F. (eds), Intraplate Strike-slip Deformation Belts. Geological Society, London, Special Publications 210, 145–158.

ROSE, J., WHITEMAN, C.A., ALLEN, P. & KEMP, R.A. 1999. The Kesgrave sands and gravels: pre-glacial Quaternary deposits of the River Thames in East Anglia and the Thames valley. Proceedings of the Geologists' Association 110, 93–116.

SANVER, M. 1968. A palaeomagnetic study of Quaternary volcanic rocks from Turkey. Physics of the Earth and Planetary Interiors 1, 403–421.

SAUNDERS, P., PRIESTLEY, K. & TAYMAZ, T. 1998. Variations in the crustal structure beneath western Turkey. Geophysical Journal International 134, 373–389.

ŞENGÖR, A.M.C., OZEREN, S., GENÇ, T. & ZOR, E. 2003. East Anatolian high plateau as a mantle-supported, north-south shortened domal structure. Geophysical Research Letters 30, 8045 [published online; doi: 10.1029/2003GL017858].

SEYREK, A., DEMIR, T., PRINGLE, M., YURTMEN, S., WESTAWAY, R., BRIDGLAND, D., BECK, A. & ROWBOTHAM, G. 2008. Late Cenozoic uplift of the Amanos Mountains and incision of the Middle Ceyhan river gorge, southern Turkey; Ar-Ar dating of the Düziçi basalt. Geomorphology, in press.

SHACKLETON, N.J., A. BERGER, A. & PELTIER, W.R. 1990. An alternative astronomical calibration of the lower Pleistocene timescale based on ODP site 677. Transactions of the Royal Society of Edinburgh, Earth Sciences 81, 251–261.

SIBSON, R.H. 1983. Continental fault structure and the shallow earthquake source. Journal of the Geological Society, London 140, 741–767.

SINGER, B.S. & PRINGLE, M.S. 1996. Age and duration of the Matuyama-Brunhes geomagnetic polarity reversal from $^{40}Ar/^{39}Ar$ incremental heating analysis of lavas. Earth and Planetary Science Letters 139, 47–61.

SINGER, B.S., ACKERT, R.P., JR., GUILLOU, H. 2004. $^{40}Ar/^{39}Ar$ and K-Ar chronology of Pleistocene glaciations in Patagonia. Geological Society of America Bulletin 116, 434–450.

SIREL, E., METIN, S. & SÖZERI, B. 1975. Palu (KD Elazığ) denizel Oligosen'in stratigrafisi ve mikropaleontolojisi [Stratigraphy and micropalaeontology of Palu (NE Elazığ) Oligocene marine units]. Bulletin of the Geological Society of Turkey 18, 175–180 [in Turkish with English abstract].

STEIGER, R.H. & JÄGER, E. 1977. Convention on the use of decay constants in geo- and cosmochronology. Earth and Planetary Science Letters 36, 359–363.

SUN, S.S. & McDONOUGH, W.F. 1989. Chemical isotopic systematics of oceanic basalts: implications for mantle composition and processes. In: SAUNDERS, A.D. & NORRY, M.J. (eds), Magmatism in Ocean Basins. Geological Society, London, Special Publications 42, 313–345.

TEZCAN, A.K. 1995. Geothermal explorations and heat flow in Turkey. In: GUPTA, M.L. & YAMANO, M. (eds), Terrestrial Heat Flow and Geothermal Energy in Asia. Science Publishers, Lebanon, New Hampshire, 23–42.

TOLUN, N. 1951. Étude géologique du bassin nord-est de Diyarbakır. Mineral Research and Exploration Institute (MTA) of Turkey Bulletin 41, 65–98.

TOLUN, N. 1962. Hatay Sheet of the Geological Map of Turkey, 1:500,000 Scale. General Directorate of Mineral Research and Exploration (MTA) Publications.

TONBUL, S. 1987. Elazığ batısının genel jeomorpholojik özellikleri ve gelişimi [General geomorphology of the area to the west of Elazığ: aspects and development]. Jeomorfoloji Dergisi 15, 37–52 [in Turkish with English abstract].

TRUA, T., SERRI, G., BIRKENMAJER, K. & PECSKAY, Z. 2006. Geochemical and Sr-Nd-Pb isotopic compositions of Mts Pieniny dykes and sills (West Carpathians); evidence for melting in the lithospheric mantle. Lithos 90, 57–76.

TURNER, G. & CADOGAN, P. 1974. Possible effects of ^{39}Ar recoil in $^{40}Ar/^{39}Ar$ dating. In: Proceedings of the 5th Lunar and Planetary Science Conference, 1601–1615.

ÜNAY, E. & DE BRUIJN, H. 1998. Plio-Pleistocene rodents and lagomorphs from Anatolia. In: The Dawn of the Quaternary; Proceedings of the 1996 SEQS-EuroMam Symposium. Mededelingen Nederlands Instituut voor Toegepaste Geowetenschappen TNO 60, 431–465.

WESTAWAY, R. 1995. Crustal volume balance during the India-Eurasia collision and altitude of the Tibetan plateau: a working hypothesis. Journal of Geophysical Research 100, 15173–15194.

WESTAWAY, R. 1998. Dependence of active normal fault dips on lower-crustal flow regimes. Journal of the Geological Society, London 155, 233–253.

WESTAWAY, R. 2001. Flow in the lower continental crust as a mechanism for the Quaternary uplift of the Rhenish Massif, north-west Europe. In: MADDY, D., MACKLIN, M. & WOODWARD, J. (eds), River Basin Sediment Systems: Archives of Environmental Change. Balkema, Rotterdam, 87–167.

WESTAWAY, R. 2002a. Geomorphological consequences of weak lower continental crust, and its significance for studies of uplift, landscape evolution, and the interpretation of river terrace sequences. Netherlands Journal of Geosciences 81, 283–304.

WESTAWAY, R. 2002b. Long-term river terrace sequences: Evidence for global increases in surface uplift rates in the Late Pliocene and early Middle Pleistocene caused by flow in the lower continental crust induced by surface processes. *Netherlands Journal of Geosciences* **81**, 305–328.

WESTAWAY, R. 2002c. The Quaternary evolution of the Gulf of Corinth, central Greece: coupling between surface processes and flow in the lower continental crust. *Tectonophysics* **348**, 269–318.

WESTAWAY, R. 2003. Kinematics of the Middle East and Eastern Mediterranean updated. *Turkish Journal of Earth Sciences* **12**, 5–46.

WESTAWAY, R. 2004a. Kinematic consistency between the Dead Sea Fault Zone and the Neogene and Quaternary left-lateral faulting in SE Turkey. *Tectonophysics* **391**, 203–237.

WESTAWAY, R. 2004b. Pliocene and Quaternary surface uplift revealed by sediments of the Loire-Allier river system, France. *Quaternaire* **15**, 103–115.

WESTAWAY, R. 2006a. Late Cenozoic extension in southwest Bulgaria: a synthesis. *In:* ROBERTSON, A.H.F. & MOUNTRAKIS, D. (eds), *Tectonic Development of the Eastern Mediterranean Region*. Geological Society, London, Special Publications **260**, 557–590.

WESTAWAY, R. 2006b. Investigation of coupling between surface processes and induced flow in the lower continental crust as a cause of intraplate seismicity. *Earth Surface Processes and Landforms* **31**, 1480–1509.

WESTAWAY, R. 2006c. Cenozoic cooling histories in the Menderes Massif, western Turkey, may be caused by erosion and flat subduction, not low-angle normal faulting. *Tectonophysics* **412**, 1–25.

WESTAWAY, R. & ARGER, J. 2001. Kinematics of the Malatya-Ovacık Fault Zone. *Geodinamica Acta* **14**, 103–131.

WESTAWAY, R. & BRIDGLAND, D. 2007. Late Cenozoic uplift of southern Italy deduced from fluvial and marine sediments: coupling between surface processes and lower-crustal flow. *Quaternary International* **175**, 86–124.

WESTAWAY, R., BRIDGLAND, D. & WHITE, M. 2006a. The Quaternary uplift history of central southern England: evidence from the terraces of the Solent River system and nearby raised beaches. *Quaternary Science Reviews* **25**, 2212–2250.

WESTAWAY, R., DEMİR, T., SEYREK, A. & BECK, A. 2006b. Kinematics of active left-lateral faulting in southeast Turkey from offset Pleistocene river gorges: improved constraint on the rate and history of relative motion between the Turkish and Arabian plates. *Journal of the Geological Society, London* **163**, 149–164.

WESTAWAY, R., GUILLOU, H., SEYREK, A., DEMİR, T., BRIDGLAND, D., SCAILLET, S. & BECK, A. 2008. Late Cenozoic surface uplift, basaltic volcanism, and incision by the River Tigris around Diyarbakır, SE Turkey. *International Journal of Earth Sciences*, in press.

WESTAWAY, R., GUILLOU, H., YURTMEN, S., BECK, A., BRIDGLAND, D., DEMİR, T., SCAILLET, S. & ROWBOTHAM, G. 2006c. Late Cenozoic uplift of western Turkey: Improved dating and numerical modelling of the Gediz river terrace staircase and the Kula Quaternary volcanic field. *Global and Planetary Change* **51**, 131–171.

WESTAWAY, R., GUILLOU, H., YURTMEN, S., DEMİR, T., SCAILLET, S. & ROWBOTHAM, G. 2005. Constraints on the timing and regional conditions at the start of the present phase of crustal extension in western Turkey from observations in and around the Denizli region. *Geodinamica Acta* **18**, 209–238.

WESTAWAY, R., MADDY, D. & BRIDGLAND, D. 2002. Flow in the lower continental crust as a mechanism for the Quaternary uplift of south-east England: constraints from the Thames terrace record. *Quaternary Science Reviews* **21**, 559–603.

WESTAWAY, R., PRINGLE, M., YURTMEN, S., DEMİR, T., BRIDGLAND, D., ROWBOTHAM, G. & MADDY, D. 2004. Pliocene and Quaternary regional uplift in western Turkey: the Gediz river terrace staircase and the volcanism at Kula. *Tectonophysics* **391**, 121–169.

WHITEMAN, C.A. & ROSE, J. 1992. Thames river sediments of the British Early and Middle Pleistocene. *Quaternary Science Reviews* **11**, 363–375.

YAZGAN, E. 1984. Geodynamic evolution of the Eastern Taurus region. *In:* TEKELİ, O. & GÖNCÜOĞLU, M.C. (eds), *Geology of the Taurus Belt, Proceedings of the 1983 Ankara Symposium*. General Directorate of Mineral Research and Exploration (MTA) Publications, 199–208.

YODER, H.S., JR. & TILLEY, C.E., 1962. Origin of basalt magmas; an experimental study of natural and synthetic rock systems. *Journal of Petrology* **3**, 342–529.

YURTMEN, S., GUILLOU, H., WESTAWAY, R., ROWBOTHAM, G. & TATAR, O. 2002. Rate of strike-slip motion on the Amanos Fault (Karasu Valley, southern Turkey) constrained by K-Ar dating and geochemical analysis of Quaternary basalts: *Tectonophysics* **344**, 207–246.

ZAGWIJN, W.H. 1992. The beginning of the Ice Age in Europe and its major subdivisions. *Quaternary Science Reviews* **11**, 583–591.

ZOR, E., SANDVOL, E., GÜRBÜZ, C., TÜRKELLİ, N., SEBER, D. & BARAZANGI, M. 2003. The crustal structure of the east Anatolian Plateau (Turkey) from receiver functions. *Geophysical Research Letters* **30**, 8044 [published online; doi: 10.1029/2003GL018192].

Appendix

Appendix: Detailed Documentation of Ar-Ar Dates.

Sample 02TR31

Information on Analysis

Sample	02TR31 E21	Material	Basaltic groundmass
Location	Çipköy, Turkey	UTM co-ordinates	EC 06704 82031
Analyst	msp	Project	Harran University, project number 442
Irradiation	cl155-	J-value	0.0003549
Standard name	tcr-2a	Standard age	28.34 Ma ± 0.01 %1s

Procedure Blanks

	$^{36}Ar \pm 1\sigma$	$^{37}Ar \pm 1\sigma$	$^{38}Ar \pm 1\sigma$	$^{39}Ar \pm 1\sigma$	$^{40}Ar \pm 1\sigma$
All splits:	0.000213 ± 0.000019	0.000255 ± 0.000038	0.000137 ± 0.000021	0.000437 ± 0.000041	0.030000 ± 0.000124

Irradiation Constants (all ± %1σ)

	$^{40}Ar/^{36}Ar(a)$	$^{38}Ar/^{36}Ar(a)$	$^{39}Ar/^{37}Ar(ca)$	$^{38}Ar/^{37}Ar(ca)$	$^{36}Ar/^{37}Ar(ca)$	$^{40}Ar/^{39}Ar(k)$	$^{38}Ar/^{39}Ar(k)$	Sensitivity	Resist
All splits	295.5 ± 0	0.1869 ± 0	0.000676 ± 0	0.000034 ± 0	0.000279 ± 0	0.00039 ± 0	0.01243 ± 0	6.000×10⁻¹⁴	001

Sample Parameters

	Standard ± %1σ	J ± %1σ	Fract ± %1σ	V.Corr	K/Ca	K/Cl	Ca/Cl
All splits	28.34 ± 0.01	0.0003549 ± 0.3	1.007 ± 0.2	1	0.49 ± 0	0 ± 0	0 ± 0

Intercept Values

Split	$^{36}Ar \pm 1\sigma$	r^2	$^{37}Ar \pm 1\sigma$	r^2	$^{38}Ar \pm 1\sigma$	r^2	$^{39}Ar \pm 1\sigma$	r^2	$^{40}Ar \pm 1\sigma$	r^2
01	0.003361 ± 0.000027	0.8633	0.010824 ± 0.000073	0.8218	0.001661 ± 0.000031	0.3527	0.035088 ± 0.000095	0.7114	0.969587 ± 0.000597	0.9711
02	0.005318 ± 0.000027	0.9531	0.043703 ± 0.000124	0.9865	0.006303 ± 0.000031	0.9970	0.189436 ± 0.000218	0.9747	1.962560 ± 0.000590	0.9992
03	0.002730 ± 0.000020	0.7724	0.075043 ± 0.000135	0.9933	0.012866 ± 0.000035	0.9996	0.502456 ± 0.000229	0.9888	2.224910 ± 0.000482	0.9996
04	0.001825 ± 0.000024	0.0837	0.056936 ± 0.000108	0.9925	0.010570 ± 0.000051	0.9993	0.479399 ± 0.000280	0.9572	1.869787 ± 0.000574	0.9984
05	0.001784 ± 0.000023	0.3746	0.049023 ± 0.000093	0.9910	0.007629 ± 0.000034	0.9991	0.366533 ± 0.000206	0.9693	1.515500 ± 0.000416	0.9970
06	0.001792 ± 0.000022	0.4820	0.046447 ± 0.000077	0.9934	0.004964 ± 0.000036	0.9995	0.269025 ± 0.000111	0.8789	1.239589 ± 0.000413	0.9815
07	0.002358 ± 0.000025	0.1901	0.061895 ± 0.000073	0.9969	0.004431 ± 0.000033	0.9987	0.275751 ± 0.000190	0.8394	1.424973 ± 0.000470	0.9954
08	0.002740 ± 0.000020	0.8188	0.067807 ± 0.000110	0.9969	0.003032 ± 0.000037	0.9993	0.168080 ± 0.000075	0.6951	1.164839 ± 0.000298	0.9809
09	0.002835 ± 0.000025	0.6905	0.079166 ± 0.000056	0.9989	0.002463 ± 0.000025	0.9977	0.124037 ± 0.000095	0.6742	1.046169 ± 0.000491	0.0004
10	0.010325 ± 0.000034	0.9717	1.667667 ± 0.001138	0.9993	0.007112 ± 0.000035	0.9995	0.301004 ± 0.000117	0.8879	3.174654 ± 0.000868	0.9994

Incremental Heating

Split	Temp.	W	^{36}Ar(a)	^{37}Ar(ca)	^{38}Ar(cl)	^{39}Ar(k)	^{40}Ar(r)	Age ± 2σ (ka)	^{40}Ar(r) (%)	^{39}Ar(k) (%)	K/Ca ± 2σ
5F041Q.01	500 °C	0	0.00305	0.04444	0.00050	0.03440	0.03851	716.6 ± 437.9	4.10	1.28	0.379 ± 0.008
5F041Q.02	600 °C	0	0.00491	0.18282	0.00282	0.18766	0.48027	1637.8 ± 101.9	24.85	6.99	0.503 ± 0.007
5F041Q.03	700 °C	0	0.00236	0.31483	0.00590	0.49858	1.49744	1922.0 ± 26.1	68.22	18.58	0.776 ± 0.010
5F041Q.04	750 °C	4	0.00150	0.23872	0.00409	0.47572	1.39615	1878.1 ± 26.7	75.89	17.73	0.976 ± 0.013
5F041Q.05	800 °C	4	0.00147	0.20549	0.00259	0.36360	1.05091	1849.6 ± 33.6	70.74	13.55	0.867 ± 0.011
5F041Q.06	850 °C	4	0.00148	0.19472	0.00116	0.26673	0.77172	1851.5 ± 44.4	63.80	9.94	0.671 ± 0.009
5F041Q.07	920 °C	4	0.00201	0.25996	0.00045	0.27337	0.79978	1872.2 ± 48.2	57.33	10.19	0.515 ± 0.007
5F041Q.08	1000 °C	0	0.00238	0.28503	0.00033	0.16637	0.43191	1661.4 ± 75.7	38.06	6.20	0.286 ± 0.004
5F041Q.09	1100 °C	0	0.00246	0.33311	0.00030	0.12258	0.29009	1514.6 ± 112.6	28.55	4.57	0.180 ± 0.002
5F041Q.10	1400 °C	0	0.00787	7.04180	0.00152	0.29387	0.81850	1782.4 ± 111.9	26.03	10.95	0.020 ± 0.000
Sum			0.02950	9.10091	0.01966	2.68288	7.57528				

Results

	^{40}Ar(r)/^{39}Ar(k) ± 2σ	Age ± 2σ (ka)	MSWD	^{39}Ar(k) (%, n)	K/Ca ± 2σ
Weighted Plateau Age	2.9148 ± 0.0275 (± 0.94%)	1865.3 ± 20.9 (± 1.12%)	0.75	51.42, 4	0.667 ± 0.195
External Error		± 20.9	3.18	Statistical T ratio	
Analytical Error		± 17.6	1.0000	Error Magnification	
Total Fusion Age	2.8236 ± 0.0309 (± 1.10%)	1806.9 ± 22.6 (± 1.25%)		10	0.144 ± 0.001
External Error		± 22.6			
Analytical Error		± 19.8			

Additional Data

Split	Temp.	W	^{40}Ar(r)/^{39}Ar(k) ± 1σ	^{40}Ar(r+a) ± 1σ	^{37}Ar(decay)	^{39}Ar(decay)	^{40}Ar(moles)	Date, time
5F041Q.01	500 °C	0	1.11939 ± 0.34213	0.93957 ± 0.00061	4.292640	1.00052058	5.638×10^{-14}	30 07 2005 17:04
5F041Q.02	600 °C	0	2.55923 ± 0.07964	1.93249 ± 0.00060	4.296057	1.00052087	1.160×10^{-13}	30 07 2005 18:02
5F041Q.03	700 °C	0	3.00343 ± 0.02044	2.19472 ± 0.00050	4.298002	1.00052103	1.317×10^{-13}	30 07 2005 18:35
5F041Q.04	750 °C	4	2.93482 ± 0.02089	1.83960 ± 0.00059	4.300007	1.00052120	1.104×10^{-13}	30 07 2005 19:09
5F041Q.05	800 °C	4	2.89028 ± 0.02629	1.48536 ± 0.00043	4.302013	1.00052136	8.913×10^{-14}	30 07 2005 19:43
5F041Q.06	850 °C	4	2.89330 ± 0.03474	1.20949 ± 0.00043	4.303960	1.00052153	7.258×10^{-14}	30 07 2005 20:16
5F041Q.07	920 °C	4	2.92565 ± 0.03769	1.39487 ± 0.00049	4.305968	1.00052169	8.370×10^{-14}	30 07 2005 20:50
5F041Q.08	1000 °C	0	2.59607 ± 0.05921	1.13477 ± 0.00032	4.307918	1.00052185	6.809×10^{-14}	30 07 2005 21:23
5F041Q.09	1100 °C	0	2.36655 ± 0.08797	1.01612 ± 0.00051	4.309927	1.00052202	6.097×10^{-14}	30 07 2005 21:57
5F041Q.10	1400 °C	0	2.78521 ± 0.08746	3.14454 ± 0.00088	4.311878	1.00052218	1.887×10^{-13}	30 07 2005 22:30

Normal Isochron

Split	Temp.	W	$^{39}Ar(k)/^{36}Ar(a) \pm 2\sigma$	$^{40}Ar(a+r)/^{36}Ar(a) \pm 2\sigma$	r.i.
5F041Q.01	500 °C	0	11 ± 0	308 ± 8	0.963
5F041Q.02	600 °C	0	38 ± 1	393 ± 8	0.975
5F041Q.03	700 °C	0	211 ± 6	930 ± 26	0.989
5F041Q.04	750 °C	4	317 ± 14	1226 ± 52	0.995
5F041Q.05	800 °C	4	247 ± 11	1010 ± 43	0.995
5F041Q.06	850 °C	4	180 ± 8	816 ± 34	0.995
5F041Q.07	920 °C	4	136 ± 5	693 ± 24	0.992
5F041Q.08	1000 °C	0	70 ± 2	477 ± 13	0.989
5F041Q.09	1100 °C	0	50 ± 1	414 ± 12	0.989
5F041Q.10	1400 °C	0	37 ± 1	399 ± 9	0.982

Results	$^{39}Ar(k)/^{36}Ar(a) \pm 2\sigma$		$^{40}Ar(r)/^{39}Ar(k) \pm 2\sigma$	Age ± 2σ (ka)	MSWD
Isochron	292.3564 ± 19.7554 (± 6.76%)		2.9276 ± 0.0905 (± 3.09%)	1873.4 ± 58.9 (± 3.15%)	1.08
External Error					± 58.9
Analytical Error					± 57.9

Statistics	Statistical F ratio	Convergence	n
	3.00	0.0000002883	4
	Error Magnification	Number of Iterations	Calculated Line
	1.0380	76	Weighted York-2

Inverse Isochron

Split	Temp.	W	$^{39}Ar(k)/^{40}Ar(a+r) \pm 2\sigma$	$^{36}Ar(a)/^{40}Ar(a+r) \pm 2\sigma$	r.i.
5F041Q.01	500 °C	0	0.036611 ± 0.000268	0.003245 ± 0.000085	0.009
5F041Q.02	600 °C	0	0.097108 ± 0.000455	0.002543 ± 0.000052	0.004
5F041Q.03	700 °C	0	0.227171 ± 0.000939	0.001075 ± 0.000030	0.002
5F041Q.04	750 °C	4	0.258599 ± 0.001092	0.000816 ± 0.000035	0.002
5F041Q.05	800 °C	4	0.244791 ± 0.001029	0.000990 ± 0.000042	0.002
5F041Q.06	850 °C	4	0.220531 ± 0.000917	0.001225 ± 0.000051	0.003
5F041Q.07	920 °C	4	0.195981 ± 0.000843	0.001444 ± 0.000049	0.003
5F041Q.08	1000 °C	0	0.146613 ± 0.000612	0.002096 ± 0.000058	0.003
5F041Q.09	1100 °C	0	0.120635 ± 0.000538	0.002418 ± 0.000072	0.008
5F041Q.10	1400 °C	0	0.093455 ± 0.000392	0.002503 ± 0.000055	0.003

Results	$^{40}Ar(a)/^{36}Ar(a) \pm 2\sigma$		$^{40}Ar(r)/^{39}Ar(k) \pm 2\sigma$	Age ± 2σ (ka)	MSWD
Isochron	292.2479 ± 19.5119 (± 6.68%)		2.9290 ± 0.0891 (± 3.04%)	1874.3 ± 58.1 (± 3.10%)	1.07
External Error					± 58.1
Analytical Error					± 57.0

Statistics	Statistical F ratio	Convergence	n
	3.00	0.0000083880	4
	Error Magnification	Number of Iterations	Calculated Line
	1.0340	3	Weighted York-2

Degassing Patterns

Split	Temp.	W	^{36}Ar(a)	^{36}Ar(ca)	^{36}Ar(cl)	^{37}Ar(ca)	^{38}Ar(a)	^{38}Ar(K)	^{38}Ar(ca)	^{38}Ar(cl)	^{39}Ar(K)	^{39}Ar(ca)	^{40}Ar(r)	^{40}Ar(a)	^{40}Ar(k)
01	500 °C	0	0.00305	0.00001	0.00000	0.04444	0.00057	0.00043	0.00000	0.00050	0.03440	0.00003	0.03851	0.90107	0.00001
02	600 °C	0	0.00491	0.00005	0.00000	0.18282	0.00092	0.00233	0.00001	0.00282	0.18766	0.00012	0.48027	1.45222	0.00007
03	700 °C	0	0.00236	0.00009	0.00000	0.31483	0.00044	0.00620	0.00001	0.00590	0.49858	0.00021	1.49744	0.69727	0.00019
04	750 °C	4	0.00150	0.00007	0.00000	0.23872	0.00028	0.00591	0.00001	0.00409	0.47572	0.00016	1.39615	0.44345	0.00019
05	800 °C	4	0.00147	0.00006	0.00000	0.20549	0.00027	0.00452	0.00001	0.00259	0.36360	0.00014	1.05091	0.43445	0.00014
06	850 °C	4	0.00148	0.00005	0.00000	0.19472	0.00028	0.00332	0.00001	0.00116	0.26673	0.00013	0.77172	0.43776	0.00010
07	920 °C	4	0.00201	0.00007	0.00000	0.25996	0.00038	0.00340	0.00001	0.00045	0.27337	0.00018	0.79978	0.59509	0.00011
08	1000 °C	0	0.00238	0.00008	0.00000	0.28503	0.00044	0.00207	0.00001	0.00033	0.16637	0.00019	0.43191	0.70286	0.00006
09	1100 °C	0	0.00246	0.00009	0.00000	0.33311	0.00046	0.00152	0.00001	0.00030	0.12258	0.00023	0.29009	0.72603	0.00005
10	1400 °C	0	0.00787	0.00196	0.00000	7.04180	0.00147	0.00365	0.00024	0.00152	0.29387	0.00476	0.81850	2.32604	0.00011
	Sum		0.02950	0.00254	0.00000	9.10091	0.00551	0.03335	0.00031	0.01966	2.68288	0.00615	7.57528	8.71624	0.00105
	Sum				0.03204	9.10091				0.05884		2.68903			16.29257

Sample 02TR31

Information on Analysis

Sample	02TR33 E22	Material	Basaltic groundmass
Location	Alaca, Turkey	UTM co-ordinates	EC 05249 89380
Analyst	msp	Project	Harran University, project number 442
Irradiation	cl155-	J-value	0.0003546
Standard name	tcr-2a	Standard age	28.34 Ma ± 0.01 %1s

Procedure Blanks

	$^{36}Ar \pm 1\sigma$	$^{37}Ar \pm 1\sigma$	$^{38}Ar \pm 1\sigma$	$^{39}Ar \pm 1\sigma$	$^{40}Ar \pm 1\sigma$
All splits:	0.000254 ± 0.000017	0.000264 ± 0.000033	0.000146 ± 0.000023	0.000455 ± 0.000049	0.040000 ± 0.000115

Irradiation Constants (all ± %1σ)

	$^{40}Ar/^{36}Ar(a)$	$^{38}Ar/^{36}Ar(a)$	$^{39}Ar/^{37}Ar(ca)$	$^{38}Ar/^{37}Ar(ca)$	$^{36}Ar/^{37}Ar(ca)$	$^{40}Ar/^{39}Ar(k)$	$^{38}Ar/^{39}Ar(k)$	$^{36}Ar/^{38}Ar(cl)$	K/Ca	K/Cl	Ca/Cl
All splits	295.5 ± 0	0.1869 ± 0	0.000676 ± 0	0.000034 ± 0	0.000279 ± 0	0.00039 ± 0	0.01243 ± 0	0 ± 0	0.49 ± 0	0 ± 0	0 ± 0

Sample Parameters

	Standard ± %1σ	J ± %1σ	Fract ± %1σ	V.Corr	Sensitivity	Resist
All splits	28.34 ± 0.01	0.0003546 ± 0.3	1.007 ± 0.2	1	6.000¥10-14	001

Intercept Values

Split	$^{36}Ar \pm 1\sigma$	r^2	$^{37}Ar \pm 1\sigma$	r^2	$^{38}Ar \pm 1\sigma$	r^2	$^{39}Ar \pm 1\sigma$	r^2	$^{40}Ar \pm 1\sigma$	r^2
01	0.001789 ± 0.000020	0.3579	0.006953 ± 0.000042	0.1088	0.000999 ± 0.000033	0.5414	0.022669 ± 0.000063	0.9720	0.529618 ± 0.000464	0.9960
02	0.003026 ± 0.000031	0.6125	0.024813 ± 0.000051	0.9876	0.002507 ± 0.000042	0.6306	0.119993 ± 0.000160	0.9940	1.218202 ± 0.000353	0.9976
03	0.003264 ± 0.000022	0.8995	0.055515 ± 0.000135	0.9880	0.006690 ± 0.000040	0.9276	0.465191 ± 0.000551	0.9975	2.355246 ± 0.002307	0.9961
04	0.002267 ± 0.000020	0.0298	0.052198 ± 0.000078	0.9940	0.007736 ± 0.000045	0.9208	0.562260 ± 0.000250	0.9996	2.364398 ± 0.000602	0.9994
05	0.002224 ± 0.000017	0.0240	0.054426 ± 0.000075	0.9947	0.008031 ± 0.000055	0.8935	0.575242 ± 0.000274	0.9995	2.433189 ± 0.000538	0.9996
06	0.002102 ± 0.000025	0.0214	0.057133 ± 0.000083	0.9950	0.007074 ± 0.000036	0.9159	0.510172 ± 0.000171	0.9997	2.264201 ± 0.000366	0.9997
07	0.002639 ± 0.000023	0.1272	0.069512 ± 0.000104	0.9942	0.007061 ± 0.000034	0.9176	0.499854 ± 0.000308	0.9991	2.455789 ± 0.000414	0.9998
08	0.003151 ± 0.000022	0.6892	0.086931 ± 0.000124	0.9954	0.006196 ± 0.000044	0.8297	0.414256 ± 0.000173	0.9996	2.256625 ± 0.000534	0.9994
09	0.003519 ± 0.000023	0.7449	0.123818 ± 0.000160	0.9962	0.006230 ± 0.000043	0.8000	0.423734 ± 0.000160	0.9997	2.493066 ± 0.000455	0.9997
10	0.017258 ± 0.000016	0.9976	1.079381 ± 0.000273	0.9999	0.016808 ± 0.000042	0.9785	1.024072 ± 0.000317	0.9998	8.038685 ± 0.001471	0.9999

Incremental Heating

Split	Temp.	W	$^{36}Ar(a)$	$^{37}Ar(ca)$	$^{38}Ar(d)$	$^{39}Ar(k)$	$^{40}Ar(r)$	Age ± 2σ (ka)	$^{40}Ar(r)$ (%)	$^{39}Ar(k)$ (%)	K/Ca ± 2σ
5F041R.01	770 °C	0	0.00149	0.02829	0.00029	0.02205	0.05072	1470.7 ± 484.5	10.36	0.48	0.382 ± 0.008
5F041R.02	870 °C	0	0.00267	0.10392	0.00035	0.11870	0.38992	2100.2 ± 128.3	33.09	2.59	0.560 ± 0.008
5F041R.03	970 °C	4	0.00286	0.23400	0.00017	0.46159	1.46909	2034.9 ± 31.1	63.45	10.08	0.967 ± 0.013
5F041R.04	1020 °C	4	0.00190	0.22005	0.00019	0.55804	1.76354	2020.5 ± 21.9	75.87	12.19	1.243 ± 0.016
5F041R.05	1070 °C	4	0.00185	0.22960	0.00033	0.57093	1.84568	2066.9 ± 20.2	77.12	12.47	1.218 ± 0.016
5F041R.06	1120 °C	4	0.00173	0.24118	0.00021	0.50628	1.71251	2162.6 ± 25.7	76.99	11.06	1.029 ± 0.013
5F041R.07	1190 °C	4	0.00224	0.29382	0.00023	0.49599	1.75424	2261.2 ± 26.7	72.62	10.83	0.827 ± 0.011
5F041R.08	1270 °C	4	0.00272	0.36789	0.00034	0.41089	1.41404	2200.2 ± 33.3	63.79	8.97	0.547 ± 0.007
5F041R.09	1370 °C	4	0.00303	0.52472	0.00019	0.42020	1.55768	2369.9 ± 35.1	63.50	9.18	0.392 ± 0.005
5F041R.10	1670 °C	0	0.01526	4.58503	0.00082	1.01393	3.48847	2199.7 ± 49.9	43.61	22.15	0.108 ± 0.001
Sum			0.03574	6.82849	0.00311	4.57861	15.44589				

Results

	$^{40}Ar(r)/^{39}Ar(k)$ ± 2σ	Age ± 2σ (ka)	MSWD	$^{39}Ar(k)$ (%, n)	K/Ca ± 2σ
Error Plateau	3.3331 ± 0.1392 (± 4.18%)	2131.0 ± 89.9 (± 4.22%)	80.52	74.78, 7	0.625 ± 0.232
External Error		± 89.9	2.45	Statistical T ratio	
Analytical Error		± 89.0	8.9735	Error Magnification	
Total Fusion Age	3.3735 ± 0.0220 (± 0.65%)	2156.8 ± 19.1 (± 0.89%)		10	0.329 ± 0.003
External Error		± 19.1			
Analytical Error		± 14.1			

Additional Data

Split	Temp.	W	$^{40}Ar(r)/^{39}Ar(k)$ ± 1σ	$^{40}Ar(r+a)$ ± 1σ	$^{37}Ar(decay)$	$^{39}Ar(decay)$	$^{40}Ar(moles)$	Date, time
5F041R.01	770 °C	0	2.29984 ± 0.37902	0.48961 ± 0.00048	4.318685	1.00052275	2.938×10^{-14}	31 07 2005 00:25
5F041R.02	870 °C	0	3.28495 ± 0.10037	1.17816 ± 0.00037	4.322123	1.00052303	7.069×10^{-14}	31 07 2005 01:23
5F041R.03	970 °C	4	3.18269 ± 0.02435	2.31507 ± 0.00231	4.324139	1.00052320	1.389×10^{-13}	31 07 2005 01:57
5F041R.04	1020 °C	4	3.16023 ± 0.01715	2.32418 ± 0.00061	4.326097	1.00052336	1.395×10^{-13}	31 07 2005 02:30
5F041R.05	1070 °C	4	3.23274 ± 0.01584	2.39297 ± 0.00055	4.328115	1.00052353	1.436×10^{-13}	31 07 2005 03:04
5F041R.06	1120 °C	4	3.38257 ± 0.02013	2.22400 ± 0.00038	4.330074	1.00052369	1.335×10^{-13}	31 07 2005 03:37
5F041R.07	1190 °C	4	3.53686 ± 0.02093	2.41560 ± 0.00043	4.332094	1.00052385	1.449×10^{-13}	31 07 2005 04:11
5F041R.08	1270 °C	4	3.44139 ± 0.02609	2.21647 ± 0.00055	4.334055	1.00052402	1.330×10^{-13}	31 07 2005 04:44
5F041R.09	1370 °C	4	3.70697 ± 0.02747	2.45290 ± 0.00047	4.336077	1.00052418	1.472×10^{-13}	31 07 2005 05:18
5F041R.10	1670 °C	0	3.44053 ± 0.03906	7.99829 ± 0.01448	4.338100	1.00052435	4.799×10^{-13}	31 07 2005 05:52

Normal Isochron

Split	Temp.	W	$^{39}Ar(k)/^{36}Ar(a)$ ± 2σ	$^{40}Ar(a+r)/^{36}Ar(a)$ ± 2σ	r.i.
5F041R.01	770 °C	0	15 ± 1	330 ± 13	0.976
5F041R.02	870 °C	0	44 ± 1	442 ± 13	0.987
5F041R.03	970 °C	4	161 ± 4	809 ± 20	0.980
5F041R.04	1020 °C	4	294 ± 9	1225 ± 39	0.992
5F041R.05	1070 °C	4	308 ± 9	1292 ± 39	0.991
5F041R.06	1120 °C	4	292 ± 11	1285 ± 48	0.994
5F041R.07	1190 °C	4	222 ± 7	1079 ± 32	0.990
5F041R.08	1270 °C	4	151 ± 4	816 ± 21	0.987
5F041R.09	1370 °C	4	139 ± 3	810 ± 20	0.987
5F041R.10	1670 °C	0	66 ± 1	524 ± 9	0.973

Results	$^{39}Ar(k)/^{36}Ar(a)$ ± 2σ	$^{40}Ar(r)/^{39}Ar(k)$ ± 2σ	Age ± 2σ (ka)	MSWD
Error Chron	376.7375 ± 90.0502 (± 23.90%)	2.9461 ± 0.4184 (± 14.20%)	1883.7 ± 267.6 (± 14.21%)	45.41
External Error			± 267.6	
Analytical Error			± 267.4	

Statistics	Statistical F ratio	Convergence	n	
	Error Magnification	Number of Iterations	Calculated Line	
	2.21	0.0000002885	7	
	6.7385	71	Weighted York-2	

Inverse Isochron

Split	Temp.	W	$^{39}Ar(k)/^{40}Ar(a+r)$ ± 2σ	$^{36}Ar(a)/^{40}Ar(a+r)$ ± 2σ	r.i.
5F041R.01	770 °C	0	0.045040 ± 0.000383	0.003034 ± 0.000115	0.012
5F041R.02	870 °C	0	0.100749 ± 0.000497	0.002264 ± 0.000068	0.003
5F041R.03	970 °C	4	0.199384 ± 0.001010	0.001237 ± 0.000031	0.032
5F041R.04	1020 °C	4	0.240103 ± 0.000993	0.000816 ± 0.000026	0.002
5F041R.05	1070 °C	4	0.238589 ± 0.000988	0.000774 ± 0.000023	0.002
5F041R.06	1120 °C	4	0.227641 ± 0.000928	0.000778 ± 0.000029	0.001
5F041R.07	1190 °C	4	0.205328 ± 0.000864	0.000927 ± 0.000027	0.001
5F041R.08	1270 °C	4	0.185381 ± 0.000765	0.001225 ± 0.000031	0.002
5F041R.09	1370 °C	4	0.171308 ± 0.000702	0.001235 ± 0.000031	0.001
5F041R.10	1670 °C	0	0.126769 ± 0.000517	0.001908 ± 0.000033	0.002

Results	$^{40}Ar(a)/^{36}Ar(a)$ ± 2σ	$^{40}Ar(r)/^{39}Ar(k)$ ± 2σ	Age ± 2σ (ka)	MSWD
Error Chron	386.1410 ± 93.7419 (± 24.28%)	2.9360 ± 0.3997 (± 13.61%)	1877.3 ± 255.7 (± 13.62%)	44.20
External Error			± 255.7	
Analytical Error			± 255.4	

Statistics	Statistical F ratio	Convergence	n	
	Error Magnification	Number of Iterations	Calculated Line	
	2.21	0.0000126132	7	
	6.6483	4	Weighted York-2	

Degassing Patterns

Split	Temp.	W	^{36}Ar(a)	^{36}Ar(ca)	^{36}Ar(cl)	^{37}Ar(ca)	^{38}Ar(a)	^{38}Ar(k)	^{38}Ar(ca)	^{38}Ar(cl)	^{39}Ar(k)	^{39}Ar(ca)	^{40}Ar(r)	^{40}Ar(a)	^{40}Ar(k)
01	770 °C	0	0.00149	0.00001	0.00000	0.02829	0.00028	0.00027	0.00000	0.00029	0.02205	0.00002	0.05072	0.43889	0.00001
02	870 °C	0	0.00267	0.00003	0.00000	0.10392	0.00050	0.00148	0.00000	0.00035	0.11870	0.00007	0.38992	0.78824	0.00005
03	970 °C	4	0.00286	0.00007	0.00000	0.23400	0.00054	0.00574	0.00001	0.00017	0.46159	0.00016	1.46909	0.84597	0.00018
04	1020 °C	4	0.00190	0.00006	0.00000	0.22005	0.00035	0.00694	0.00001	0.00019	0.55804	0.00015	1.76354	0.56064	0.00022
05	1070 °C	4	0.00185	0.00006	0.00000	0.22960	0.00035	0.00710	0.00001	0.00033	0.57093	0.00016	1.84568	0.54728	0.00022
06	1120 °C	4	0.00173	0.00007	0.00000	0.24118	0.00032	0.00629	0.00001	0.00021	0.50628	0.00016	1.71251	0.51149	0.00020
07	1190 °C	4	0.00224	0.00008	0.00000	0.29382	0.00042	0.00617	0.00001	0.00023	0.49599	0.00020	1.75424	0.66135	0.00019
08	1270 °C	4	0.00272	0.00010	0.00000	0.36789	0.00051	0.00511	0.00001	0.00034	0.41089	0.00025	1.41404	0.80243	0.00016
09	1370 °C	4	0.00303	0.00015	0.00000	0.52472	0.00057	0.00522	0.00002	0.00019	0.42020	0.00035	1.55768	0.89522	0.00016
10	1670 °C	0	0.01526	0.00128	0.00000	4.58503	0.00285	0.01260	0.00016	0.00082	1.01393	0.00310	3.48847	4.50982	0.00040
	Sum		0.03574	0.00191	0.00000	6.82849	0.00668	0.05691	0.00023	0.00311	4.57861	0.00462	15.44589	10.56134	0.0017
	Sum			0.03765		6.82849		0.06694			4.58323				26.00902

Sample 02TR35

Information on Analysis

Sample	02TR35 E23
Location	Gümüşbağlar, Turkey
Analyst	msp
Irradiation	cl155-
Standard name	tcr-2a

Material	Basaltic groundmass
UTM co-ordinates	EC 18088 88361
Project	Harran University, project number 442
J-value	0.0003540
Standard age	28.34 Ma ± 0.01 %1s

Procedure Blanks

	^{36}Ar ± 1σ	^{37}Ar ± 1σ	^{38}Ar ± 1σ	^{39}Ar ± 1σ	^{40}Ar ± 1σ
All splits:	0.000309 ± 0.000022	0.000489 ± 0.000022	0.000219 ± 0.000031	0.000492 ± 0.000038	0.055921 ± 0.000415

Irradiation Constants (all ± %1σ)

	^{40}Ar/^{36}Ar(a)	^{38}Ar/^{36}Ar(a)	^{39}Ar/^{37}Ar(ca)	^{38}Ar/^{37}Ar(ca)	^{36}Ar/^{37}Ar(ca)	^{40}Ar/^{39}Ar(k)	^{38}Ar/^{39}Ar(k)	^{36}Ar/^{38}Ar(cl)	K/Ca	K/Cl	Ca/Cl
All splits	295.5 ± 0	0.1869 ± 0	0.000676 ± 0	0.000034 ± 0	0.000279 ± 0	0.00039 ± 0	0.01243 ± 0	0 ± 0	0.49 ± 0	0 ± 0	0 ± 0

Sample Parameters

	Standard ± %1σ	J ± %1σ	Fract ± %1σ	V.Corr	Sensitivity	Resist
All splits	28.34 ± 0.01	0.0003540 ± 0.3	1.007 ± 0.2	1	6.000¥10-14	001

Intercept Values

Split	^{36}Ar ± 1σ	r²	^{37}Ar ± 1σ	r²	^{38}Ar ± 1σ	r²	^{39}Ar ± 1σ	r²	^{40}Ar ± 1σ	r²
01	0.003364 ± 0.000024	0.8872	0.011170 ± 0.000043	0.9513	0.001743 ± 0.000031	0.5364	0.055801 ± 0.000101	0.9611	1.092858 ± 0.000254	0.9987
02	0.002586 ± 0.000028	0.5584	0.022026 ± 0.000084	0.9623	0.002734 ± 0.000028	0.7829	0.157435 ± 0.000115	0.9985	1.266037 ± 0.000431	0.9973
03	0.002529 ± 0.000022	0.7473	0.063885 ± 0.000087	0.9963	0.009202 ± 0.000030	0.9858	0.700603 ± 0.000278	0.9997	2.877892 ± 0.001222	0.9990
04	0.001476 ± 0.000020	0.4523	0.057441 ± 0.000060	0.9974	0.012097 ± 0.000049	0.9557	0.988303 ± 0.000255	0.9999	3.354715 ± 0.000752	0.9998
05	0.001326 ± 0.000021	0.5886	0.055148 ± 0.000091	0.9931	0.014251 ± 0.000065	0.9553	1.140046 ± 0.000283	0.9999	3.723360 ± 0.000762	0.9998
06	0.001236 ± 0.000018	0.4829	0.046341 ± 0.000066	0.9938	0.010425 ± 0.000034	0.9671	0.823280 ± 0.000275	0.9998	2.736845 ± 0.000440	0.9998
07	0.001445 ± 0.000014	0.7051	0.054763 ± 0.000095	0.9914	0.007505 ± 0.000032	0.9482	0.575259 ± 0.000244	0.9996	2.052278 ± 0.000455	0.9992
08	0.001906 ± 0.000022	0.0802	0.081659 ± 0.000104	0.9963	0.004830 ± 0.000030	0.8198	0.338727 ± 0.000270	0.9981	1.444859 ± 0.000475	0.9930
09	0.002422 ± 0.000014	0.3197	0.140543 ± 0.000085	0.9992	0.005401 ± 0.000025	0.9181	0.357670 ± 0.000257	0.9986	1.607769 ± 0.000386	0.9979
10	0.011389 ± 0.000018	0.9938	0.855257 ± 0.000784	0.9985	0.006040 ± 0.000020	0.9505	0.267718 ± 0.000250	0.9969	3.654186 ± 0.001112	0.9995

Incremental Heating

Split	Temp.	W	^{36}Ar(a)	^{37}Ar(ca)	^{38}Ar(cl)	^{39}Ar(k)	^{40}Ar(r)	Age ± 2σ (ka)	^{40}Ar(r) (%)	^{39}Ar(k) (%)	K/Ca ± 2σ
5F041S.01	500 °C	0	0.00296	0.04577	0.00026	0.05492	0.16261	1889.8 ± 269.3	15.68	1.02	0.588 ± 0.009
5F041S.02	600 °C	0	0.00219	0.09235	0.00013	0.15587	0.56336	2306.7 ± 94.0	46.55	2.91	0.827 ± 0.012
5F041S.03	700 °C	0	0.00208	0.27198	0.00000	0.69543	2.20614	2024.9 ± 20.6	78.18	12.97	1.253 ± 0.016
5F041S.04	750 °C	4	0.00107	0.24445	0.00000	0.98130	2.98311	1940.4 ± 14.0	90.43	18.30	1.967 ± 0.025
5F041S.05	800 °C	4	0.00092	0.23471	0.00000	1.13207	3.39427	1913.8 ± 12.8	92.55	21.12	2.363 ± 0.031
5F041S.06	850 °C	4	0.00085	0.19699	0.00000	0.81737	2.43048	1898.0 ± 15.2	90.66	15.25	2.033 ± 0.026
5F041S.07	920 °C	4	0.00104	0.23327	0.00000	0.57092	1.68893	1888.3 ± 19.2	84.60	10.65	1.199 ± 0.016
5F041S.08	1000 °C	0	0.00146	0.34904	0.00009	0.33583	0.95876	1822.4 ± 37.3	69.03	6.26	0.471 ± 0.006
5F041S.09	1100 °C	0	0.00189	0.60252	0.00033	0.35448	0.99413	1790.2 ± 32.8	64.06	6.61	0.288 ± 0.004
5F041S.10	1400 °C	0	0.00975	3.67898	0.00052	0.26302	0.71667	1739.3 ± 128.1	19.92	4.91	0.035 ± 0.00
Sum			0.02420	5.95008	0.00134	5.36120	16.09846				

Results

	^{40}Ar(r)/^{39}Ar(k) ± 2σ	Age ± 2σ (ka)		MSWD	^{39}Ar(k) (%, n)	K/Ca ± 2σ
Error Plateau	2.9982 ± 0.0341 (± 1.14%)	1913.8 ± 24.6 (± 1.28%)		8.61	65.31, 4	1.647 ± 0.533
		± 24.6			Statistical T ratio	3.18
		± 21.7			Error Magnification	2.9349
External Error						
Analytical Error						

	^{40}Ar(r)/^{39}Ar(k) ± 2σ	Age ± 2σ (ka)		^{39}Ar(k) (%, n)	K/Ca ± 2σ
Total Fusion Age	3.0028 ± 0.0153 (± 0.51%)	1916.7 ± 15.1 (± 0.79%)		10	0.442 ± 0.003
External Error		± 15.1			
Analytical Error		± 9.8			

Additional Data

Split	Temp.	W	^{40}Ar(r)/^{39}Ar(k) ± 1σ	^{40}Ar(r+a) ± 1σ	^{37}Ar(decay)	^{39}Ar(decay)	^{40}Ar(moles)	Date, time
5F041S.01	500 °C	0	2.96061 ± 0.21109	1.03692 ± 0.00049	4.374790	1.00052736	6.222×10^{-14}	31 07 2005 16:06
5F041S.02	600 °C	0	3.61423 ± 0.07366	1.21006 ± 0.00060	4.378271	1.00052764	7.261×10^{-14}	31 07 2005 17:04
5F041S.03	700 °C	0	3.17236 ± 0.01612	2.82170 ± 0.00129	4.380314	1.00052781	1.693×10^{-13}	31 07 2005 17:38
5F041S.04	750 °C	4	3.03996 ± 0.01095	3.29841 ± 0.00086	4.382297	1.00052797	1.979×10^{-13}	31 07 2005 18:11
5F041S.05	800 °C	4	2.99828 ± 0.01005	3.66700 ± 0.00087	4.384341	1.00052814	2.200×10^{-13}	31 07 2005 18:45
5F041S.06	850 °C	4	2.97354 ± 0.01195	2.68060 ± 0.00060	4.386386	1.00052831	1.609×10^{-13}	31 07 2005 19:19
5F041S.07	920 °C	4	2.95829 ± 0.01506	1.99613 ± 0.00062	4.388372	1.00052847	1.198×10^{-13}	31 07 2005 19:52
5F041S.08	1000 °C	0	2.85494 ± 0.02924	1.38881 ± 0.00063	4.390419	1.00052863	8.334×10^{-14}	31 07 2005 20:26
5F041S.09	1100 °C	0	2.80450 ± 0.02569	1.55171 ± 0.00057	4.392407	1.00052880	9.311×10^{-14}	31 07 2005 20:59
5F041S.10	1400 °C	0	2.72475 ± 0.10036	3.59816 ± 0.00119	4.394456	1.00052896	2.159×10^{-13}	31 07 2005 21:33

Normal Isochron

Split	Temp.	W	$^{39}Ar(k)/^{36}Ar(a) \pm 2\sigma$	$^{40}Ar(a+r)/^{36}Ar(a) \pm 2\sigma$	r.i.
5F041S.01	500 °C	0	19 ± 1	350 ± 9	0.978
5F041S.02	600 °C	0	71 ± 3	553 ± 20	0.992
5F041S.03	700 °C	0	334 ± 11	1355 ± 45	0.992
5F041S.04	750 °C	4	920 ± 52	3091 ± 174	0.997
5F041S.05	800 °C	4	1227 ± 82	3973 ± 264	0.998
5F041S.06	850 °C	4	966 ± 65	3167 ± 213	0.998
5F041S.07	920 °C	4	549 ± 28	1920 ± 98	0.997
5F041S.08	1000 °C	0	231 ± 10	954 ± 43	0.995
5F041S.09	1100 °C	0	188 ± 6	822 ± 26	0.991
5F041S.10	1400 °C	0	27 ± 1	369 ± 7	0.971

Results	$^{39}Ar(k)/^{36}Ar(a) \pm 2\sigma$	$^{40}Ar(r)/^{39}Ar(k) \pm 2\sigma$	Age ± 2σ (ka)	MSWD
No Convergence	268.6120 ± 108.8344 (± 40.52%)	3.0233 ± 0.1252 (± 4.14%)	1929.8 ± 80.7 (± 4.18%)	11.11
External Error			± 80.7	
Analytical Error			± 79.9	

Statistics	Statistical F ratio	Convergence	n	
	3.00	0.0000242816	4	
	Error Magnification	Number of Iterations	Calculated Line	
	3.3332	100	Weighted York-2	

Inverse Isochron

Split	Temp.	W	$^{39}Ar(k)/^{40}Ar(a+r) \pm 2\sigma$	$^{36}Ar(a)/^{40}Ar(a+r) \pm 2\sigma$	r.i.
5F041S.01	500 °C	0	0.052967 ± 0.000300	0.002853 ± 0.000076	0.006
5F041S.02	600 °C	0	0.128814 ± 0.000567	0.001809 ± 0.000064	0.006
5F041S.03	700 °C	0	0.246457 ± 0.001031	0.000738 ± 0.000024	0.006
5F041S.04	750 °C	4	0.297506 ± 0.001210	0.000323 ± 0.000018	0.001
5F041S.05	800 °C	4	0.308719 ± 0.001253	0.000252 ± 0.000017	0.001
5F041S.06	850 °C	4	0.304919 ± 0.001245	0.000316 ± 0.000021	0.001
5F041S.07	920 °C	4	0.286011 ± 0.001184	0.000521 ± 0.000027	0.002
5F041S.08	1000 °C	0	0.241809 ± 0.001066	0.001048 ± 0.000047	0.004
5F041S.09	1100 °C	0	0.228442 ± 0.000987	0.001216 ± 0.000039	0.004
5F041S.10	1400 °C	0	0.073099 ± 0.000330	0.002710 ± 0.000050	0.005

Results	$^{40}Ar(a)/^{36}Ar(a) \pm 2\sigma$	$^{40}Ar(r)/^{39}Ar(k) \pm 2\sigma$	Age ± 2σ (ka)	MSWD
Error Chron	273.1873 ± 120.1076 (± 43.97%)	3.0227 ± 0.1346 (± 4.45%)	1929.4 ± 86.7 (± 4.49%)	12.27
External Error			± 86.7	
Analytical Error			± 85.9	

Statistics	Statistical F ratio	Convergence	n	
	3.5034	0.0000008250	4	
	Error Magnification	Number of Iterations	Calculated Line	
		7	Weighted York-2	

Degasing Patterns

Split	Temp.	W	^{36}Ar(a)	^{36}Ar(ca)	^{36}Ar(cl)	^{37}Ar(ca)	^{38}Ar(a)	^{38}Ar(k)	^{38}Ar(ca)	^{38}Ar(cl)	^{39}Ar(k)	^{39}Ar(ca)	^{40}Ar(r)	^{40}Ar(a)	^{40}Ar(k)
01	500 °C	0	0.00296	0.00001	0.00000	0.04577	0.00055	0.00068	0.00000	0.00026	0.05492	0.00003	0.16261	0.87431	0.00002
02	600 °C	0	0.00219	0.00003	0.00000	0.09235	0.00041	0.00194	0.00000	0.00013	0.15587	0.00006	0.56336	0.64670	0.00006
03	700 °C	0	0.00208	0.00008	0.00000	0.27198	0.00039	0.00864	0.00001	0.00000	0.69543	0.00018	2.20614	0.61556	0.00027
04	750 °C	4	0.00107	0.00007	0.00000	0.24445	0.00020	0.01220	0.00001	0.00000	0.98130	0.00017	2.98311	0.31530	0.00038
05	800 °C	4	0.00092	0.00007	0.00000	0.23471	0.00017	0.01407	0.00001	0.00000	1.13207	0.00016	3.39427	0.27273	0.00044
06	850 °C	4	0.00085	0.00005	0.00000	0.19699	0.00016	0.01016	0.00001	0.00000	0.81737	0.00013	2.43048	0.25013	0.00032
07	920 °C	4	0.00104	0.00007	0.00000	0.23327	0.00019	0.00710	0.00001	0.00000	0.57092	0.00016	1.68893	0.30720	0.00022
08	1000 °C	0	0.00146	0.00010	0.00000	0.34904	0.00027	0.00417	0.00001	0.00009	0.33583	0.00024	0.95876	0.43005	0.00013
09	1100 °C	0	0.00189	0.00017	0.00000	0.60252	0.00035	0.00441	0.00002	0.00033	0.35448	0.00041	0.99413	0.55758	0.00014
10	1400 °C	0	0.00975	0.00103	0.00000	3.67898	0.00182	0.00327	0.00013	0.00052	0.26302	0.00249	0.71667	2.88149	0.00010
	Sum		0.02420	0.00166	0.00000	5.95008	0.00452	0.06664	0.00020	0.00134	5.36120	0.00402	16.09846	7.15104	0.00209
	Sum				0.02586	5.95008				0.07270		5.36522			23.25159